國立交通大學

環境工程研究所

碩 士 論 文

製備高光催化活性之有機修飾中孔洞二氧化鈦

Fabrication of organic modified mesoporous TiO_2 with high photocatalytic activity

研 究 生：石佳璇

指導教授：張淑閔　博士

中 華 民 國 九 十 九 年 七 月

製備高光催化活性之有機修飾中孔洞二氧化鈦

Fabrication of organic modified mesoporous TiO_2 with high photocatalytic activity

研 究 生：石佳璇　　Student：Chia-Hsuan Shih

指導教授：張淑閔　　Advisor：Sue-Min Chang

國 立 交 通 大 學

環 境 工 程 研 究 所

碩 士 論 文

A Thesis
Submitted to Institute of Environmental Engineering
College of Engineering
National Chiao Tung University
In partial Fulfillment of the Requirements
for the Degree of
Master
in

Environmental Engineering

July 2010

Hsinchu, Taiwan, Republic of China

中華民國九十九年七月

中文摘要

本研究中首次以非水解性溶膠-凝膠法 (non-hydrolytic sol-gel)，使用三辛基氧化膦 (TOPO) 與 1,3,5-三甲基苯 (TMB) 分別作為模板劑及擴張劑，以單一步驟製備有機修飾的中孔洞二氧化鈦 (TiO_2) 結晶體。樣品比表面積介於 2-103 m^2/g，且數值隨TOPO濃度增加而減小，當TOPO/Ti = 0.05 (sample TP 1) 時，TiO_2顆粒間隙可形成中孔洞結構，而當TOPO/Ti比例提升到 0.1 (sample TP 2) 時，TOPO形成的微胞使樣品隨即轉變為微孔洞結構，進一步提高TOPO/Ti比例則製備出TOPO披覆的奈米顆粒。添加TMB之後，微孔洞與連續孔洞樣品皆呈現Type Ⅳ isotherm，並且大幅提升了比表面積與孔洞數量和孔洞尺寸，由此可知TMB擴大微胞尺寸並幫助TOPO形成微胞而驅使TiO_2形成中孔洞材料。其中TMB/TOPO/Ti為 0.12/0.1/1 的條件下，可得到高比表面積 236 m^2/g，平均孔洞尺寸為 3.6 nm的樣品，且未經鍛燒即得到高程度的anatase 晶體，晶粒大小約為 4.4 nm。在紅外光光譜分析中可以清楚看到C-H的波峰出現在 2760-3150 cm^{-1}，且P-O-Ti的波峰出現在 1100 cm^{-1}，相對於原TOPO的P=O在 1150 cm^{-1}，此紅位移的結果顯示TOPO以化學鍵結修飾於二氧化鈦上。由X光光電子能譜儀分析顯示，樣品表面的Ti-O/(Ti + P)比例大約 1.3~1.8，略小於二氧化鈦的理論值 2，因此樣品表面有缺陷形成。並且，從元素分析結果得到約有 45-70%的TOPO會在合成的過程中遺失。有機修飾中孔洞二氧化鈦降解環境荷爾蒙-酚甲烷 (Bisphenol-A, BPA) 的光催化能力高於純TiO_2。吸附結果顯示TOPO修飾的孔洞結構藉由疏水性物質間非特定性吸附與毛細作用力對BPA展現極高的吸附能力，因此除高比表面積外，孔洞結構與表面有機修飾物協同性的增進光催化活性。

Abstract

In this study, an organically modified mesoporous TiO_2 is prepared using a non-hydrolytic sol-gel method when trioctylphosphine oxide (TOPO) and 1,3,5-trimethylbenzene (TMB) are used as the template and auxiliary swelling agent, respectively. The specific surface areas of the samples ranged 2-103 m^2/g and increased with decreasing the TOPO concentrations. The critical TOPO/Ti ratio for microporous structure was 0.1. Addition of TMB led micro- and continuous porous samples exhibiting Type Ⅳ isotherm. In addition, remarkable increases in specific surface areas, pore volumes and pore sizes were obtained. This finding indicates that TMB assists the formation of TOPO micelles and expands the size of the micelles to form mesoporous TiO_2. The optimal TMB/TOPO/Ti ratio for the mesoporous TiO_2 was 0.12/0.1/1, at which the TiO_2 exhibited the largest surface area of 236 m^2/g and an average mesopore size of 3.6 nm. Highly anatase structures with a mean crystallite size of 4.4 nm were obtained. The mesoporous TiO_2 clearly shows C-H and P-O-Ti stretching absorptions at 2760-3150 and 1100 cm^{-1}, respectively, in the FTIR spectra. Moreover, the red shift of the P=O peak from 1150 to 1100 cm^{-1} indicates that the TOPO is chemically bound to the surface through the formation of P-O-Ti bonds. Surface Ti-O/(Ti + P) ratios ranged 1.3-1.8, which were smaller than the theoretical ratio of 2 of TiO_2. It suggested that many defects are introduced into the surface lattice. The mesoporous TiO_2 shows higher photocatalytic activity than pure TiO_2 for degradation of bisphenol-A (BPA). The TOPO-modified mesoporous TiO_2 samples not only contained large surface areas but also surface hydrophobic property and proper porous structures that exhibit extraordinarily high affinity for BPA, thus synergistically enhancing the photoactivity.

謝誌

三年的研究歷程終於告一段落，承蒙指導教授 張淑閔老師辛勤的指導，給了我這三年的辛苦磨練與訓練，培養我做實驗的態度及精神。感謝口試委員 董瑞安教授、楊家銘教授和徐雍鎣教授，在口試時給予的寶貴指正及建議，以及對於論文撰寫和修改提供許多建議，使得本論文更臻完整。

特別感謝清大醫環董老師實驗室的學長姐 Michelle、Judy、Barry 及同學 Grace 總是無私得出借任何我需要的儀器、耗材及藥品，以及提供許多寶貴意見。感謝實驗室的學長姐 Evelyn、Brad、Claire、Wes，在實驗上的指導，學弟妹 Adam、Karen、Ian、Ashley、Jiphi、Jerome，在苦悶的實驗當中總是帶來無窮的歡樂，另外從美國飛來的候鳥 Charles，那陣子天天陪我熬夜寫 proposal，吃關東煮，耍寶，度過好幾個風強雨大的颱風夜。當然不能忘記一路陪我到畢業的陳姿姿，總是能夠互相扶持彼此，在我低潮時後給予我鼓勵，在我遇到瓶頸時幫我想辦法解決，這三年的研究中有妳真好。同窗好友狗狗、金門、馬路、安安、百百，讓我的碩班生涯不無聊。感謝最正的助理靖宜，在我生活有困難的時候適時的伸出援手，也扮演著心靈導師讓我有個抒發管道，感激在心頭。另外感謝文彬學長和 susu 學妹，在最後階段讓我無條件的使用 HPLC，並教導我儀器分析的知識。感謝材料系學長達哥，認識你是我這輩子修來的福氣，謝謝你給予我許多材料合成鑑定上的專業知識，當然還有 TEM 的支援及指導。此外，感謝交大貴儀歐哥，清大貴儀羅先生和張小姐，讓我的實驗數據得以順利完成。感謝，環工排球隊大王、家馨、恰恰、阿嚕、信元、珖儀、展帆、京澄和燒餅，能跟你們一起打球是一件很快樂的事情，謝謝你們陪我度過苦悶的碩三生涯；其中大王、家馨謝謝妳們常常陪我聊天打屁，替我舒壓。最後特別感謝沈佩、Ginny、ug、阿信和矮人這群麻吉們，妳們總是在背後給我最大的支持，在我無助的時候提供一個避風港，不時的給我打氣讓我可以走到今天。

當然由衷地感謝我的家人，給予無虞的精神支持與無匱乏的經濟。感謝我的母親無盡的包容我，讓我這碩班期間沒有後顧之憂的專心在研究上，雖然您一直不懂我為什麼這麼忙碌及我在做什麼研究，但也從不過問我，不給我過多的壓力；謝謝老哥，我念書這段時間家裡都靠你支撐了，辛苦你了。

僅以本文獻給所有曾經關心過我與幫助過我的家人朋友們!

佳璇　謹誌

中華民國九十九年七月

Content Index

中文摘要 I

Abstract II

謝誌 III

Figure Index VII

Table Index IX

Chapter 1. Introduction 1

1-1. Motivation 1

1-2. Objectives 2

Chapter 2. Background and theory 4

2-1. Photocatalysis 4

2-1-1. Principle of photocatalysis 4

2-1-2. TiO_2 photocatalysis 6

2-2. Mesoporous materials 8

2-2-1. Synthesis and templates 9

2-2-2. Mesoporous TiO_2 11

2-2-3. The photocatalytic activity of mesoporous TiO_2 14

2-3. Surface modification 16

2-3-1. Metal deposition 16

2-3-2. Transition metal modification 17

2-3-3. Organic modification 17

2-4. Non-hydrolytic sol-gel process 18

2-5. Endocrine disrupted chemicals 20

Chapter 3. Experimental materials and methods 24

3-1. Chemicals 24

3-2. Preparation of TOPO modified mesoporous TiO_2 via NHSG process 27
3-3. Characterization 31
3-3-1. High Resolution Transmission Electron Microscopy (HRTEM) 31
3-3-2. Nitrogen adsorption and desorption isothermal 31
3-3-3. X-ray powder diffractmeter (XRPD) 31
3-3-4. UV-vis Spectrometer 32
3-3-5. Fourier Transform Infrared Spectrometer (FTIR) 32
3-3-6. Zeta Potential 33
3-3-7. Thermo Gravimetric Analysis / Differential Scanning Calorimetry (TGA/DSC) 33
3-3-8. X-ray photoelectron Spectroscopy (XPS) 33
3-4. Adsorption behavior 34
3-5. Photodegradation of BPA 35
Chapter 4. Results and Discussion 36
4-1. The pore structure and morphology 36
4-2. Crystalline structure and optical property 44
4-3. Surface property 48
4-3-1. Surface functional groups 48
4-3-2. Surface chemical composition 50
4-4. Adsorption isotherm 56
4-5. Photocatalytic activity 60
Chapter 5. Conclusions 65
References 66
Appendix A. Zeta potential of TOPO-TiO_2 and Pure TiO_2 74
Appendix B. JCPDS database of TiO_2 (anatase) 76
Appendix C. EDX patterns of TP and TP 2-B samples 78

Appendix D. TGA/DSC curve of TP and TP 2-B samples 82

Appendix E. Calibration curve of BPA solution..... 87

Appendix F. Photodegradation of various BPA concentrations 89

Figure Index

Figure 2-1 Reaction diagram of photocatalysis at a semiconductor by illumination. 5

Figure 2-2 Schematic photoexcitation in a solid followed by excitation events.[34] 5

Figure 2-3 Energies for various semiconductors in aqueous electrolytes at pH = 1.[34] 7

Figure 2-4 The structures of (a) brookite, (b) anatase, (c) rutile.[37] 8

Figure 2-5 Structure of rutile and anatase TiO_2.[34] 8

Figure 2-6 Liquid-crystal templating mechanism showing two possible pathways for the formation of MCM-41.[43] 10

Figure 2-7 Illustrations of mesoporous M41S materials: (a) MCM-41, (b) MCM-48, and (c) MCM-50.[44,45] 10

Figure 2-8 The *Pm3n* cubic phase, in which the polyhedral represent micelles.[49] 11

Figure 2-9 Conventional sol-gel process.[76] 19

Figure 2-10 Proposed reaction pathways of BPA degradation.[101] 23

Figure 3-1 Flow chart of experimental design in this study. 26

Figure 3-2 A flow diagram for the preparation of TOPO modified mesoporous TiO_2 via a NHSG method. 29

Figure 3-3 A flow diagram for preparation of TOPO modified mesoporous TiO_2 in the presence of TMB. 30

Figure 3-4 Photolysis of BPA under illumination of 305 nm UV light. 35

Figure 4-1 N_2 adsorption and desorption isotherm and BJH pore size distribution of TP 1and TP 2. 38

Figure 4-2 (a) N_2 adsorption/desorption isotherm and (b) the pore size distribution of TP 1-B0.3, TP 1-B0.5, TP 1-B0.8, TP 1-B1.0 and TP 1-B1.2. 40

Figure 4-3 (a) N_2 adsorption/desorption isotherm and (b) the pore size distribution of TP 2-B0.3, TP 2-B0.5, TP 2-B0.8, TP 2-B1.0 and TP 2-B1.2. 41

Figure 4-4 (a) N_2 adsorption/desorption isotherm and (b) the pore size distribution of TP 3-B0.3, TP 3-B0.5, TP 3-B0.8, TP 3-B1.0 and TP 3-B1.2. 42

Figure 4-5 TEM and HRTEM images of (a and b) TiO_2, (c and d) TP 1, (e and f) TP 2 and (g and h) TP 2-B0.3. 43

Figure 4-6 XRD patterns of (a) TOPO-TiO_2 and pure TiO_2, (b) the TOPO-TiO_2 adding TMB. 45

Figure 4-7 UV-vis spectra of TOPO-TiO_2 and pure TiO_2..... 46

Figure 4-8 The FTIR spectra of TOPO-TiO_2 and pure TiO_2. 49

Figure 4-9 The wide-ranged XP spectra of TOPO-TiO_2..... 50

Figure 4-10 The evolution of O (1s) XP spectra of TOPO-TiO_2. 52

Figure 4-11 The TGA/DSC curve of TP 2. 55

Figure 4-12 Adsorption of BPA in the suspensions of (a) TP samples and pure TiO_2, (b) the TP 2-B samples. 58

Figure 4-13 Adsorption equilibrium of 10 mg/L BPA in the suspensions of (a) TP samples and pure TiO_2, (b) the TP 2-B samples. 59

Figure 4-14 The photodegradation of 10 mg/L BPA by (a) TP samples and pure TiO_2, (b) TP 2-B samples. 62

Figure 4-15 A plot of the linear fit of 1/r versus 1/C of (a) TP 2 and (b) P25. 63

Figure 5-1 The TOPO concentration has influenced of pore structure. 65

Table Index

Table 2-1 Pore-size regimes and representative porous inorganic materials.[42] 9

Table 2-2 Preparation of mesoporous TiO_2..... 13

Table 2-3 Mesoporous TiO_2 affects photoactivtive efficiency. 15

Table 2-4 Characteristics of BPA[102] 22

Table 3-1 The structures of chemicals used in this study. 25

Table 3-2 The preparation conditions and corresponding sample names..... 28

Table 4-1 The specific surface area, pore size and pore volumes of TOPO-TiO_2 and TiO_2. .. 38

Table 4-2 The specific surface area, pore size and pore volumes of TOPO-TiO_2 with TMB.. 39

Table 4-3 Crystalline size of TOPO-TiO_2 and pure TiO_2. 45

Table 4-4 Band gap energy of TOPO-TiO_2 and pure TiO_2. 47

Table 4-5 Surface chemical composition of TOPO-TiO_2. 52

Table 4-6 Elemental analysis of TOPO-TiO_2 and pure TiO_2 using EDX. 53

Table 4-7 The weight loss of TP and TP-B samples. 55

Table 4-8 The rate constants (k_r) and adsorption coefficients (K_a) of BPA in the TP 2 and P25 suspensions. 64

Chapter 1. Introduction

1-1. Motivation

Titanium dioxide (TiO_2) is a kind of inorganic semiconductors. Moreover, TiO_2 is the mostly used photocatalyst for photocatalytic decomposition of organic pollutants because it has the ideal band gap structure (3.2 eV), chemical and thermal stability, high decomposition efficiency, low operating temperature and low cost[1-3]. The improvement of the photocatalytic performance of TiO_2 through structural and compositional modifications has attracted much attention not only because of scientific interests but also application importance. Surface modification of TiO_2 with inorganic or organic material has been demonstrated to effectively reduce charge recombination, to improve contact opportunity between the catalysts and reactants and to promote interfacial charge transfer[4-8]. In addition, porous materials with high surface areas provide high quantities of active sites, thus greatly increasing their photocatalytic efficiency[9-15].

Templating method is currently employed to prepare porous materials. Mobil Oil Company has used quaternary ammonium surfactants as a template to synthesize the ordered mesoporous M41S material in 1992[16]. Up to dates, various methods including sol-gel[17], hydrothermal[18], and microwave-assisted method[3] have been developed to prepare mesoporous TiO_2. Among these methods, sol-gel is the simple and feasible manner which is easy to be developed in laboratories. Surfactants including cetrimonium bromide (CTAB)[19-21], triblock poly(ethylene oxide)-poly(propylene oxide)-poly(ethylene oxide) (P123)[9,13,14,18,22-24] and anime surfactants (doddecylamin[25,26], tetracdecylamin[3]) have been used as the templates for mesoporous TiO_2. Prompt hydrolysis and condensation at room temperature generally result in amorphous TiO_2. To crystallize the TiO_2 and remove the organic template, the samples need to be calcined above 500°C. The

resulting TiO_2 has the pore size ranging 5.7-14 nm and the high specific surface area of 395-467 m^2/g[3,14,18,24,27-30].

Surface organically modified TiO_2 were generally prepared by post immersion of TiO_2 in the modifier solutions. Organic modifiers including ascorbic acid[31] and salicylic acid[5] , have been demonstrated to be adsorbed onto TiO_2 with complex form. They could improve the photocatalytic efficiency, but also desorbed easily during the reaction process. Yu et al.[32] used trifluoroacetic acid (TFA) to modify mesoporous TiO_2 thin films by dipping TiO_2-coated glass slide into TFA solution and post heating at 250°C for chemisorption. But this method is time-consuming and requires complicated synthesis. Chang et al.[8] used a non-hydrolytic sol-gel method to prepare trioctylphosphine oxide (TOPO) modified TiO_2 nanocrystals. In addition, they have demonstrated that the TOPO-modified TiO_2 exhibited 1.4- and 3.2-times higher photocatalytic activity than P25 for the degradation of phenol and bisphenol A, respectively. However, the modified TiO_2 lacked industrial potential because of its low specific surface areas (~ 7.0 m^2/g) and low production yield.

1-2. Objectives

This study aims to develop a facile non-hydrolytic sol-gel method for preparation of surface modified mesoporous TiO_2 in a single process. Trioctylphosphine oxide (TOPO) was used as the template as well as the modifier. The influence of TOPO concentration (TOPO/Ti = 0.05-0.25) and the addition of 1,3,5-trimethylbanzene (TMB) on the mechanism of porous material formation, pore structures and sizes were investigated. The micro-structural and compositional properties of the surface modified mesoporous TiO_2 were characterized by high resolution transmission electron microscopy (HRTEM), nitrogen adsorption and desorption model, X-ray powder diffractometer (XRPD), UV-vis

spectrophotometer, Fourier transform infrared spectrometer (FTIR), thermo-gravimetric analysis/differential scanning calorimetry (TGA/DSC) and X-ray photoelectron spectroscopy (XPS). Furthermore, adsorption and decomposition of BPA by the surface modified mesoporous TiO_2 and pure TiO_2 were examined and compared to elucidate the contribution of the surface modifiers on the improved photocatalyic activity.

Chapter 2. Background and theory

2-1. Photocatalysis

2-1-1. Principle of photocatalysis

The treatment techniques for environmental pollution with semiconductor photocatalysis have been developed rapidly in recent years. Photocatalysis involves semiconductors which utilize photons to produce electron-hole pairs and then induce oxidation or reduction of adsorbed contaminants through interfacial charge transfer. In general, semiconductors such as TiO_2, ZnO_2, SnO_2 and WO_3 have been used to degrade organic compounds under UV or visible light irradiation[33]. Usually a semiconductor has different band gap energy that can influence the optical and physicochemical properties. A large band gap range has a high reactivity, but also needs more excitation energy. However, a small band gap range can easily recombine the electron-hole pairs to reduce photocatalyic activity.

At room temperature, an electron is bound by the nucleus; the most electrons stay in the valence band. When the energy of a photon is higher than the band gap of a semiconductor, the semiconductor will separate the electron and hole pairs (Figure 2-1). But the electron and hole pairs still have an opportunity for recombination (Figure 2-2). Therefore, the excited electrons reach the conduction band, those reduce surface absorbed oxygen to form superoxide radicals ($O_2^{\cdot -}$). Furthermore, the holes may react with OH^- and H_2O absorbed at the surface to convert to hydroxyl radicals (·OH). The redox reaction that occurred at the surface of the semiconductor can transform organic compounds into oxidized or reduced products.

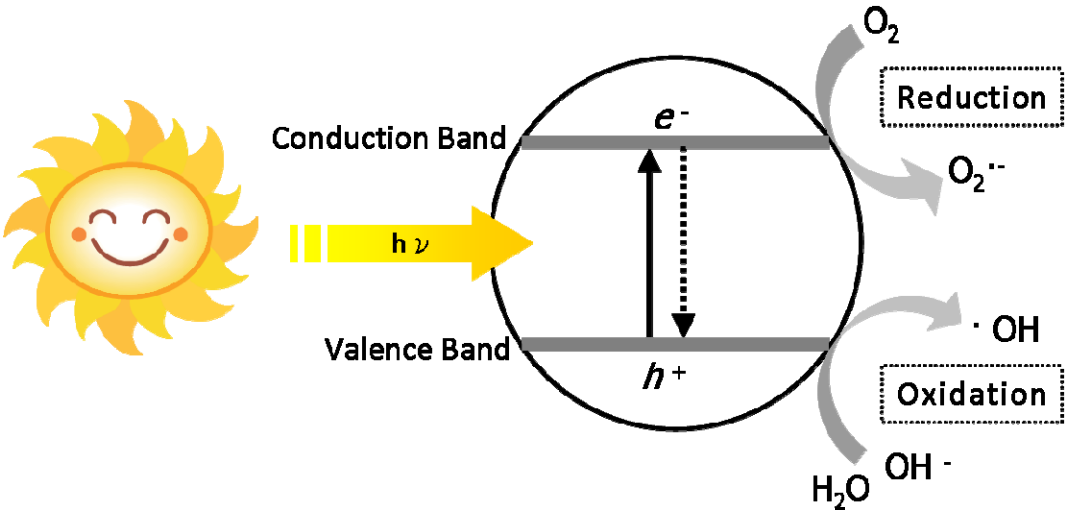

Figure 2-1 Reaction diagram of photocatalysis at a semiconductor by illumination.

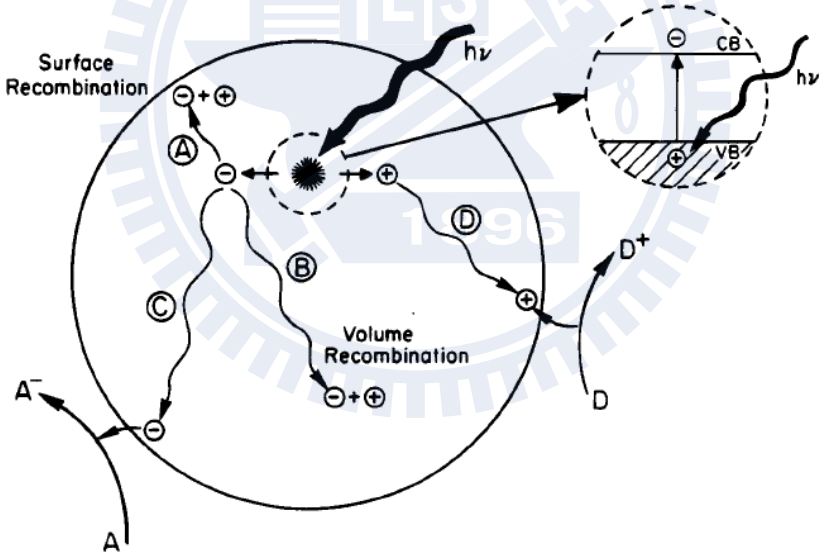

Figure 2-2 Schematic photoexcitation in a solid followed by excitation events.[34]

In general, photocatalysis can be observed in continues steps of oxidation-reduction.

Illumination

$$TiO_2 + h\nu \rightarrow e^+ + h^- \quad (2\text{-}1)$$

Oxygen

$$2H_2O + 4h^+ \rightarrow O_2{}^+ 4H^+ \quad (2\text{-}2)$$

Peroxide

$$O_2 + 2H^+ + 2e^- \rightarrow H_2O_2 \quad (2\text{-}3)$$

Superoxide

$$O_2 + e^- \rightarrow O_2^- \quad (2\text{-}4)$$

Radical

$$H_2O + h^+ \rightarrow OH\bullet + H^+ \quad (2\text{-}5)$$

2-1-2. TiO_2 photocatalysis

Since the discovery of photochemical water splitting using TiO_2 electrode by Fujishima and Honda[35], a multitude of studies have been focused on chemical systems that implicate the absorption of photoirradiation by chemical agents, followed by reactions leading to the splitting of water into H_2 and O_2[36]. TiO_2 has been commonly used because their physical and chemical properties are very stable, resist acidity, have high photocatalytic activity, are cheaper, easily prepared, non-toxic, and oxidizes or reduces the majority of organic pollutants[1-3]. The band gap of anatase TiO_2 is about 3.2 eV, so their critical wavelength is 380 nm, in ultraviolet range.

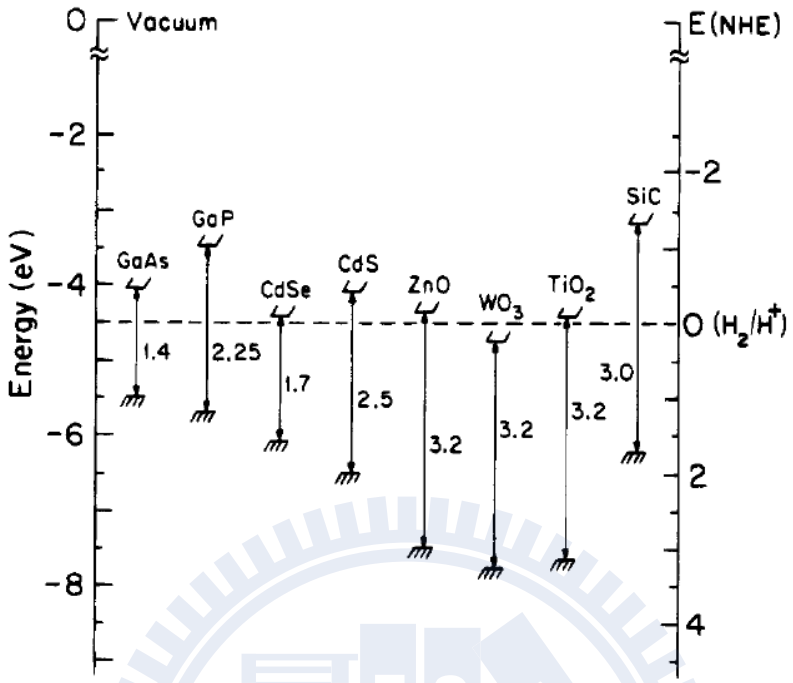

Figure 2-3 Energies for various semiconductors in aqueous electrolytes at pH = 1.[34]

TiO_2 is the n-type semiconductor. The basic structure is a titanium atom in the center, surrounded by six oxygen atoms to form an octahedral structure with 6 coordinations. A titanium atom has 22 electronics with 3d orbit electron and four oxygen atoms to form a covalent bond. TiO_2 has three types of crystal phases: anatase, rutile and brookite (Figure 2-4, 2-5). Anatase and rutile phase are usually used in photocatalytic reactions, where band gaps are 3.2 eV and 3.0 eV, respectively. Moreover, anatase is the metastable structure, which will cover to rutile phase at about 400-500°C[34].

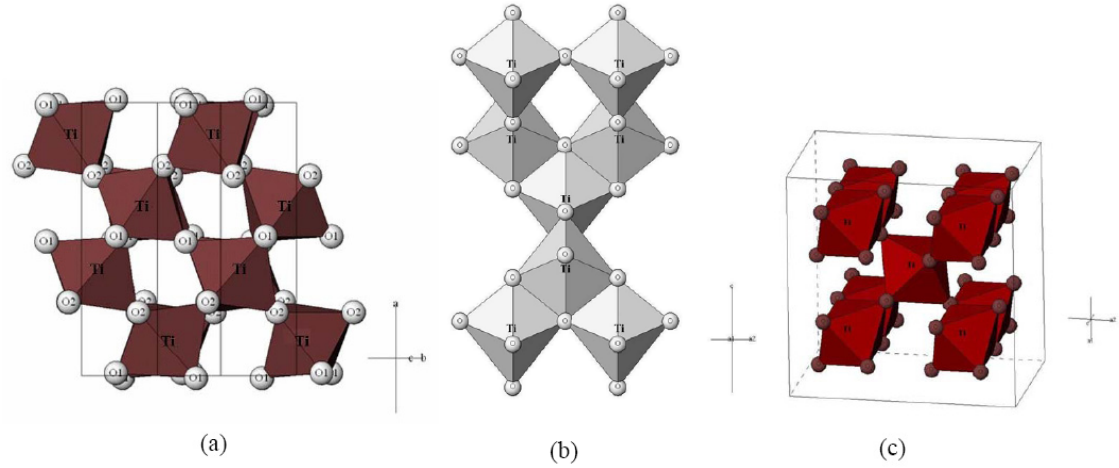

Figure 2-4 The structures of (a) brookite, (b) anatase, (c) rutile.[37]

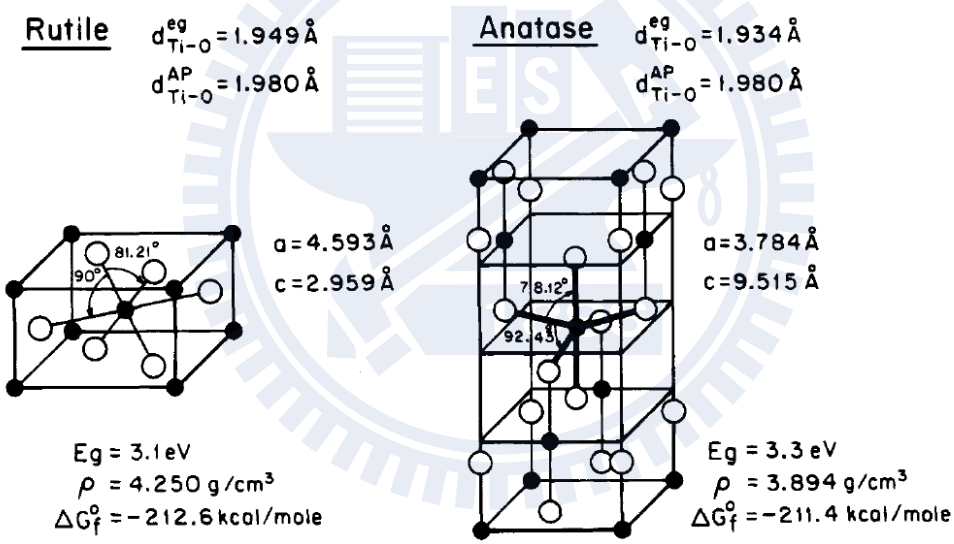

Figure 2-5 Structure of rutile and anatase TiO_2.[34]

2-2. Mesoporous materials

According to IUPAC definition, pore sizes can be divided into: microporous (< 2 nm), mesoporous (2-50 nm) and macroporous (> 50 nm). Porous materials were interesting and focused on designing materials that have extremely high surface areas and tunable pore

sizes. Recently, porous materials have been widely used in adsorption, catalysts, sensors and other areas[38-41].

Table 2-1 Pore-size regimes and representative porous inorganic materials.[42]

Pore-size regimes	Definition	Examples	Actual size range
macroporous	> 500 Å	glasses	> 500 Å
mesoporous	20-500 Å	aerogels	> 100 Å
		pillared layered clays	10 Å, 100 Å[(a)]
		M41S	16-100 Å
microporous	< 20 Å	zeolites, zeotypes	< 14.2 Å
		activated carbon	6 Å

(a)Bimodal pore-size distribution

2-2-1. Synthesis and templates

In 1992, Mobil Oil Company used quaternary ammonium surfactants as a template with negatively charged aluminate silicate to synthesize order mesoporous M41S material first[16]. The scheme is shown in Figure 2-6. The pore sizes of M41S were about 20-30 Å. The series of M41S can be divided into three structures based on the method of each molecular array. (1) MCM-41 has a hexagonal array of noninterconnecting cylindrical pores (Figure 2-7a), (2) the structure of cubic space group *Ia3d* was MCM-48 (Figure 2-7b); and (3) the structure of MCM-50 is lamellar[16,43] (Figure 2-7c). These porous materials have some advantages such as high specific surface area (BET surface area of about 1000 m^2/g), thermal stability, adjustable pores, order structures, and uniform pore size.

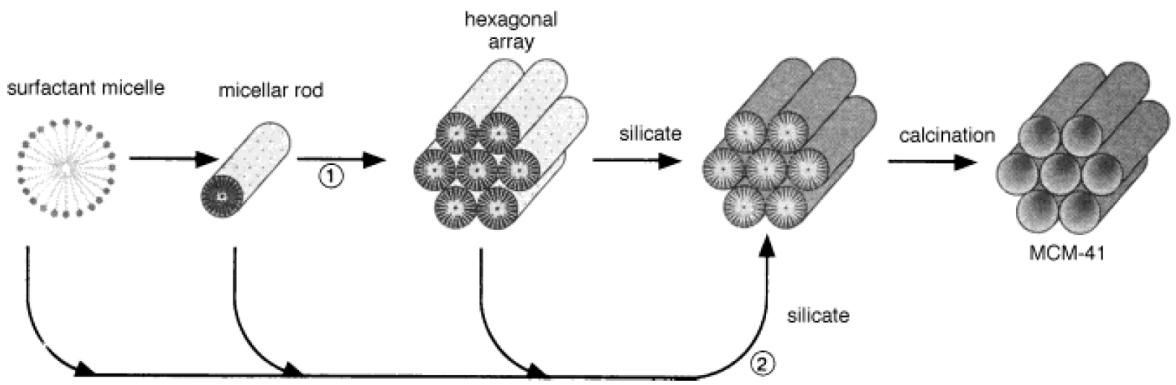

Figure 2-6 Liquid-crystal templating mechanism showing two possible pathways for the formation of MCM-41.[43]

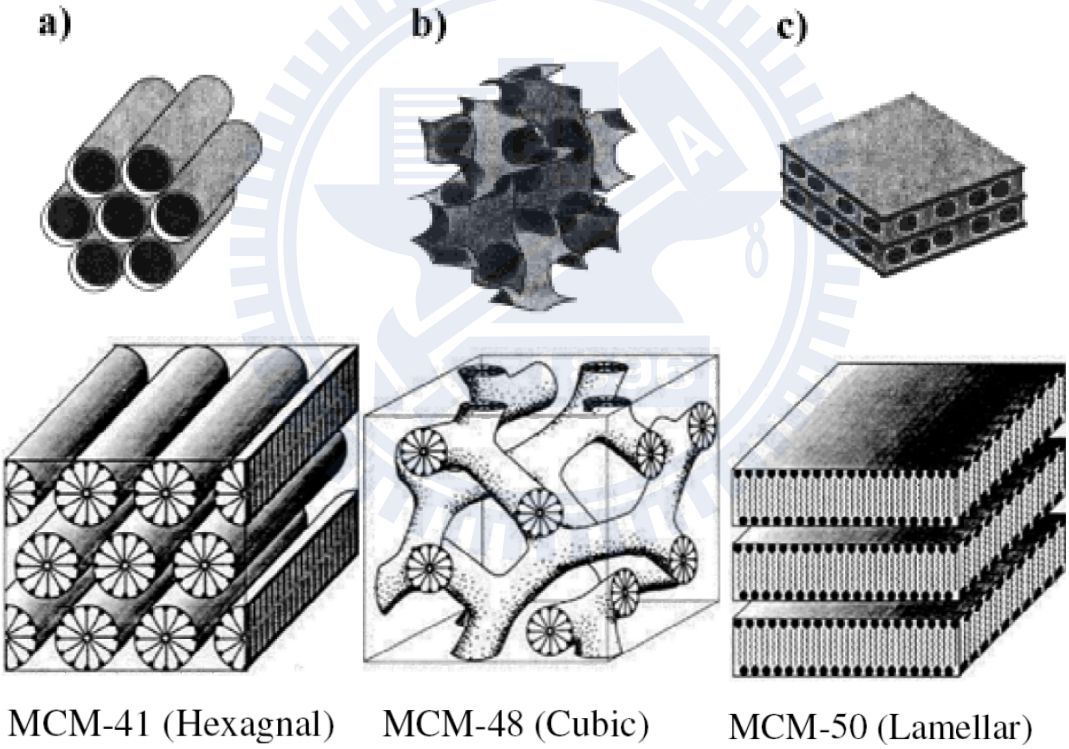

Figure 2-7 Illustrations of mesoporous M41S materials: (a) MCM-41, (b) MCM-48, and (c) MCM-50.[44,45]

Subsequently, the SBA (Santa Barbara) amorphous materials were synthesized in 1994. Syntheses of SBA structures used both organic and inorganic salts to form electrostatic

interaction forces. Furthermore, the order structure of SBA-1 was under strong acidic conditions. Cetyltriethylammonium bromide (CTEABr) and tetraethyl orthosilicate (TEOS) were used as a surfactant and silicon source for the successful synthesis of a space group *Pm3n* cubic structure[46] (Figure 2-8). The tunable pore size property of the SBA materials was better than that of MCM materials, and SBA materials have higher hydrothermal stability as well. As the demand for application of scientific interest, increases ideas about using surfactants as templates to prepare porous inorganic metal oxides were discussed, using materials such as Al_2O_3, SiO_2[47], SiC, ZrO_2, and TiO_2[48], etc.

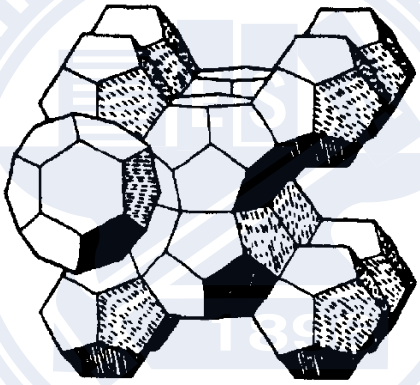

Figure 2-8 The *Pm3n* cubic phase, in which the polyhedral represent micelles.[49]

2-2-2. Mesoporous TiO_2

It has been demonstrated that TiO_2 has high surface area, which can enhance the photocatalytic activity by physical methods. Template method has been utilized mostly for the preparation of porous photocatalysts mostly. In 1995, mesoporous TiO_2 were synthesized using phosphate as a surfactant and titanium alkoxide utilized sol-gel method[48]. At present, preparation of mesoporous TiO_2 have been developed in different ways, including the sol-gel method[48], hydrothermal method[18], microwave-assisted method[3],

sonochemistry method[27], block copolymers[50], ionic liquid containing cellulose[51], phosphotungstic acid assisted sol-gel method[17], and deposition method[52]. In general, TiO_2 prepared by the use of titanium chloride or alkoxide as the precursor, processed hydrolysis-condensation and recrystallization, resulted in a pore size range of 5.7-14 nm and a highly specific surface area of 395-467 m^2/g[27]. Many researches focus on discussing the influence of the different synthetic parameters on the materials in the synthesized process of mesoporous TiO_2. Callreja et al.[14] used the nonionic co-polymer, triblock poly(ethylene oxide)-poly(propylene oxide)-poly(ethylene oxide) ($PEO_{20}PPO_{70}PEO_{20}$, P123) as the template by sol-gel synthesis. They discussed water/Ti source ratio, and the effect of solvent and surfactants concentration. The results found that the water/titanium ratio was greater than 10, and the surfactant make it difficult to form micelle to lead to the pore structure. Moreover, this study showed that using ethanol as a solvent can reduce the hydrolytic condensation to enhance the surface area. Serrano et al.[53] discussed the effect of using different acidic reagents to synthesize TiO_2. Results show that sulfate and phosphate have larger interaction with Ti ion, leading to the collapsing of the pore structure. Furthermore, nitric acid and hydrochloric acid can stabilize the pore structure to enhance photocatalytic activity. Wang et al.[54] utilized the titanium phosphate (TiPO) and CTAB to synthesize porous materials by hydrothermal method and observed under temperature can influence the structure. Results showed that when the synthesis occurred at room temperature, the outcome was a hexagonal structure, and a lamellar structure formed at $100^{o}C$. The preparations of mesoporous TiO_2 are summarized in Table 2-2.

Table 2-2 Preparation of mesoporous TiO_2.

Method	Precursor	Template	Surface area (m^2/g)	Pore diameter (nm)	Ref.
Sol-gel	Titanium isopropoxide	TX-100	187-487	3.8-4.6	[30]
	Titanium isopropoxide	P123	137-582	2.0-4.2	[14]
Ligand-assisted templating	Titanium isopropoxide	Dodecyl phosphate	90-712	-	[55]
Template-free sol-gel	Titanium *n*-propoxide	Formamide	150	5	[56]
Surfactant-templated sol-gel	Titanium isopropoxide	P123	200-250	4.9-6.4	[53]
Nonhydrolytic evaporation-induced self-assembly	Titanium chloride and Titanium butoxide	P123	80-135	3.5-6.1	[24]
Hydrothermal treatment	Titanium tetrapropoxide	$C_{16}(EO)_{10}$	101-215	9.1-9.9	[29]
	Tetrabutyl titanate	CTAB	117-205	2.2-2.8	[33]
	Tetrabutyl titanate	-	100-400	3-4	[28]
	Titanium isopropoxide	-	49-126	8-10	[57]

2-2-3. The photocatalytic activity of mesoporous TiO_2

Mesoporous TiO_2 has a larger surface area because of its confined porous structure and high surface to volume ration, and enhanced high photocatalytic activity, because of improved access to the active sites of TiO_2. Kim et al.[22] used titanium isopropoxide and diblock copolymer surfactants to synthesis mesoporous TiO_2. They discussed the photocatalytic activity was increased with decrease of crystallite size, larger surface area, and smaller pore-size distribution. In comparison with commercial TiO_2, Ishihara ST-01, the mesoporous TiO_2 materials exhibit better photocatalytic activities in the decomposition of methylene blue. Yu et al.[12] prepared bimodal nanocrystalline mesoporous anatase TiO_2 powder photocatalyst using tetrabutylorthotitanate as precursor via a hydrothermal method. The results show that optimal hydrothermal condition (180°C for 10 h) was determined. The photocatalytic activity of the TiO_2 powders prepared under an optimal hydrothermal condition exceeds that of P25 by a factor of more than three times. Peng et al.[19] apply a hydrothermal method to synthesize mesoporous anatase TiO_2 nanoparticles by using CTAB as a surfactant-directing agent. This literature indicated the large surface area, small crystalline size, and well-crystallized anatase mesostructure can explain the high photocatalytic activity of mesoporous TiO_2 nanoparticles calcined at 400°C. Therefore, the obtained mesoporous TiO_2 nanopowders exhibit higher photocatalytic activity than the commercial nonporous photocatalyst P25. Many researches have been discussed the mesoporous TiO_2 enhanced photocatalytic activity are summarize in Table 2-3.

Table 2-3 Mesoporous TiO_2 affects photoactivtive efficiency.

Precursor	Target compound	The photoactivtive efficiency	Ref
Titanium isopropoxide	Methylene blue	The MT-18 was higher than ST-01 by 5.8 times.	[22]
		The mesoporous TiO_2 with high surface areas, which exhibit photocatalytic activity superior to P25.	[3]
	Mordant Yellow	All mesoporous samples show higher photocatalytic activity than P25.	[58]
	Dibenzothiophene (DBT)	The 98% removal efficiency of 300 mg/L DBT is within 2 min reaction.	[59]
Titanium butoxide	2,4,6-tribromophenol (TBP)	The degradation efficiencies increased from 89.48% to 95.87% with PEG molecule was increased from 200 to 20000.	[10]
	VOC_s	The photocatalytic activity was about 3 times higher than P25.	[12]
	Phenol	The sample calcined at 800°C was removal 90% phenol than P25 (20%) within 120min.	[20]
$Ti(SO_4)_2$	Rhodamine B (RhB)	The optimum reactivity is observed at the sample calcined at 400°C, which causes 97% RhB to be degraded after 2h irradiation.	[19]

2-3. Surface modification

The limiting factors of the reactive dynamics of photocatalysts include large surface area, in addition to the pollutants absorbed capacity on the photocatalyst surface and the surface charge transfer. Consequently, the research and technology focused on photocatalyst surface modification has received great attention in recent years. The material for modification can be divided into metals, transition metal and organic compounds.

2-3-1. Metal deposition

Adding metals (such as Pt, Pd, Au, Ag) in photocatalysts is for the purpose of separating electrons and hole pairs, inhibiting electron and hole recombination[7,60-64]. After the photocatalyst is excited, electrons are produced which effectively improving can transfer to metal particles quickly because of electric potential difference, leading to electron and hole separation and the increase of the efficiency of photodegradation. Adding rare metals to photocatalysis will change the mechanism of the photocatalysis because of a transformation of the surface property. The results would enhance the reaction rate of photocatalysis, stabilize the yield of the specific product, and alter the final product. Li et al.[61] prepared mesoporous titania photocatalysts by embedding gold nanoparticles. This result shows that Au nanoparticles embedded within the TiO_2 pore tunnel may also serve as an electron conductor, which facilitates photoelectron transfer to pore surface and further reduces the probability of charge recombination. In addition, enhanced light absorption and improved quantum efficiency were the main factors leading to improved photocatalytic activity.

2-3-2. Transition metal modification

Transition metals, such as V, Mn, Fe, Co, Ni and Cu have been extensively used as dopants to enhance the photocatalytic activity of TiO_2[65-67]. These doping ions in the TiO_2 structure has caused a significant absorption shift to the visible region compared to pure TiO_2[68]. Adding transition metals in the photocatalyst can promote the efficiency of electron capture and thus restrain electron and hole unification. In addition, the transition metals will be forming a new independent band between with the conduction band and valence band. Therefore, it can use lower energy to excite electrons, which expand the light range. Huo et al.[69] prepared La-doped TiO_2 photocatalysts via ultrasound-assisted sol-gel method, followed by supercritical treatment. This literature indicated the La-modification could increase the oxygen vacancies and surface defects in the TiO_2 photocatalysts which might capture photoelectrons and thus, inhibit the recombination between photoelectrons and holes, resulting in enhanced quantum efficiency.

2-3-3. Organic modification

In recent years, bonding of TiO_2 with organic moieties attracted large attention. The surface electronic structure as well as hydrophicility of TiO_2 change with organic modifiers, and consequently enhance the photocatalytic activity by three ways: (1) by inhibiting charge recombination[31,32,70], (2) by exploring the wavelength response range[71,72] and (3) by changing the selectivity or yield of a particular product[31,73]. Organic modifiers are chemisorbed on the TiO_2 surface via chelation or formation of covalent bonds. Ou et al.[31] used an ascorbic acid as modifier for TiO_2 and found that the modified TiO_2 was more photoactive for oxidation of azo-dye than pure TiO_2 both under UV and solar irradiation. Chang et al.[8] used a non-hydrolytic sol-gel method to prepare trioctylphosphine oxide

(TOPO) modified TiO_2 and compared the photodegradation ability of the TOPO-capped TiO_2 with that of P25 in terms of degradation of different hydrophilic and hydrophobic of endocrine disrupting chemicals (EDCs). Relative to P25, the TOPO-capped TiO_2 showed 1.4 and 3.2 times higher activity for the degradation of phenol and bisphenol A, respectively. Chang and Chen[5] used microwave-assisted method to prepare salicylic acid modified TiO_2. The modified salicylic acid extends absorption wavelength of the TiO_2 to visible light (452 nm) and enhances surface charge transfer and the adsorption of reactants on the catalyst surface. Therefore the photocatalytic activity of the salicylic acid modified TiO_2 was higher than commercial photocatalysts (Degussa P25) by 1.6 times. Comparelli et al.[74] prepared oleic acid (OLEA)- and tri-n-octylphosphine oxide (TOPO)-capped anatase TiO_2 nanocrystal powders. They indicated that the organic-capped TiO_2 exhibited lower degradation rates than the P25. The organic capping prevents dye access to the catalyst and/or limit the local density of –OH groups. If it combines surface modification and high surface area of the porous structure, it can be expected that the photocatalytic efficiency will be enhanced. Angelome et al.[75] prepared the surface modified porous structure in two steps: synthesis of mesoporous materials, and then surface modification of the inner pore with organic compounds. However, the post adsorption was inefficient and many adsorbed modifier could detach from the surface.

2-4. Non-hydrolytic sol-gel process

As we know, the sol-gel method is a simple process for transition metal oxides (including titania) with nanoscale microstructures and provides for excellent chemical homogeneity. Sol-gel derived unique metastable structures occur at low reaction temperature. The conventional sol-gel routes are based on the hydroxylation and polycondensation of molecular precursors. Figure 2-9 expresses the conventional sol-gel

process. Hydrolysis and polymerization of the precursors occurs, usually involving which are usually inorganic metal salts or metal organic compounds such as metal alkoxides. Finally the condensation reaction is two molecules or moieties (functional groups) combining to form one single molecule, with the loss of a small molecule[76-78].

Hydrolysis

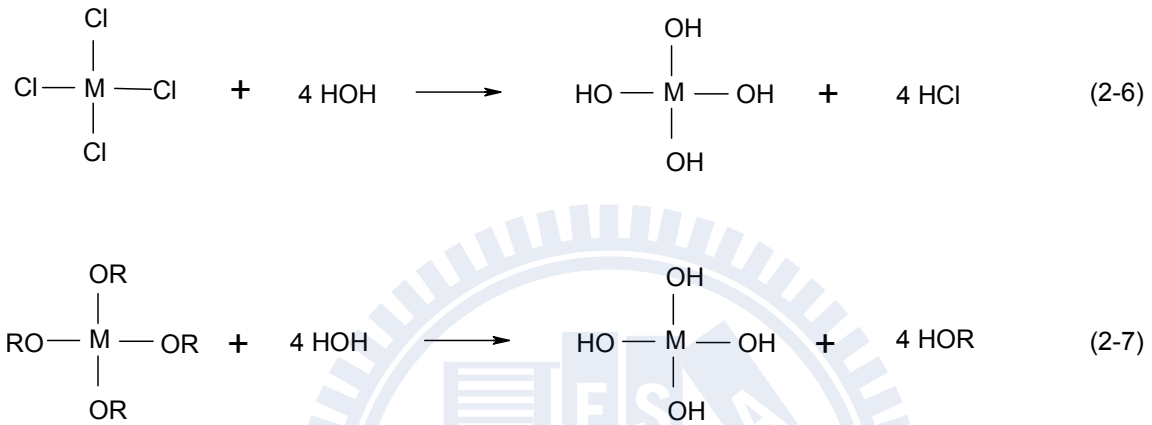

Condensation

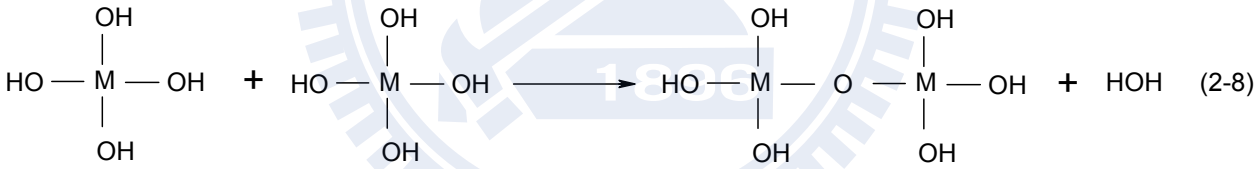

Gelatin

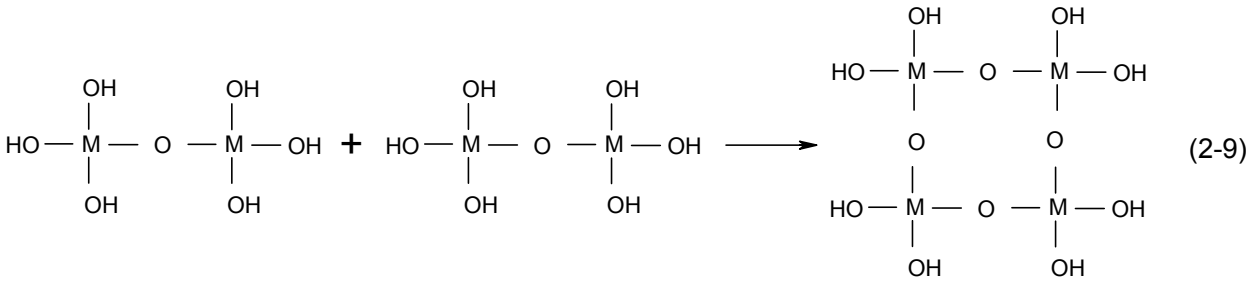

Figure 2-9 Conventional sol-gel process.[76]

The hydrolytic sol-gel process has been studied extensively over the last 2 decades as a facile route to transition metal oxides. It was only in the last 10 years that the corresponding non-hydrolytic sol-gel (NHSG) process has been recognized as a useful route to inorganic oxides. The NHSG route has been evaluated for the synthesis of silica, titania, alumina1 and mixed or binary oxides such as aluminosilicates and silica-titania systems. The NHSG process involves the reaction of a metal halide with an oxygen donor such as an alkoxide, ether, alcohol and so forth under nonaqueous conditions to form an inorganic oxide. Subsequently, when metal chlorides and metal alkoxides are mixed, ligand-exchange reactions occur, giving rise to a mixture of metal chloroalkoxides[79-82].

Condensation

$$MCl_n + M(OR)_n \rightarrow 2\ MO_{n/2} + nRCl \qquad (2\text{-}10)$$

Etherolysis or Alcoholysis

$$\equiv MCl + H\text{-}O\text{-}R \rightarrow \equiv MOH + RCl \qquad (2\text{-}11)$$

$$\equiv MCl + R\text{-}O\text{-}R \rightarrow \equiv MOR + RCl \qquad (2\text{-}12)$$

$$MCl_n + n/2\ R\text{-}O\text{-}R \rightarrow MO_{n/2} + nRCl \qquad (2\text{-}13)$$

Ligand Exchange

$$MCl_n + M'(OR)_n \leftrightarrow MCl_{n-x}(OR)_x + M'Cl_x(OR)_{n-x} \qquad (2\text{-}14)$$

2-5. Endocrine disrupted chemicals

Recently, scientists have found that some chemicals in the environment have high potential to interfere the endocrine system, which called “endocrine disrupters” or

“endocrine disrupting chemicals” (EDC_s). The Organization of Economic and Cooperate Development define EDC_s as “an exogenous substance or mixture that alters the function(s) of the endocrine systems and consequently causes adverse health effect in an intact organism, or its progeny or (sub) pollution”[83]. EDC_s are highly toxic and carcinogenic. They remain in the environment for a long time due to their stability and bioaccumulation. The effects associated with the presence of EDC_s in the environment are: (1) toxic to the reproductive system and development in mammals, fishes and birds, (2) feminization of male fishes, (3) changes in the immunologic system of marine mammals, (4) causing irreversible damage to the aquatic life[84]. Moreover, the EDC_s can lead some adverse effects in human health and the function of the endocrine system by binding to nuclear receptors[85]. The effects of EDC_s in human beings reported so far have been: (1) low sperm count, (2) increases in the incidences of breast cancer, (3) early puberty and (4) the endometriosis[83,84]. Therefore, EDC_s are a great concern because of their potential in altering the normal endocrine function and physiological status of organism.

Bisphenol-A (BPA) has been used for the production of epoxy resins, polycarbonates and polysulfones, and has been suspected as one of endocrine disruptors[86]. Recently, BPA was widely applied in various polycarbonate plastics, poly(vinylchloride) (PVC) and epoxy resins such as the inner coating of food cans, powder paints, plastic containers, dental fillings and baby bottles[87-89]. BPA is often contained in environmental water and now is attracting attention. Various methods have been developed to remove BPA from water, such as a biological method[90,91], chemical oxidation[92,93], electrochemical oxidation[94], Fenton[95], and a photocatalytic method[30,89,96-98]. One of the most promising methods is photocatalytic degradation due to its high mineralization efficiency, low toxigenicity, ideally producing carbon dioxide, water and inorganic mineral ions as end products. Wang et al.[99] carried out the photocatalysis in a horizontal circulating bed photocatalytic reactor

(HCBPR). An optimum condition for HCBPR operation was achieved as follows, initial BPA concentration at 10 mg/L, initial pH at 12.3, TiO_2 dosage at 1% and temperature at 24.3^{o}C, under which 95% TOC removal and nearly 97% BPA degradation were achieved after 6 h of UV radiation. Gao et al.[100] utilized Zr-doped TiO_2 to degradation of BPA under UV irradiation and indicated that the Zr-doped TiO_2 show enhanced efficiency in comparison with a pure anatase TiO_2. Furthermore, nearly complete removal of TOC can be achieved. Guo et al.[101] reported two different 3D mesoporous TiO_2 to degradation of BPA under UV irradiation and proposed the degradation mechanism of BPA. The mechanism involves reactions of hydroxyl radicals. In addition, photogenerated holes also can oxidize the organic molecule directly, while the electrons can react with the adsorbed molecular oxygen on the Ti(III)-surface to generate superoxide radical anion HOO•. In the TiO_2 photocatalysis toward aromatic compounds, initial hydroxylation of aromatic rings by hydroxyl radicals is believed to play a dominate role in a sequential ring cleavage. The reaction pathways of BPA degradation mechanism showed in Fig 2-10.

Table 2-4 Characteristics of BPA[102]

Structure of BPA	**Formula**	**MW**	**Water solubility (mg/L at 25°C)**	**Octanol-water partition coefficient (log K_{ow})**
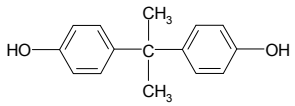	$C_{15}H_{16}O_2$	228.28	120 mg/L	3.32

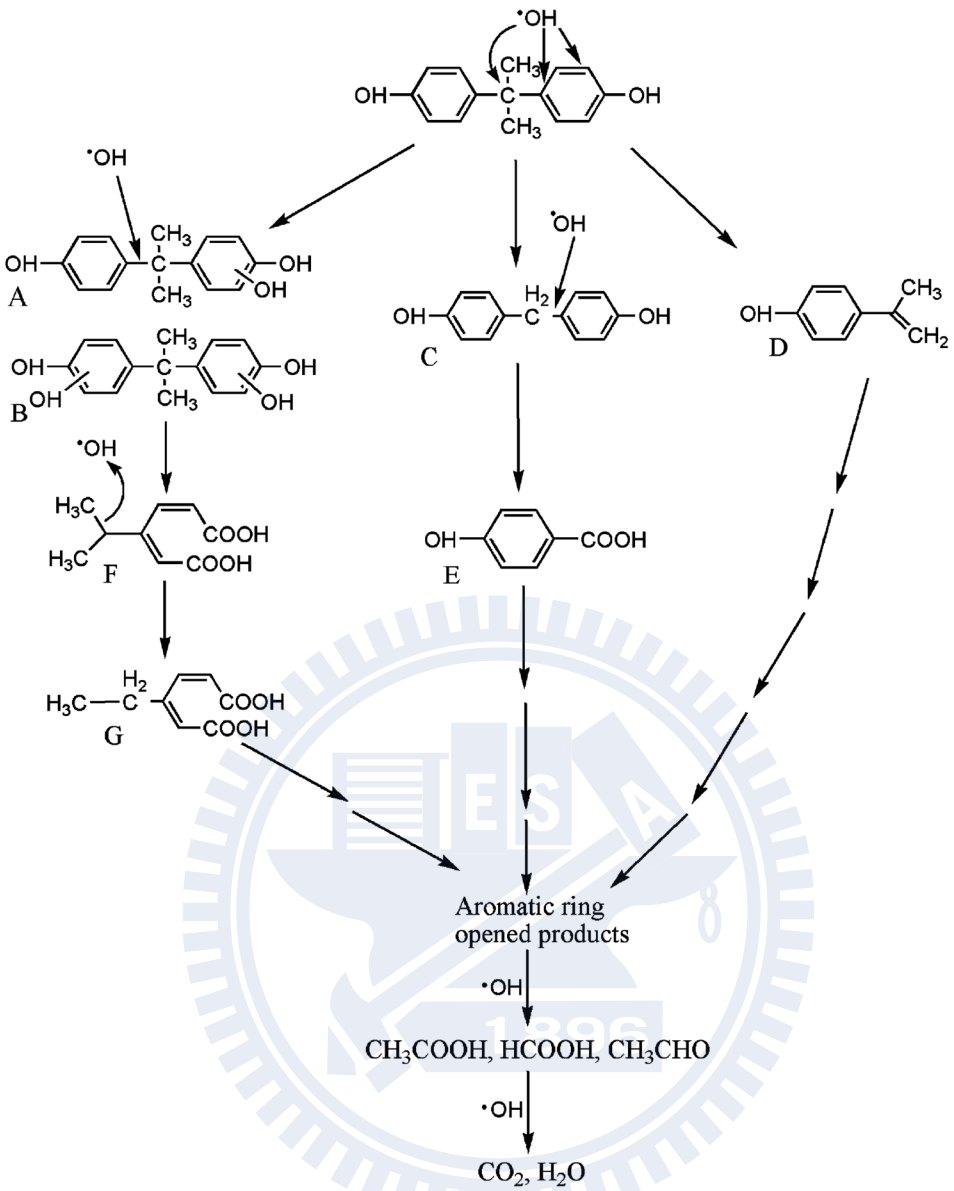

Figure 2-10 Proposed reaction pathways of BPA degradation.[101]

Chapter 3. Experimental materials and methods

Figure 3-1 indicates the experimental framework in this study. TOPO-modified TiO_2 are prepared through a non-hydrolytic sol-gel method. Afterward, the resulting samples are characterized using TEM, FTIR, UV-vis, XRD, TGA, XPS and N_2 adsorption and desorption isothermal to understand their microstructures and physiochemical properties. Adsorption and decomposition of BPA was by the surface modified mesoporous TiO_2 and pure TiO_2 was examined to evaluate their photocatalyic activity.

3-1. Chemicals

Titanium chloride ($TiCl_4$, Showa, 99%) and titanium isopropoxide (TTIP, $Ti(OC_3H_7)_4$, Acros, 98%) were used as the precursors of TiO_2. Trioctylphosphine oxide (TOPO, $[CH_3(CH_2)_7]_3PO$, Strem Chemicals, 99%) was used as the organic modifier as well as template. 1,3,5-trimethylbenzene (TMB, C_9H_{12}, Alfa, 98%) was used as a swelling agent to expand pore sizes. Bisphenol A (BPA, $C_{15}H_{16}O_2$, Sigma Aldrich, 99+%) was used as the target compounds for photocatalysis activity. All chemicals were shown in Table 3-1.

Table 3-1 The structures of chemicals used in this study.

Chemical	Structure
Titanium chloride	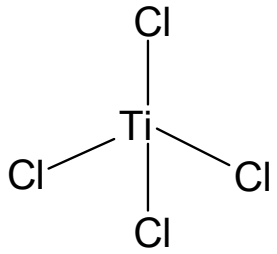
Titanium isopropoxide	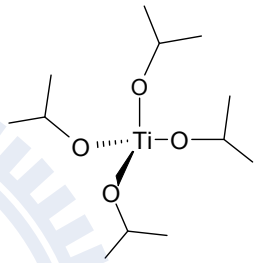
Trioctylphosphine oxide	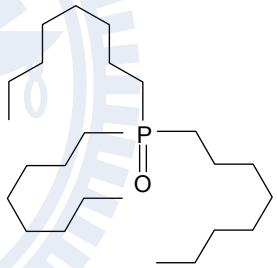
1,3,5-trimethylbenzene	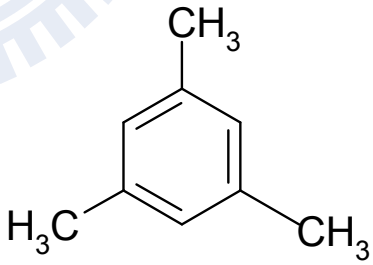
Bisphenol A	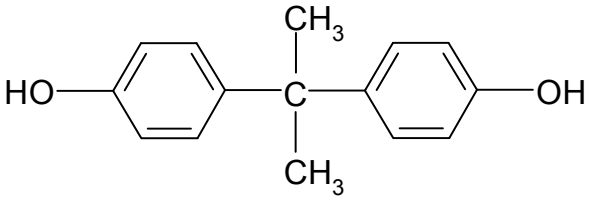

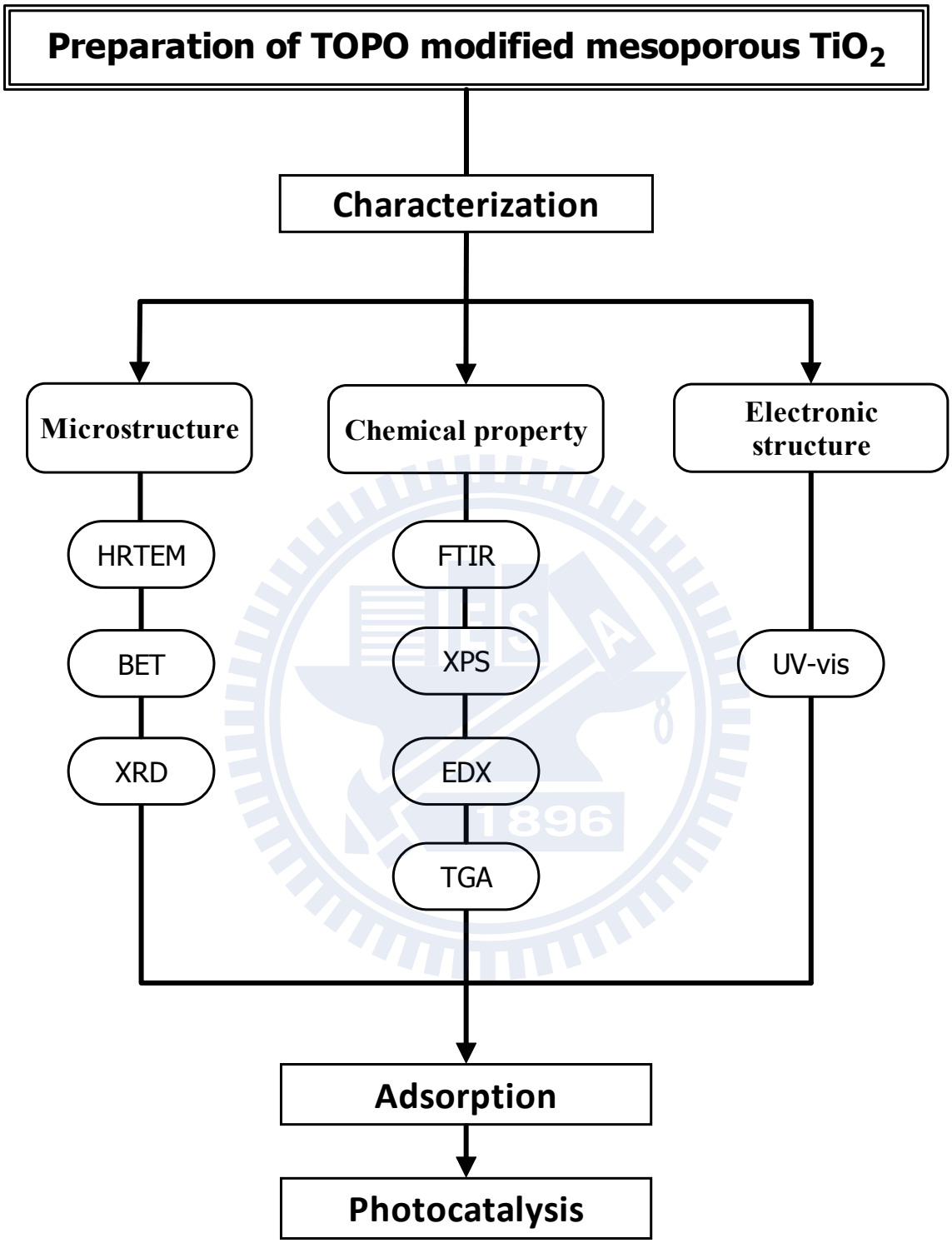

Figure 3-1 Flow chart of experimental design in this study.

3-2. Preparation of TOPO modified mesoporous TiO_2 via NHSG process

TOPO-modified mesoporous TiO_2 were prepared by a non-hydrolytic sol-gel process. TOPO (0.967 g, 2.5 mmol) was added into a tight vial and melted at 90°C. Afterward, TTIP (7.48 mL, 25 mmol) and $TiCl_4$ (2.74 mL, 25 mmol) were injected into the molten TOPO at 400 rpm. The temperature was initially raised to 150°C and kept for 15 minutes. Then, it was further increased to 320°C under a N_2 flow. The color of solution gradually became deep yellow as the temperature increased. When the temperature reached to 320°C, the solution suddenly became solid gel. At this moment, the solution cooled down to 50°C. Acetone was used to wash out the residual TOPO and the powders were harvested via centrifugation at 10000 rpm for 6 minutes. This step was repeated for three times. Finally, the samples were dried at room temperature and then ground into fine powders.

To expand pore sizes of the TOPO-TiO_2, TMB (0.213 mL, 1.5 mmol) was added into the molten TOPO (1.933 g, 5 mmol) prior to the addition of TTIP (7.48 mL, 25 mmol) and $TiCl_4$ (2.74 mL, 25 mmol). All procedures for TOPO-TiO_2-TMB samples were the same as those for the TOPO-TiO_2 except the final temperature was raised to 350°C. In addition, toluene was used to remove the TMB from the pores of the TiO_2. Pure TiO_2 was prepared from cross-condensation between 8.98 mL of TTIP (30 mmol) and 3.29 mL $TiCl_4$ (30 mmol). All the procedures for the TiO_2 were also the same as those for the TOPO-TiO_2 except the final temperature was 290°C. To discuss the influence of the different synthesis parameters on the structure and the surface characteristics of TiO_2, various TOPO/Ti and TOPO/TMB ratios were adapted for the preparation. The detailed synthesis conditions were listed in Table 3-2. TPX and TPX-Y were given to the TOPO-TiO_2 and TOPO-TiO_2-TMB samples, where X and Y represent the TOPO/TTIP and TMB/TOPO ratios, respectively, when the TTIP/$TiCl_4$ ratio was set as 1.

Table 3-2 The preparation conditions and corresponding sample names.

Sample name	**TOPO : TTIP : $TiCl_4$**
TP 1	0.1 : 1 : 1
TP 2	0.2 : 1 : 1
TP 3	0.3 : 1 : 1
TP 4	0.4 : 1 : 1
TP 5	0.5 : 1 : 1

Sample name	**TOPO : TTIP : $TiCl_4$**	**TOPO : TMB**
TP 2-B0.3	0.2 : 1 : 1	1 : 0.3
TP 2-B0.8	0.2 : 1 : 1	1 : 0.8
TP 2-B1.2	0.2: 1 : 1	1 : 1.2

Sample name	**TTIP : $TiCl_4$**
Pure TiO_2	1 : 1

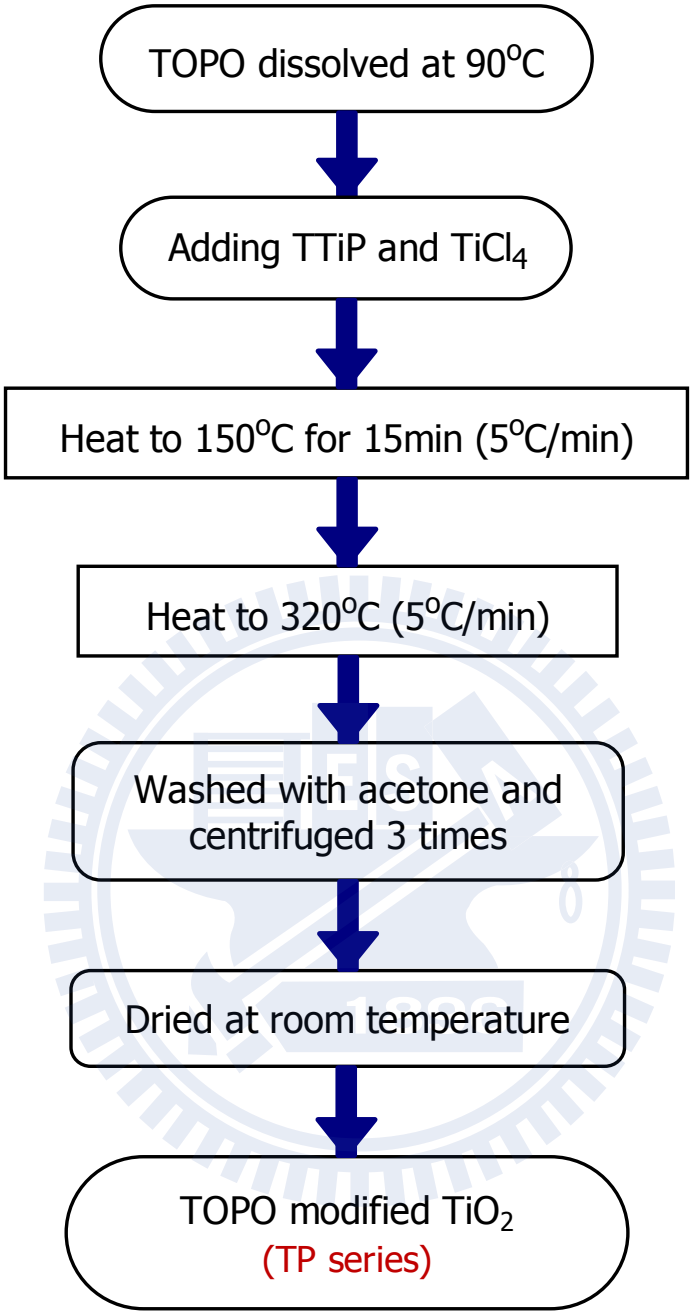

Figure 3-2 A flow diagram for the preparation of TOPO modified mesoporous TiO_2 via a NHSG method.

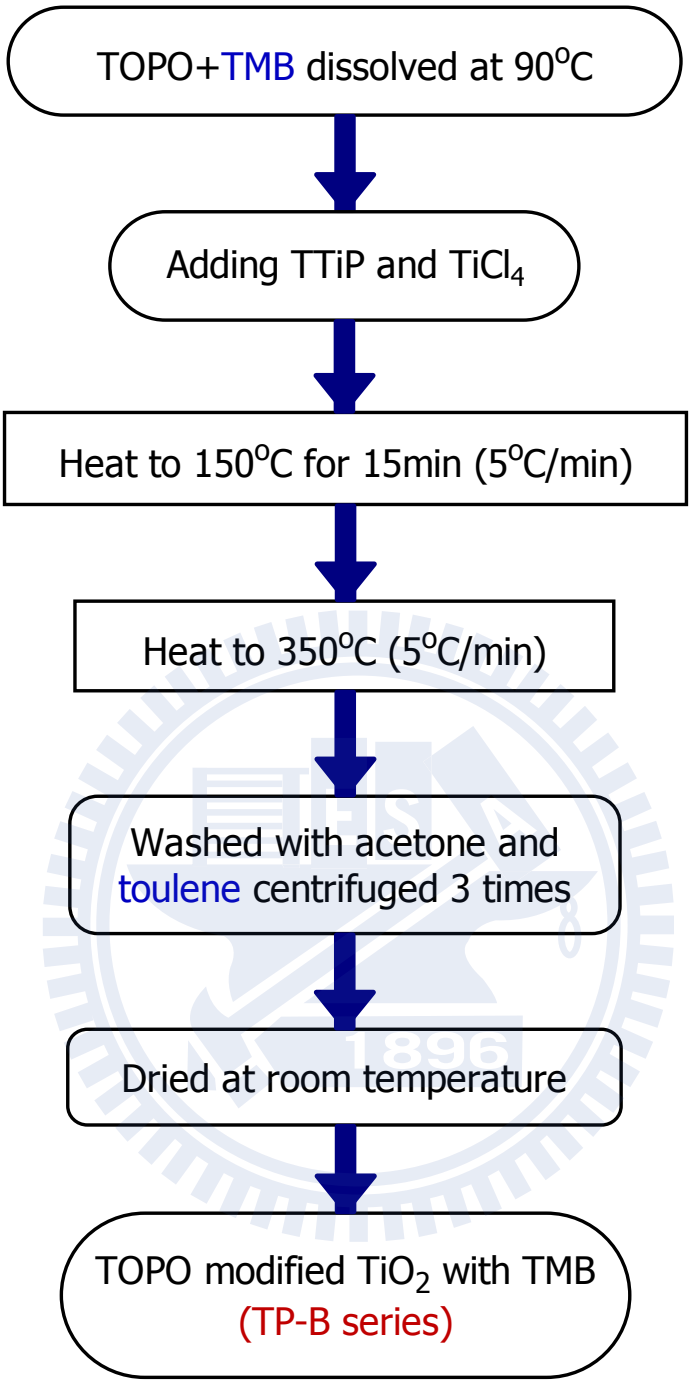

Figure 3-3 A flow diagram for preparation of TOPO modified mesoporous TiO_2 in the presence of TMB.

3-3. Characterization

3-3-1. High Resolution Transmission Electron Microscopy (HRTEM)

The pore structure and shape of TOPO-TiO_2 were identified using high resolution transmission electron microscopy (HRTEM, Philips TECNAI 20) operated at a 200 kV accelerating voltage. The samples were prepared by dispersing of powders into acetone with ultrasonic for 30 minutes. Following, the suspension was dropped on the holey carbon film supported on a Cu grid.

3-3-2. Nitrogen adsorption and desorption isothermal

The specific surface area, S_{BET}, and pore sizes were determined from Brunaner, Emmett and Teller model (BET) and Barrett, Joyner and Halenda formula (BJH), respectively. This based on the N_2 adsorption and desorption isothermal at 77K by Micromeritics, Tristar 3000. Prior to the adsorption experiment, the samples were pre-dried at 120°C for 4 hours. Afterward, the samples were degassed at 120°C under vacuum for 12 hours.

3-3-3. X-ray powder diffractmeter (XRPD)

The crystalline structure and crystallite sizes were identified via X-ray powder diffractmeter (XRPD, MAC Sience, MXP18) using Cu Kα irradiation (λ = 0.1546 nm). The operating conditions were at an accelerating voltage of 30 kV and an emission current of 20 mA. The X-ray patterns were obtained from 20° to 80° 2θ at a sampling width of 0.02^o and scanning speed of 4°/min. The crystalline size of each sample was calculated by Scherrer's equation[103]:

$$D = \frac{K\lambda}{\beta \cos\theta} \tag{3-1}$$

D: crystalline size

K: shape constant, 0.89

λ: wavelength of X-ray source (Cu Kα = 0.1546 nm)

β: full width at half-maximum (FWHM)

θ: scattering angle

3-3-4. UV-vis Spectrometer

The optical properties and band gaps of the TOPO modified TiO_2 were determined using UV-vis diffuse reflectance spectrophotometer (HITACHI U-3010) scanning from 900 to 200 nm. All the analysis used aluminum oxide (Al_2O_3) as the reference. The band gap of the TiO_2 was determined from the absorption spectra converted from the reflectance spectra using Kubelka-Munk equation[104]:

$$F(R) = \frac{(1-R)^2}{2R} = \frac{k}{S} \tag{3-2}$$

k: absorption coefficient

S: scattering coefficient

R: *%R* reference

3-3-5. Fourier Transform Infrared Spectrometer (FTIR)

The functional groups of the TOPO modified mesoporous TiO_2 were identified using Fourier transform infrared spectrometer (FTIR, Thermo Scientific Nicolet iS10) scanning

from 400 to 4000 cm^{-1} with the resolution of 4 cm^{-1} for 100 scans. The samples were mixed with KBr (Merck) and than pressed as a flake for the FTIR measurement.

3-3-6. Zeta Potential

The zeta potential was measured by Zetasizer nano ZS (Malbern, Britain). The concentration of catalysts in the DI water was 1 mg/mL. The pH value of suspension was adjusted by NaOH (0.1 M) and HCl (0.1 M) solution.

3-3-7. Thermo Gravimetric Analysis / Differential Scanning Calorimetry (TGA/DSC)

The organic volume and energy flow of the samples were measured using thermo gravimetric analysis (TGA, TA 5100) and differential scanning calorimetry (DSC, Netzsch 404). The samples were heated from room temperature to 900°C at a heating rate of 10°C/min under an air flow with a flow rate of 50 mL/min.

3-3-8. X-ray photoelectron Spectroscopy (XPS)

The surface chemical compositions and chemical states of the TOPO-modified mesoporous TiO_2 were characterized using X-ray photoelectron spectroscopy (XPS, ESCA PHI 1600) using an Al Kα X-ray source (1486.6 eV). The photoelectron was collected into the analyzer with pass energy of 23.5 eV. The collection step size in wide range scan and high-resolution analysis were 1.0 and 0.1 eV, respectively. All analytical process was controlled under ultrahigh vacuum conditions at pressure less than 1.4×10^{-9} Torr. The chemical shift in binding energy of XPS spectra was reference to the Ti (2p) line at 458.8 eV.

In order to quantify and qualify each element, curve fitting of the XPS spectra was performed. After subtraction of the "Shirley-shaped" background, the original spectra were fitted using a nonlinear least-square fitting program and combination of Gaussian-Lorentzian peak shapes was adapted for all peaks. The parameters used for the curve fitting of the Ti 2p, O 1s, C 1s and P 2p, including the binding energies, doublet separation, and full-width at half maximum. The integrated peak areas were normalized atomic sensitive factors to calculate atomic ratios. The equation for atomic ratio calculation is shown below[105]:

$$\frac{n_1}{n_2} = \frac{I_1 / ASF_1}{I_2 / ASF_2} = \frac{A_1 / ASF_1}{A_2 / ASF_2} \qquad (3\text{-}3)$$

n: atomic number

I: intensity of XPS spectra

ASF: atomic sensitivity factor

A: peak area of XPS spectra

3-4. Adsorption behavior

Batch sorption equilibriums were conducted in the dark at room temperature. The TiO_2 samples were added into the BPA solutions (5-80 mg/L) under stirring for 30 minutes. The dosage of TiO_2 in each batch test was maintained 1 g/L. After adsorption, the suspension was centrifuged at 15000 rpm for 3 minutes to remove the photocatalysts. The BPA concentration in the supernatant was analyzed by high performance liquid chromatography (HPLC, Waters Alliance 2695) equipped with a Photodiode Array Detector (PDA, Waters 2996, 190-400 nm) and a C18 column (5 μm, 4.6 mm × 250 mm). The mobile phase was acetonitrile-water mixture (50/50, v/v) at flow rate of 1.0 mL/min.

Signal was detected at 280 nm.

3-5. Photodegradation of BPA

The BPA was selected as the hydrophobic target compounds. The powder samples (20.0 mg) were dispersed into 20 mL BPA solutions. The initial concentration of BPA solution was 10 mg/L. Before illumination, the suspension was stirred and purged with oxygen in the dark for 30 minutes for equilibrium of adsorption and desorption of BPA. The degradation of BPA was irradiation by 305 nm UV light in the reactor. These suspensions were periodically sampled by withdrawing the aliquots from the reactor, and then were centrifuged at 15000 rpm for 3 minutes to separate the BPA solutions from the solid TiO_2 catalysts. The photodegradation of BPA solutions were analyzed by high performance liquid chromatography (HPLC). BPA was almost stable under illumination with 305 nm UV lamp (Figure 3-4).

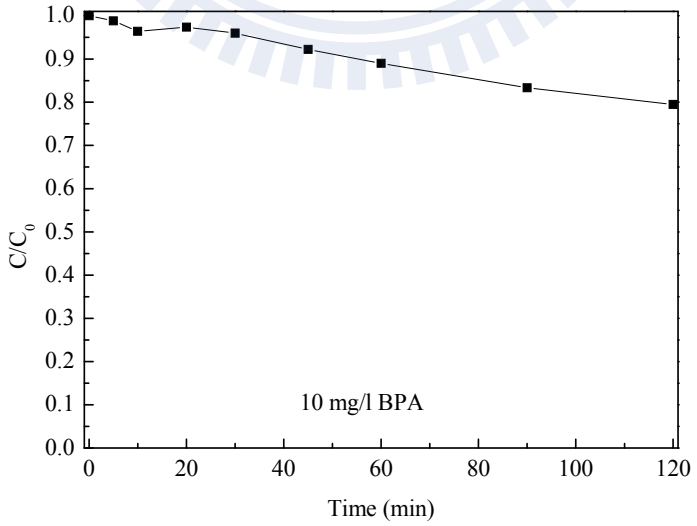

Figure 3-4 Photolysis of BPA under illumination of 305 nm UV light.

Chapter 4. Results and Discussion

4-1. The pore structure and morphology

Figure 4-1 shows N_2 adsorption and desorption isotherm and BJH pore size distribution of TP 1 and TP 2. The TP 1 exhibited Type Ⅳ adsorption isotherm and H4 type hysteresis loop, indicating a mesoporous material. The pore size distributions of the samples were analyzed using the BJH model for the adsorption branch. The specific surface areas and pore sizes of the modified TiO_2 are summarized in Table 4-1. Pure TiO_2 contained a specific surface area of 15 m^2/g. The specific surface area ranged 2-103 m^2/g and increased with decreasing TOPO concentrations. The TP 1 contained largest surface area of 103.0 m^2/g and a typical mesopore size of 3.6 nm. The mesoporous were formed in the interstitial space between TiO_2 nanoparticles. At the TOPO/Ti concentration was 0.1 (sample TP 2), the pore shape changed to a wormhole-like structure. Moreover, Type Ⅰ adsorption was observed for the TP 2, indicating microporous properties. TOPO-capped nanoparticles were gradually formed when the TOPO/Ti concentrations were higher than 0.2. Strong hydrophobic interaction between the TOPO-capped TiO_2 resulted in low specific surface areas. Thus, the critical TOPO/Ti ratio for the porous structure was 0.1. Some studies reported that the critical surfactant/Ti were 0.6 and 0.12 when P123[14] and CTAB[19] were used as the structure directing agent, respectively. Comparatively, the required critical concentration was lower in this study because the carbon chains of TOPO are much shorter than CTAB and P123.

TMB is a hydrophobic substance and can assist TOPO to self-assemble micelles in hydrophilic media. Figure 4-2, 4-3 and 4-4 shows the N_2 adsorption/desorption and pore size distribution of TP 1、TP 2 and TP 3 formed in the presence of various mounts of TMB. Table 4-2 summarizes the specific surface areas and pore sizes of TP-B samples. Addition

of TMB into the precursor solutions led to Type Ⅳ isotherm for most of the TP samples except for TP 3-B0.3, TP 3-B0.5 and TP 3-B1.2. In addition, remarkable increases in specific surface areas, pore volumes and pore size were obtained. This finding indicates that TMB assists formation of porous structure expand the pore size of TiO_2. In the TP 1 sample, the TOPO/Ti ratio 0.05/1 was too low to form well micelles and to result in well-resolved porous structure. However, emulsion effect caused by the presence of TMB led to large micelles and large pore size. For TP 1 series, the narrowest pore distribution was formed when the TMB/TOPO/Ti at 0.05/0.05/1 (TP 1-B1.0). Too low or too high TMB concentration was unable to form homogenous micelles. In the TP 2 series, narrow pore size distribution with average pore size of 3.0-3.7 nm was found for all the added concentrations of TMB. TP 3 was at the margin stage which a continuous porous structure starts to transit to a non-porous structure. However, obvious mesoporous structures were found at the TMB/TOPO/Ti of 0.4/0.15/1 (TP 3-B0.8) and 0.5/0.15/1 (TP 3-B1.0), while microporous feature was found for the other TMB/TOPO ratios. TMB assists TOPO to self-assemble micelles and an appropriate TMB/TOPO concentration is required to form mesoporous structures.

Figure 4-5 shows the TEM and HRTEM images of pure TiO_2 and the modified TiO_2 prepared with different TOPO concentrations. Pure TiO_2 was nonporous structure and composed of aggregated nanocrystals (Figure 4-5a). The TP 1 had the main mesoporousity due to the interparticle porosity (Figure 4-5c). The HRTEM image of TP 1 showed clear lattice fringes which allows for the identification of crystallographic spacing. It indicates that the prepared TiO_2 powders had well anatase crystalline with a d-spacing of (101) crystallographic plan of 0.37 nm. TP 1 had a single crystallize size about 4.6 nm. Figure 4-5g and e displays the TEM images of TP 2-B0.3 and TP 2, respectively. This finding reveals that the addition of TMB could form obvious pore structures.

Table 4-1 The specific surface area, pore size and pore volumes of TOPO-TiO_2 and TiO_2.

Sample	S_{BET} (m^2/g)	V_{pore} (cm^3/g)	*D_{pore} (nm)
TP 1	103	0.16	3.6
TP 2	100	0.16	3.1
TP 3	11	0.11	8.8
TP 4	2	0.09	22.1
TP 5	3	0.02	11.4
TiO_2	15	0.14	131.0

*Average pore size was calculated by using the BJH formula for the adsorption branch.

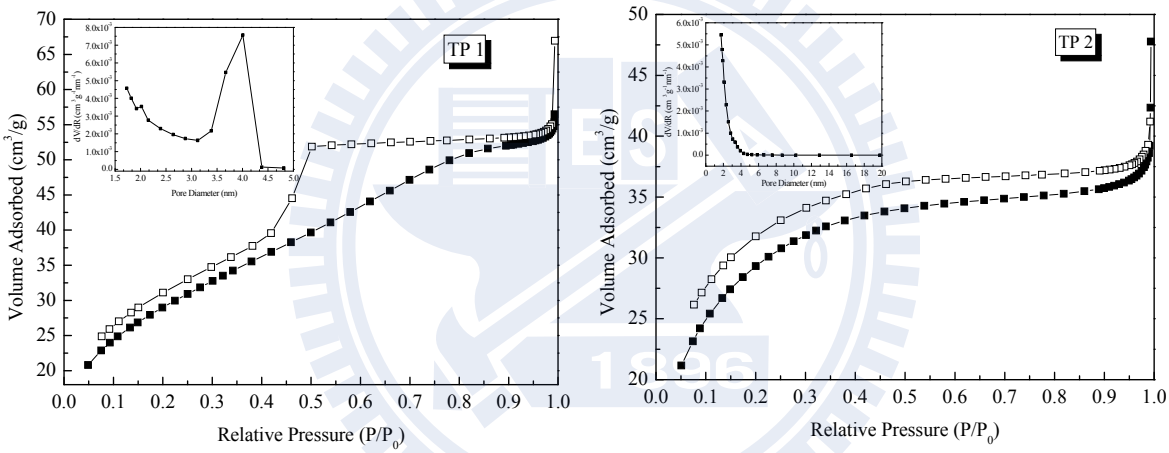

Figure 4-1 N_2 adsorption and desorption isotherm and BJH pore size distribution of TP 1and TP 2.

Table 4-2 The specific surface area, pore size and pore volumes of TOPO-TiO_2 with TMB.

Sample	S_{BET} (m^2/g)	V_{pore} (cm^3/g)	*D_{pore} (nm)
TP 1-B0.3	270	0.52	6.8
TP 1-B0.5	190	0.29	5.2
TP 1-B0.8	110	0.27	5.9
TP 1-B1.0	272	0.33	4.3
TP 1-B1.2	264	0.48	6.2

Sample	S_{BET} (m^2/g)	V_{pore} (cm^3/g)	*D_{pore} (nm)
TP 2-B0.3	234	0.29	3.7
TP 2-B0.5	206	0.27	3.7
TP 2-B0.8	158	0.22	3.0
TP 2-B1.0	208	0.22	3.7
TP 2-B1.2	236	0.27	3.6

Sample	S_{BET} (m^2/g)	V_{pore} (cm^3/g)	*D_{pore} (nm)
TP 3-B0.3	117	0.15	3.5
TP 3-B0.5	113	0.08	2.7
TP 3-B0.8	170	0.21	4.7
TP 3-B1.0	145	0.11	2.7
TP 3-B1.2	101	0.13	2.6

*Average pore size was calculated by using the BJH formula for the desorption branch.

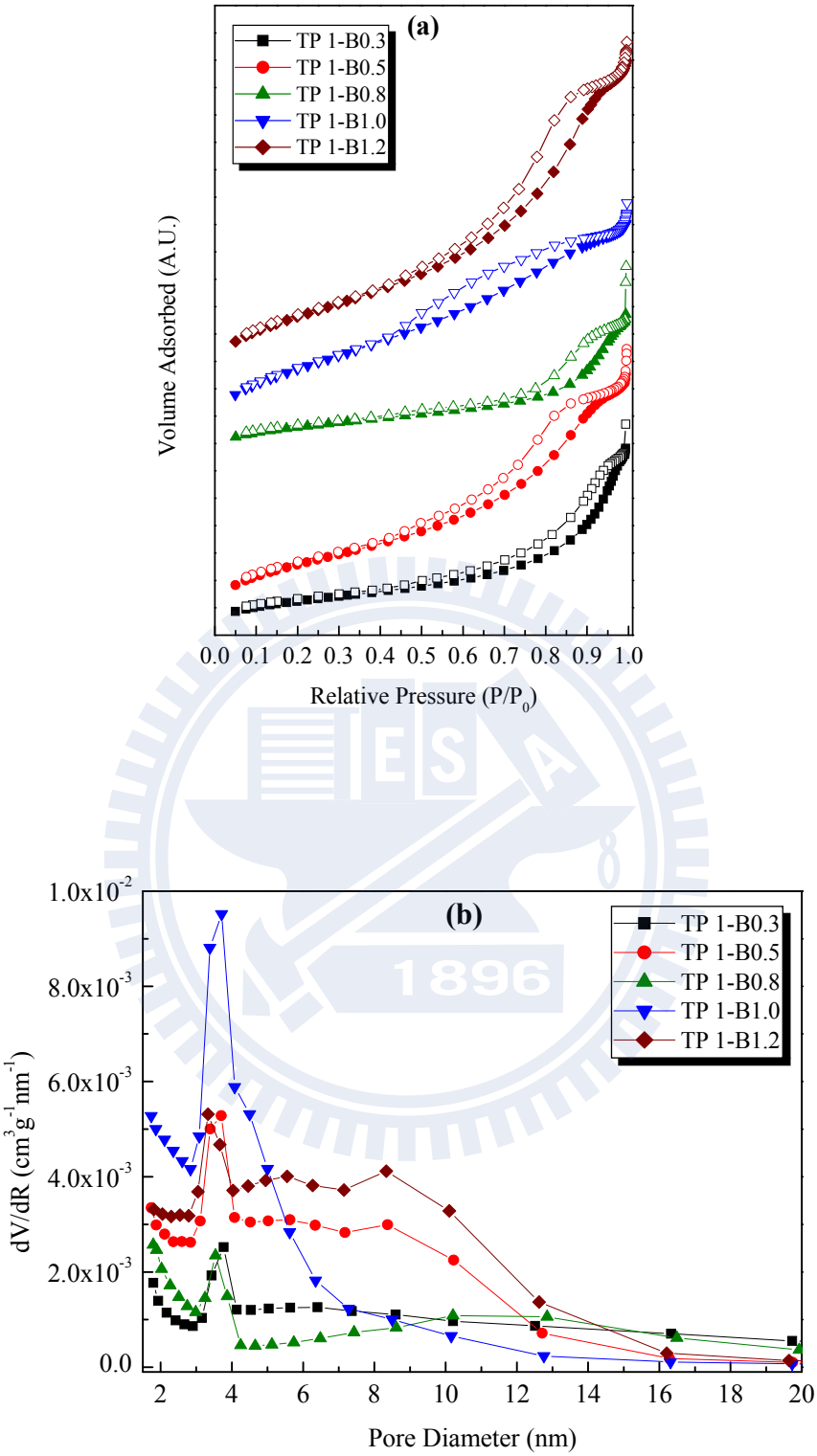

Figure 4-2 (a) N_2 adsorption/desorption isotherm and (b) the pore size distribution of TP 1-B0.3, TP 1-B0.5, TP 1-B0.8, TP 1-B1.0 and TP 1-B1.2.

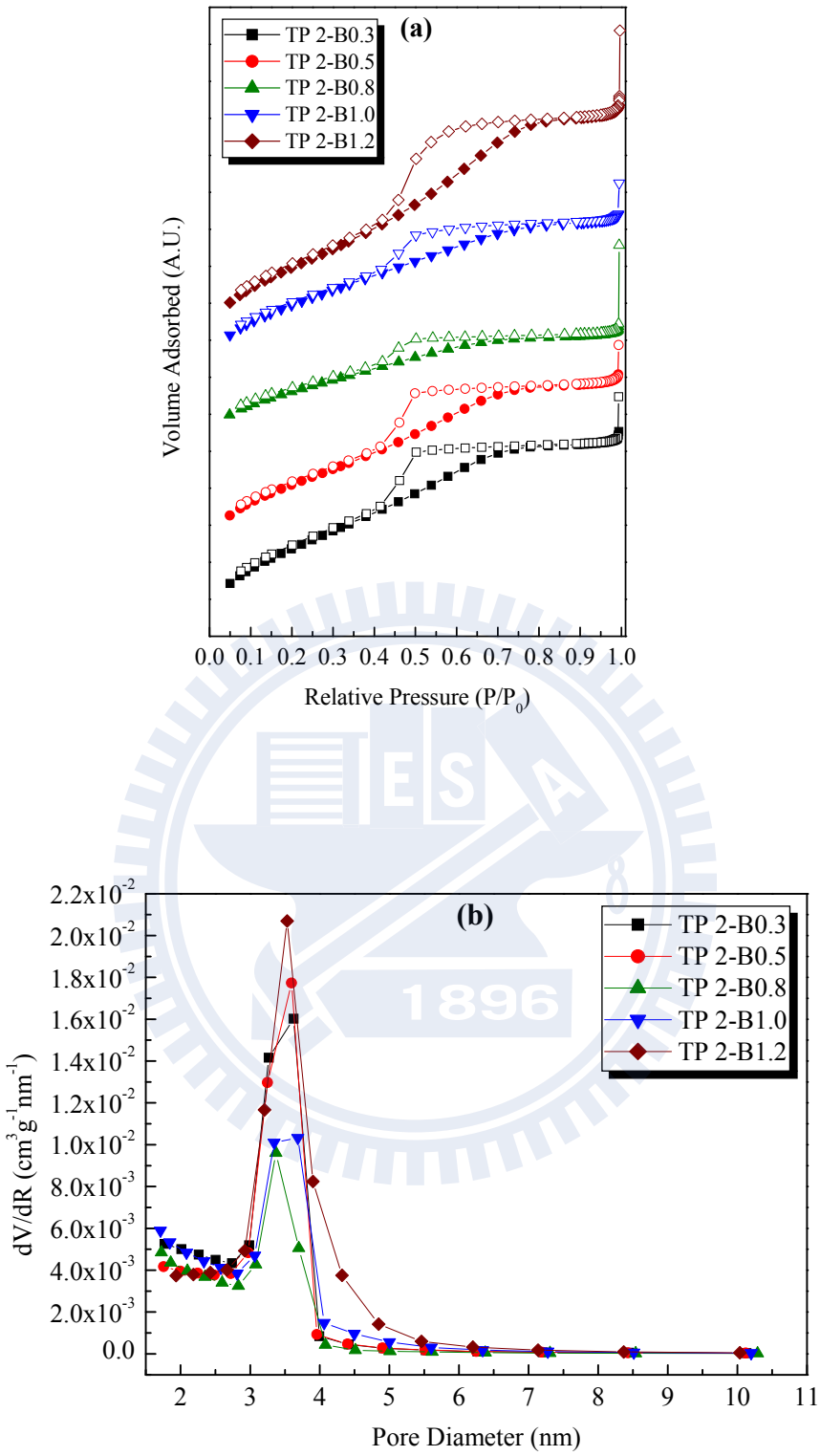

Figure 4-3 (a) N_2 adsorption/desorption isotherm and (b) the pore size distribution of TP 2-B0.3, TP 2-B0.5, TP 2-B0.8, TP 2-B1.0 and TP 2-B1.2.

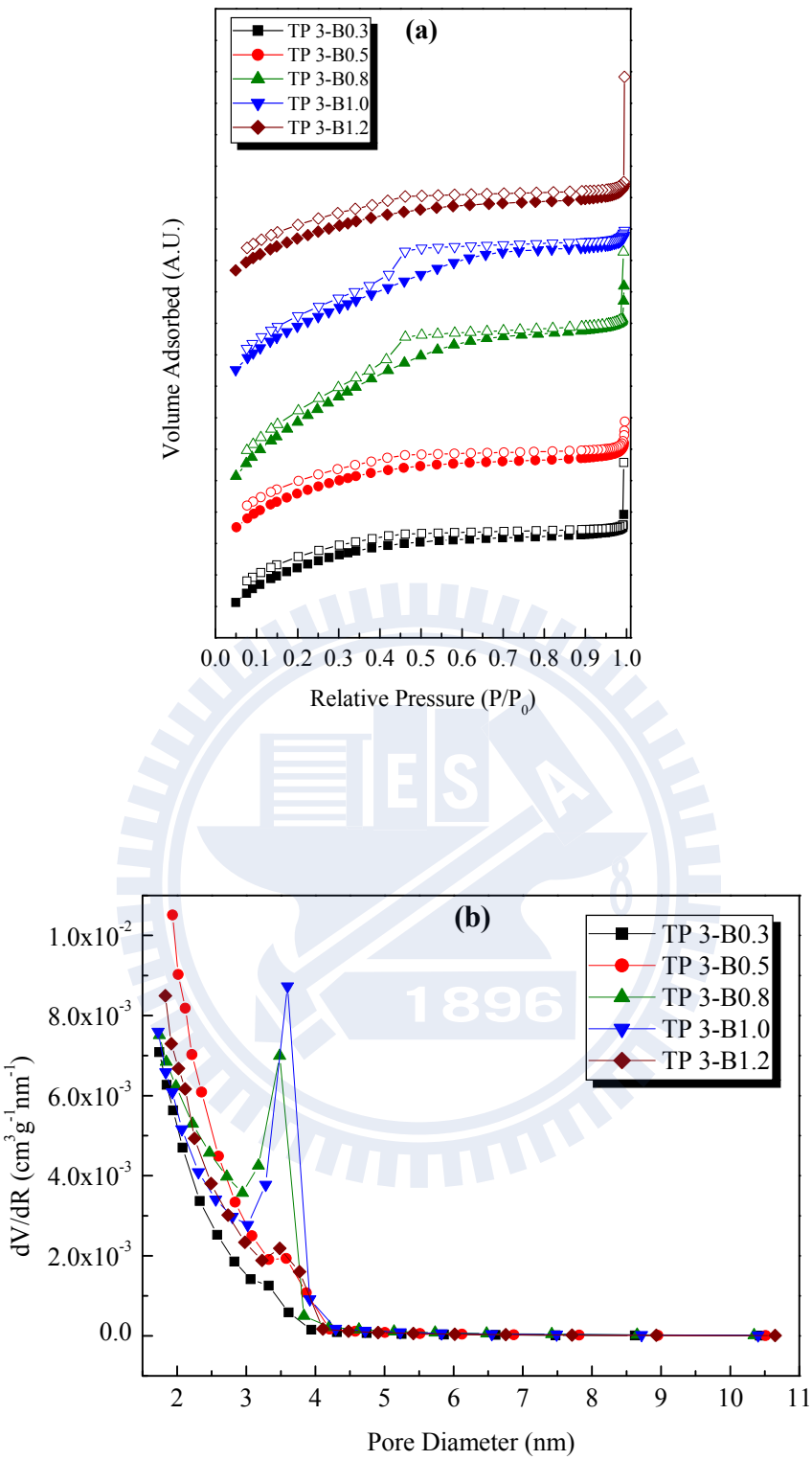

Figure 4-4 (a) N_2 adsorption/desorption isotherm and (b) the pore size distribution of TP 3-B0.3, TP 3-B0.5, TP 3-B0.8, TP 3-B1.0 and TP 3-B1.2.

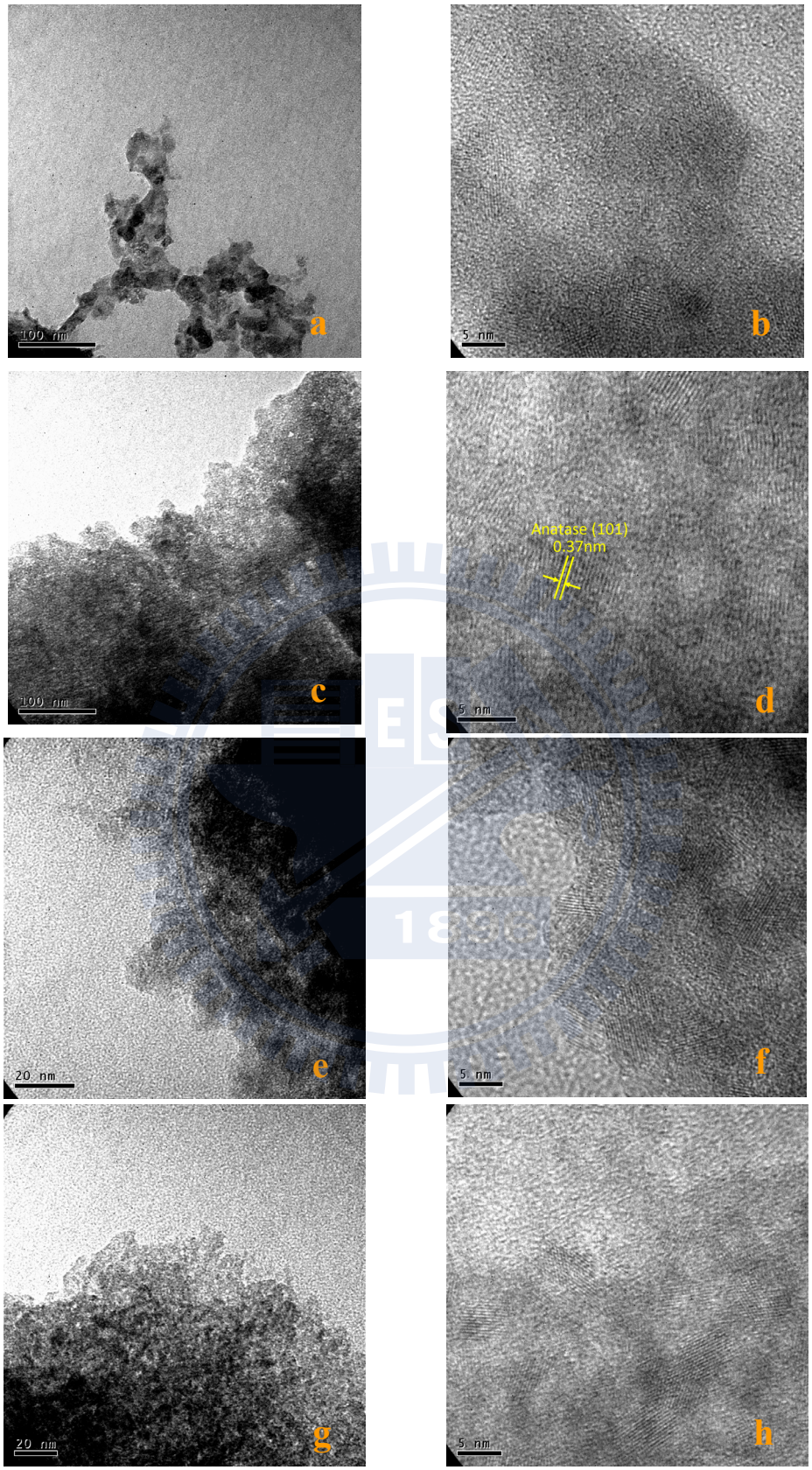

Figure 4-5 TEM and HRTEM images of (a and b) TiO_2, (c and d) TP 1, (e and f) TP 2 and (g and h) TP 2-B0.3.

4-2. Crystalline structure and optical property

Figure 4-6 shows the XRD patterns of the pure and modified TiO_2. Anatase was the major crystalline phase presented in all TOPO-TiO_2 and pure TiO_2 samples (JCPDS NO.21-1272, see Appendix B). The crystalline sizes, which were calculated using Scherrer formula, are listed in Table 4-3. The crystalline sizes of the pure TiO_2 and TOPO-TiO_2 were 2.3 and 3.4-4.7 nm, respectively. Participation of TMB in the preparation changed the crystalline properties of TP samples insignificantly. Consequently, the synthetic temperature even is higher, the crystalline phases are unobvious. Chang et al.[8] used the similar preparation condition (TOPO/Ti = 2.7) to synthesize TOPO-capped TiO_2 nanocrystals at 400°C and found an average crystalline size of 5 nm. The low crystallite size (3.4-4.7 nm) in this study is attributed to low temperature of 320°C used for the synthesis. Moreover, TOPO/Ti ratio thermodynamically effect the generation of TiO_2. It is noted that the critical temperature for the TiO_2 generation increased with increasing TOPO/Ti ratios. This phenomenon is due to the high energy required to break the interaction between TOPO and $TiCl_x(OC_3H_7)_{4-x}$.

Although templating sol-gel methods are frequently used to prepare porous materials, calcination step at temperature 450-550°C is needed to remove templates and induce crystallization. The resulted crystalline sizes were from 6 to 8 nm[22]. Thus, two steps are necessary for proration of organically modified mesoporous TiO_2. In this study, it clearly demonstrates that the non-hydrolytic sol-gel templating method can achieve crystallization and organic modification in single step process.

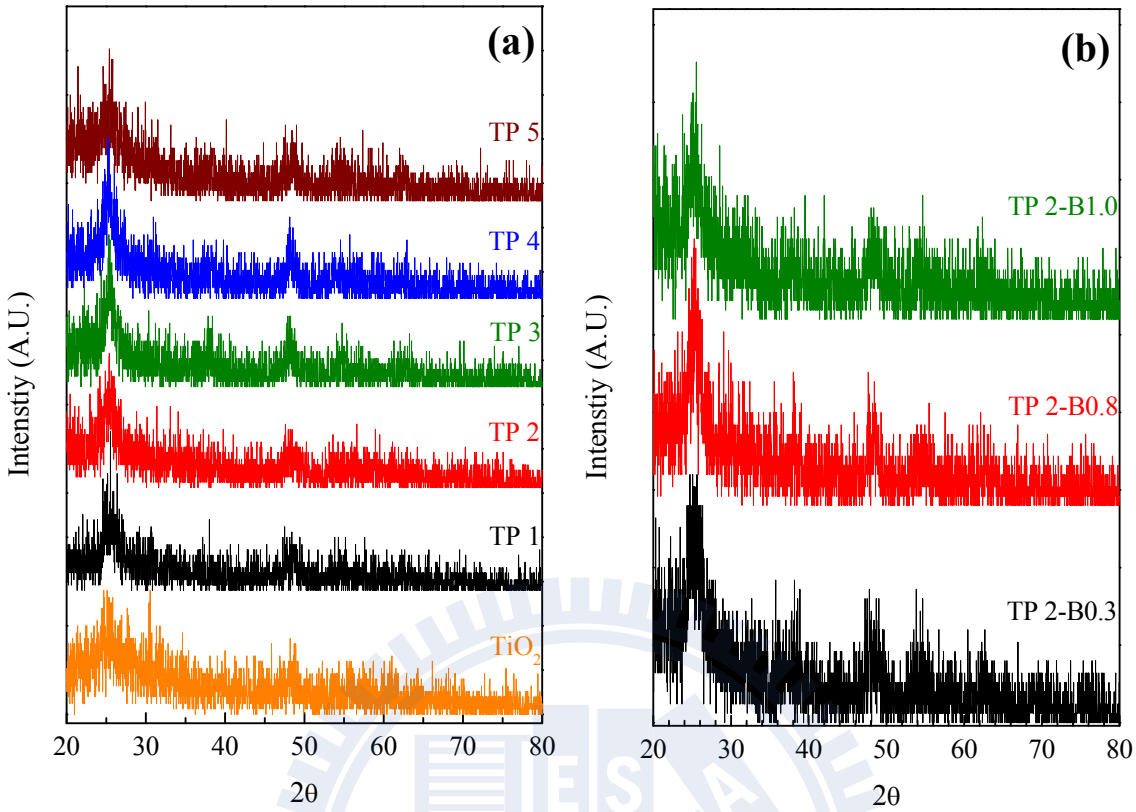

Figure 4-6 XRD patterns of (a) TOPO-TiO_2 and pure TiO_2, (b) the TOPO-TiO_2 adding TMB.

Table 4-3 Crystalline size of TOPO-TiO_2 and pure TiO_2.

Sample	Crystalline size (nm)
TP 1	4.5
TP 2	4.0
TP 3	4.6
TP 4	4.7
TP 5	3.4
TP 2-B0.3	4.2
TP 2-B0.8	4.2
TP 2-B1.2	4.4
TiO_2	2.3

The band gap of the TOPO modified TiO_2 was determined by UV-vis spectrophotometry. Figure 4-7 shows UV-vis spectra of TOPO-TiO_2 and pure TiO_2. Based on the adsorption edges, their bandgaps are listed in Table 4-4. The bandgap of the pure and modified TiO_2 was 3.6 and 3.3-3.4 eV, respectively. These band gaps were slightly larger than that of a bulk anatase TiO_2 (3.2 eV)[106]. The finding indicates that a quantum size effects took place in the non-hydrolytic sol-gel derived TiO_2.

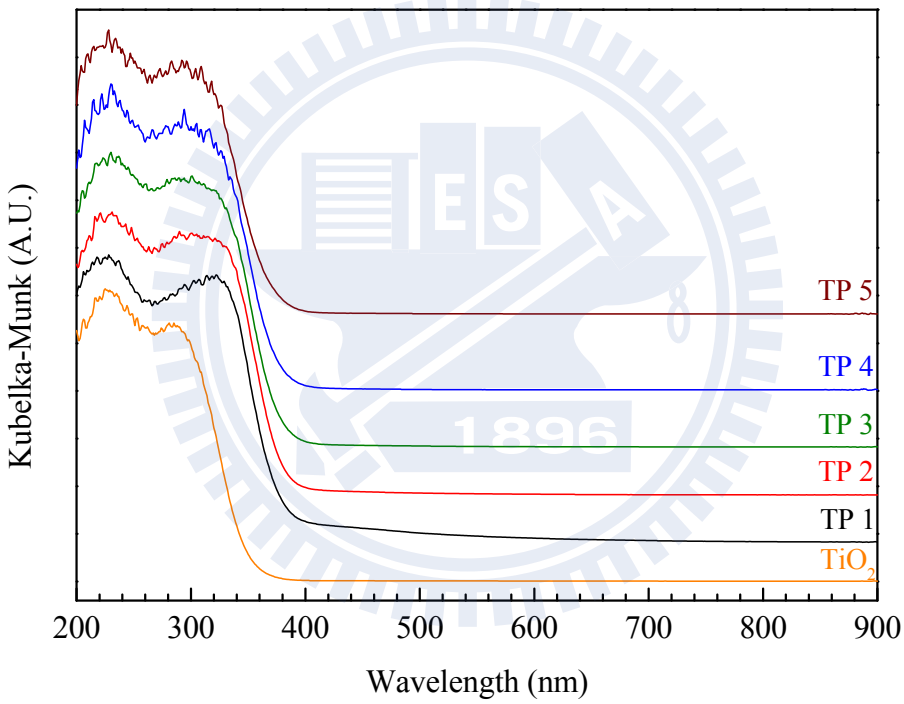

Figure 4-7 UV-vis spectra of TOPO-TiO_2 and pure TiO_2.

Table 4-4 Band gap energy of TOPO-TiO_2 and pure TiO_2.

Sample	**Band gap (eV)**
TP 1	3.3
TP 2	3.3
TP 3	3.3
TP 4	3.3
TP 5	3.3
TP 2-B0.3	3.4
TP 2-B0.8	3.3
TP 2-B1.2	3.4
TiO_2	3.6

4-3. Surface property

4-3-1. Surface functional groups

Figure 4-8 shows the FTIR spectra of TOPO-TiO_2 and pure TiO_2. TP samples all showed $–CH_3$, $–CH_2$ and P=O stretching absorptions at 2760-3150 cm^{-1} and 1100 cm^{-1}, respectively[6]. Compared to the FTIR spectrum of TOPO, the shift of the P=O absorption indicates the formation of a P-O-Ti bond[6]. These characteristic absorptions demonstrate that TOPO was chemically bonded to TiO_2 during the non-hydrolytic sol-gel process. Furthermore, the intensity of P-O-Ti absorption increased with increasing TOPO/Ti concentrations. On the other hand, intensive O-H stretching and bending peaks located at 3400 and 1600 cm^{-1} were observed[9]. The surface hydroxyl groups were formed by hydrolysis of the remained Ti-Cl and Ti-OR in the TiO_2 with water vapor after the non-hydrolytic sol-gel reaction. These results indicate the TOPO-TiO_2 samples contained hydrophilic and hydrophobic regions.

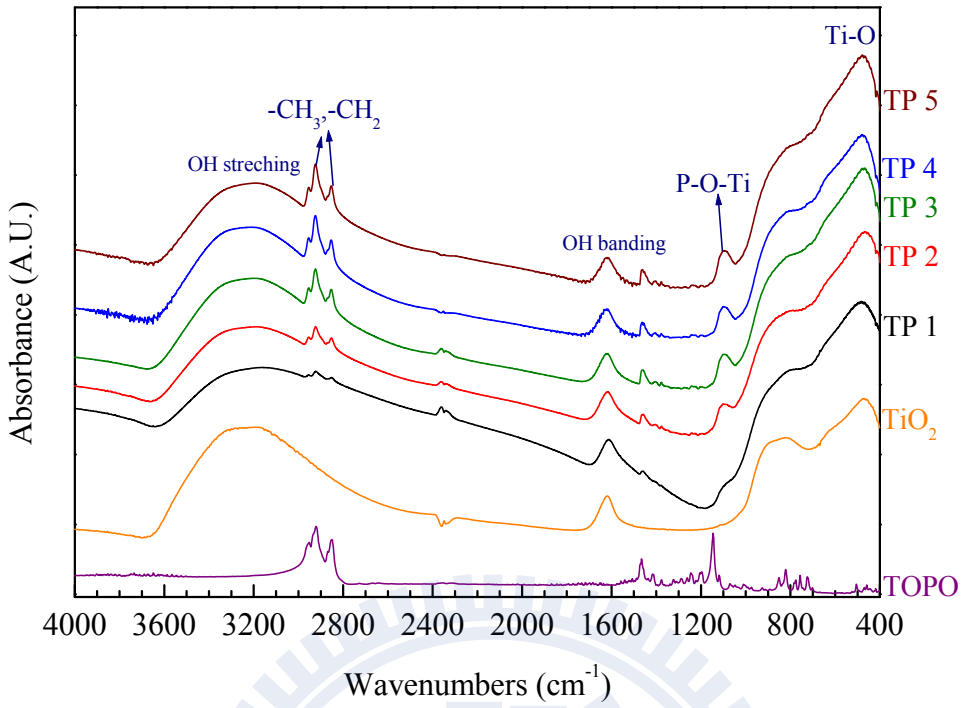

Figure 4-8 The FTIR spectra of TOPO-TiO_2 and pure TiO_2.

4-3-2. Surface chemical composition

Figure 4-9 shows the wide-range XP spectra of TOPO-TiO_2. The Ti (2p), O (1s), C (1s) and P (2p) photoelectron peaks were observed in the spectra, confirming the existence of TOPO on the TiO_2 surface.

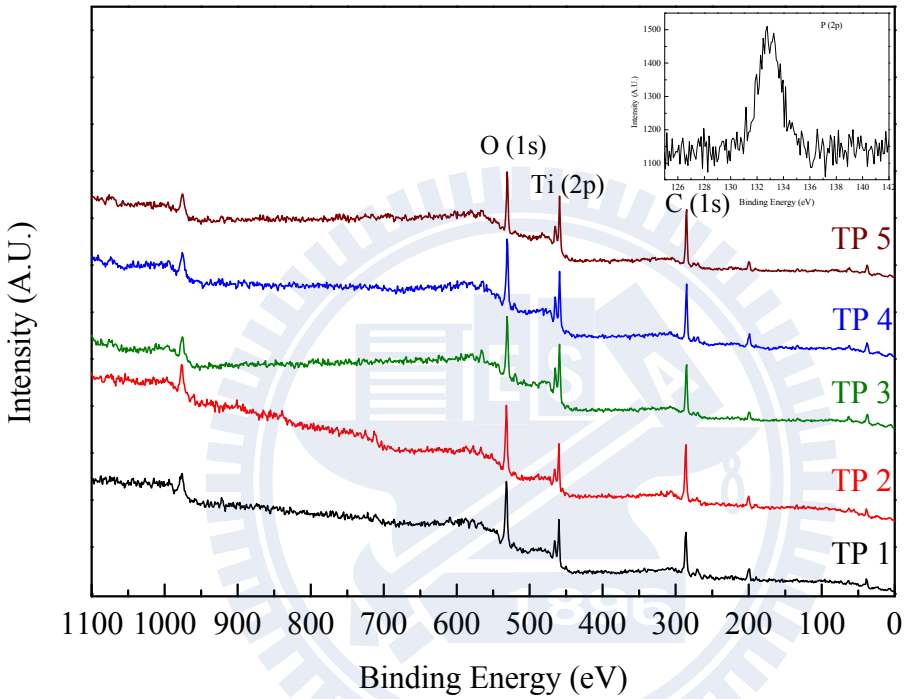

Figure 4-9 The wide-ranged XP spectra of TOPO-TiO_2.

Figure 4-10 displays the high resolution scanned XP spectra of O (1s). The O 1s spectra can be fitted into Ti-O-Ti and Ti-OH with the binding energy of 530.3 and 531.7 eV, respectively[4,6,107]. The peak intensity of the Ti-O relative to that of the Ti-OH peak was decreased when TOPO/Ti ratio was increased, indicating the increased coverage of TOPO on the surface. The P/Ti, C/P and O/(Ti + P) of TOPO-TiO_2 atomic ratios were calculated from the integrated peak areas normalized to their atomic sensitive factors and are summarized in Table 4-5. The C/P ratios of 11.73-18.57 were lower than the theoretical ratio of 24.0 of TOPO molecules, indicating that some carbon chains of TOPO were decomposed during the synthetic process. The ratios of Ti-O/(Ti + P) in the TP samples were 1.3-1.8, that were smaller than the theoretical ratio of 2 of TiO_2. It suggests many defects on the surface. The P/Ti ratios were 0.37-0.43. Participation of TMB in the sol-gel process decreased the P/Ti ratios of TP 2 from 0.39 to 0.19-0.24. It is presumably due to that TMB expands the size of micelles, thus reducing TOPO-to-surface area of the micelle ratios.

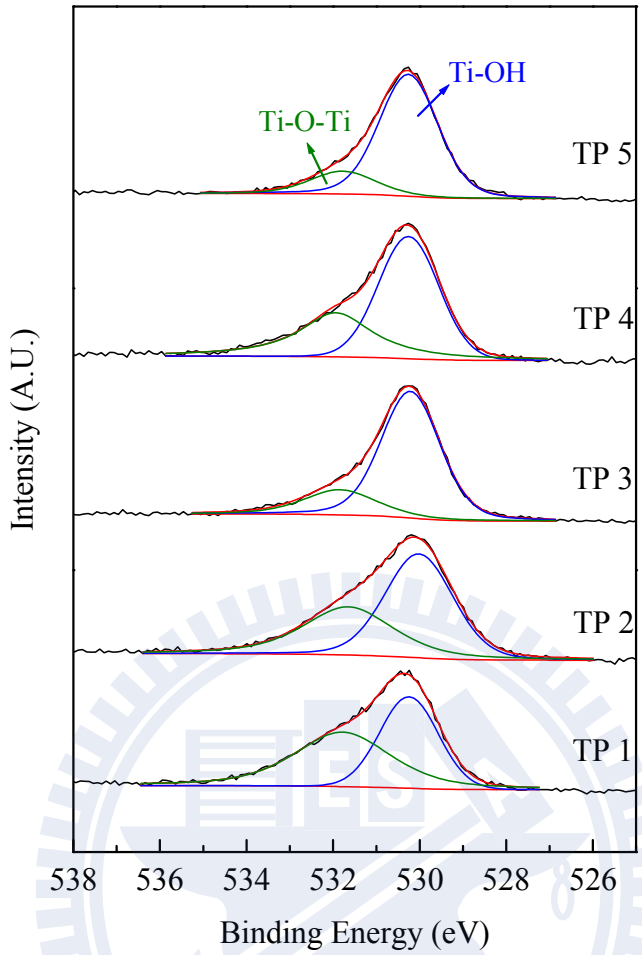

Figure 4-10 The evolution of O (1s) XP spectra of TOPO-TiO_2.

Table 4-5 Surface chemical composition of TOPO-TiO_2.

	P/Ti	C/P	Ti-O/(Ti + P)
TP 1	0.37	16.86	1.33
TP 2	0.39	18.57	1.84
TP 3	0.41	11.99	1.45
TP 4	0.44	12.72	1.36
TP 5	0.42	12.66	1.49
TP 2-B0.3	0.24	16.84	1.81
TP 2-B0.8	0.22	19.54	1.75
TP 2-B1.2	0.19	22.92	1.81

To estimate the quantity of the bonded TOPO, the fractions of the P, O, Cl and Ti of the TOPO-TiO_2 was carried out using EDX (see Appendix C). Table 4-6 shows P/Ti, O/Ti, and Cl/Ti ratios in the TOPO-TiO_2 samples and pure TiO_2. The percentages of P increased with the increasing TOPO concentration. In addition, substantial amounts of Cl ions were left in all samples. Theoretically, Ti-O-Ti oxo-bonds are formed by cross-condensation between Ti-OR and Ti-Cl, and the by-product is volatile RCl. The remained Cl ions should be resulted from the hydrolysis of Ti-Cl. This finding proved again that the generation of OH groups observed in the FTIR spectra. The ratio of P/Ti ranged from 1.4 $\times 10^{-2}$ to 9.0 $\times 10^{-2}$. These values were all smaller than the theoretical addition amount (P/Ti = 0.05-0.25). Approximately, 45-70% TOPO was lost from the synthesis. The loss could be resulted from the thermal evaporation of TOPO at the high reaction temperature. The addition of TMB has a little influence on the percentages of P. Based on the texture and chemical composition analysis, it can conclude that TMB dominate the structure of TOPO-TiO_2 only.

Table 4-6 Elemental analysis of TOPO-TiO_2 and pure TiO_2 using EDX.

Atomic (%)	P/Ti	O/Ti	Cl/Ti
TiO_2	-	2.38	0.23
TP 1	1.4×10^{-2}	2.71	0.14
TP 2	4.8×10^{-2}	2.71	0.14
TP 3	7.6×10^{-2}	3.32	0.16
TP 4	7.8×10^{-2}	3.88	0.17
TP 5	9.0×10^{-2}	2.51	0.18
TP 2-B0.3	3.0×10^{-2}	2.93	0.20
TP 2-B0.8	5.3×10^{-2}	3.17	0.10
TP 2-B1.2	4.6×10^{-2}	3.17	0.23

The quantity of TOPO bonded to the TiO_2 surface was determined by thermo gravimetriv analysis (TGA). Figure 4-11 displays the typical heat flow and weight loss of TP 2 (The other TP samples see Appendix D). There are three weight loss stages in the measuring temperature range. Below 100°C, 6-12% weight loss is denoted to the removal of surface physisorbed water molecules. From 100 to 260°C, 5-10% weight loss indicated partially oxidized or pyrolysis of TOPO. At 250-550°C, 14% weight loss accompanied with an exothermic peak centered at 300°C indicates complete burnout of the carbon moiety from the bonded TOPO. The organic-related weight loss of TP 1 was 9%. However, it increased to 21-22% when TOPO/Ti concentration was higher than 0.15 (sample TP 3, TP 4 and TP 5). This result indicates that the bonding of TOPO to the surface of TiO_2 reached saturation. The presence of TMB did not alter the bonding. The TP 2-B samples contained 17% of the organic loss, which is similar to that of TP 2 (14%). This result is in agreement with that obtained from EDX, in which the P/Ti ratio of the TP 2 (4.8×10^{-2}) was similar to that in the TP 2-B samples (3.0×10^{-2}-5.3×10^{-2}).

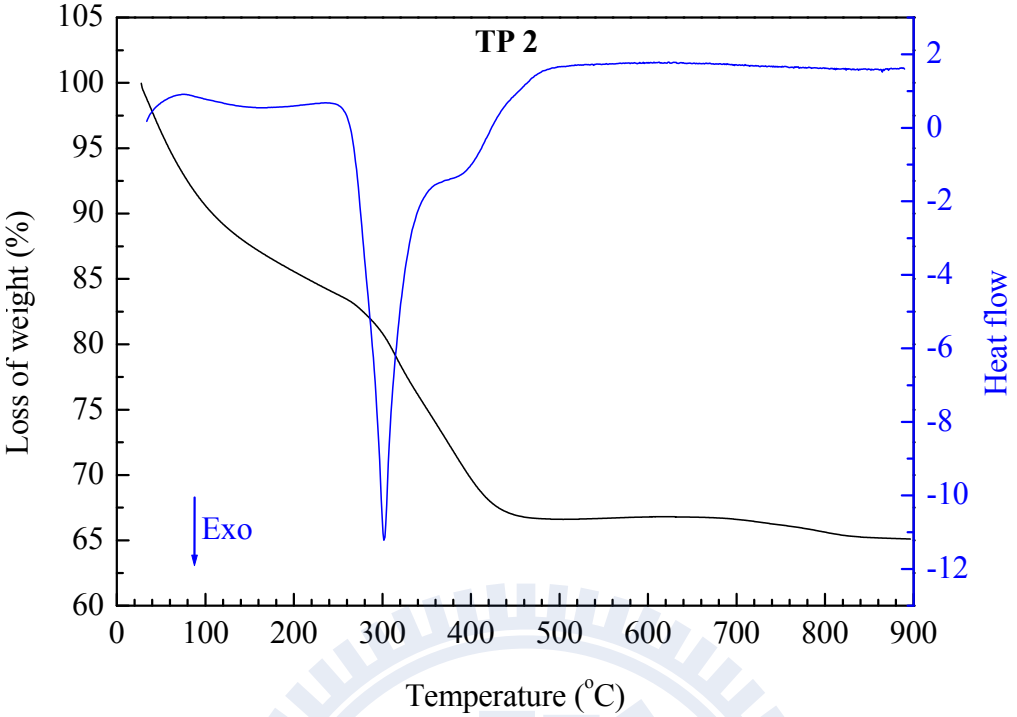

Figure 4-11 The TGA/DSC curve of TP 2.

Table 4-7 The weight loss of TP and TP-B samples.

Weight loss (%)	RT-100°C	100-260°C	260-550°C
TP 1	7	10	9
TP 2	12	6	14
TP 3	7	5	21
TP 4	8	5	22
TP 5	7	6	22
TP 2-B0.3	6	6	17
TP 2-B0.8	6	6	17
TP 2-B1.2	7	6	17

4-4. Adsorption isotherm

Surface modifier and surface areas play an important role in the photocatalytic activities because they dominate the adsorption ability and reaction sites of the catalysts. Figure 4-12 displays the adsorption isotherms of the TOPO-TiO_2 and pure TiO_2 toward BPA. Both P25 and the non-hydrolytic sol-gel derived TiO_2 adsorbed little amount of BPA. This phenomenon reveals that surface Ti-OH has small affinity toward the target compound. In contrast, all TOPO-TiO_2 samples showed high level of adsorptions. Linear dependence of the adsorption amounts upon equilibrium concentration in the TP 4 and TP 5 suspensions indicates that BPA is partitioned to the surface of the samples. The nonspecific physisorption is resulted from their TOPO-capped surface. The TP 2 and TP 3 exhibited a sigmoid adsorption. The concave upward curve at low BPA concentrations followed Type Ⅲ adsorption isotherm, suggesting the interactions between the adsorbates were stronger than those between the adsorbate and the samples[108]. This phenomenon was induced by the π-π interaction between the BPA molecules adsorbed in the meso- or micro-pores. In addition, capillary force assists BPA molecules rapidly congealed into the pores. Due to the pore size of the TP 2 was smaller than the TP 3, the TP 2 exhibited a higher adsorption ability than the TP 3. Apparently, TP 1 reached a saturated adsorption of 25.6 mg/g. The low amounts of the bonded TOPO restricted its adsorption capacity. However, the TP 1 showed similar adsorption ability to the TP 2 at low BPA concentrations, indicating their similar TOPO-contained pore structures. After addition of TMB, the adsorption capacity of the TP 2 decreased from 54.9 to 21.1-46.3 mg/g at the initial concentration of 80 mg/g. The decreased adsorption ability was due to the expanded pore sizes caused by the presence of BPA.

Figure 4-13 shows the time domain of 10 mg/L BPA adsorption on P25, pure non-hydrolytic sol-gel derived TiO_2, the TP and TP-B samples. The P25 and pure TiO_2,

TP 2, TP 3, TP 4 and TP 5 reached adsorption equilibrium within 10 minutes. However, the adsorption equilibrium time of the TP 1 extended to 30 minutes. This phenomenon reveals that large surface tension resulted from microporous structures initially inhibit the diffusion of BPA into the pores. It is noted that the equilibrium time of the TP 2 was largely shorten to 2 minutes after addition of TMB. The expanded pores sizes reduced the surface tension, thus promoting the adsorption kinetics.

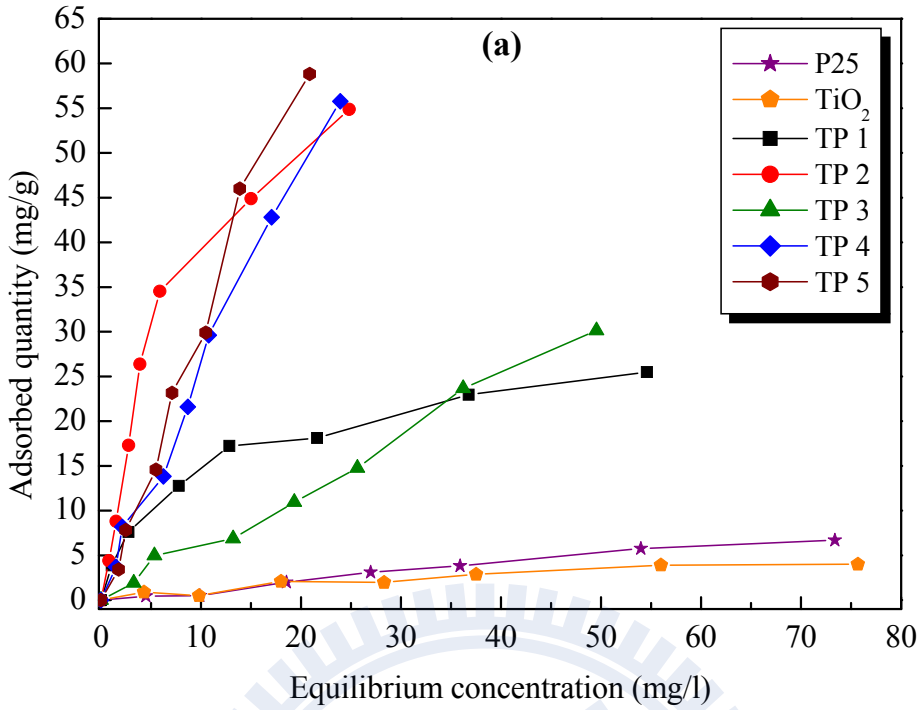

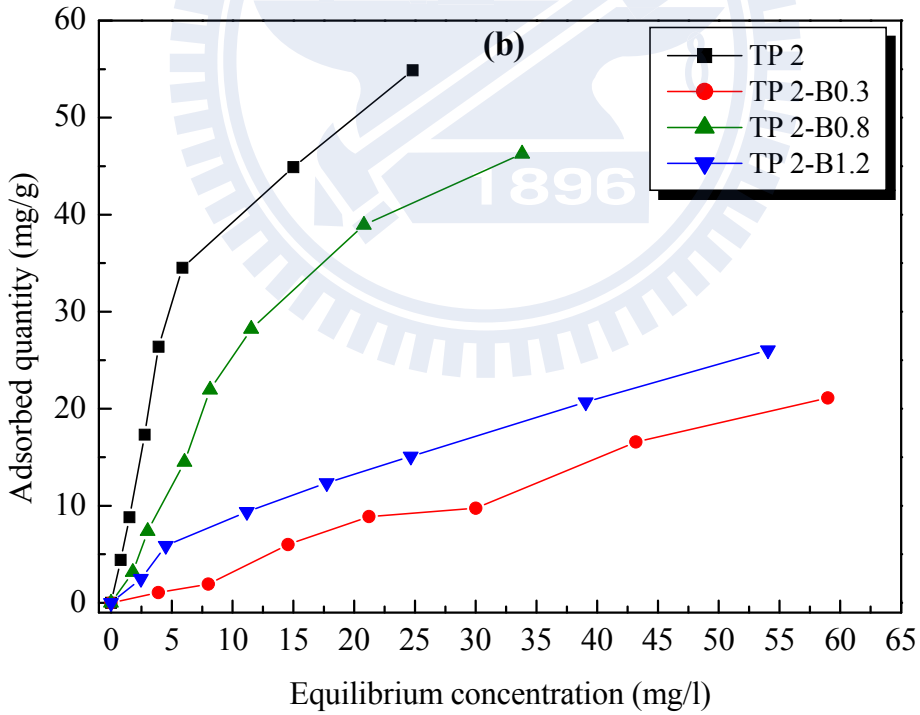

Figure 4-12 Adsorption of BPA in the suspensions of (a) TP samples and pure TiO_2, (b) the TP 2-B samples.

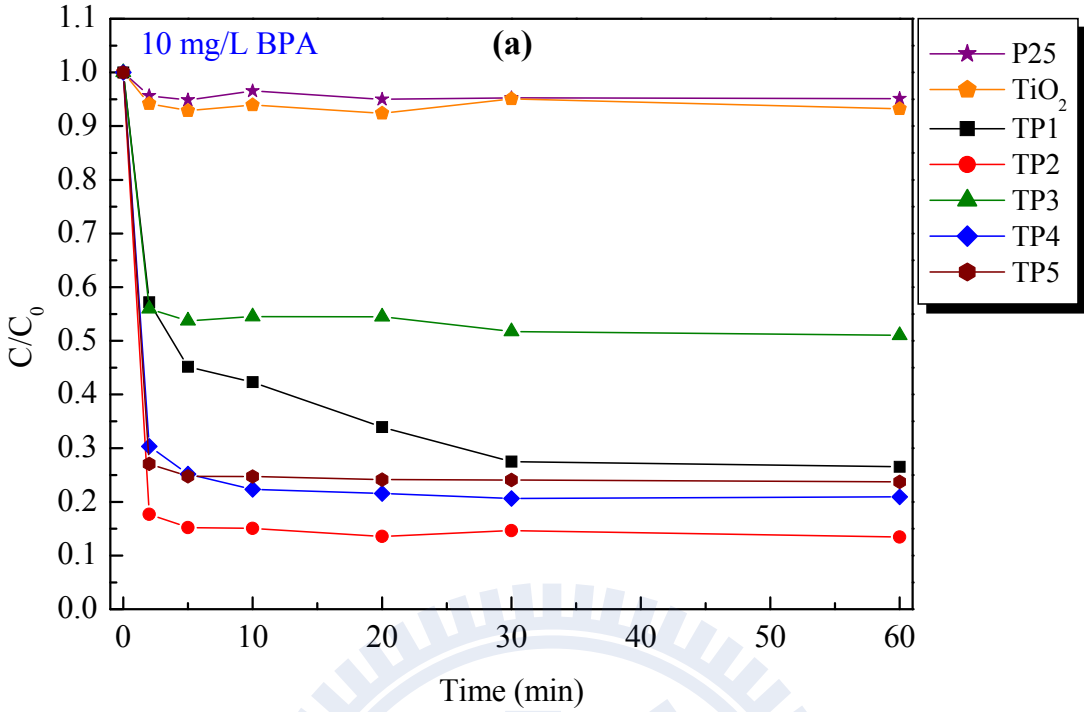

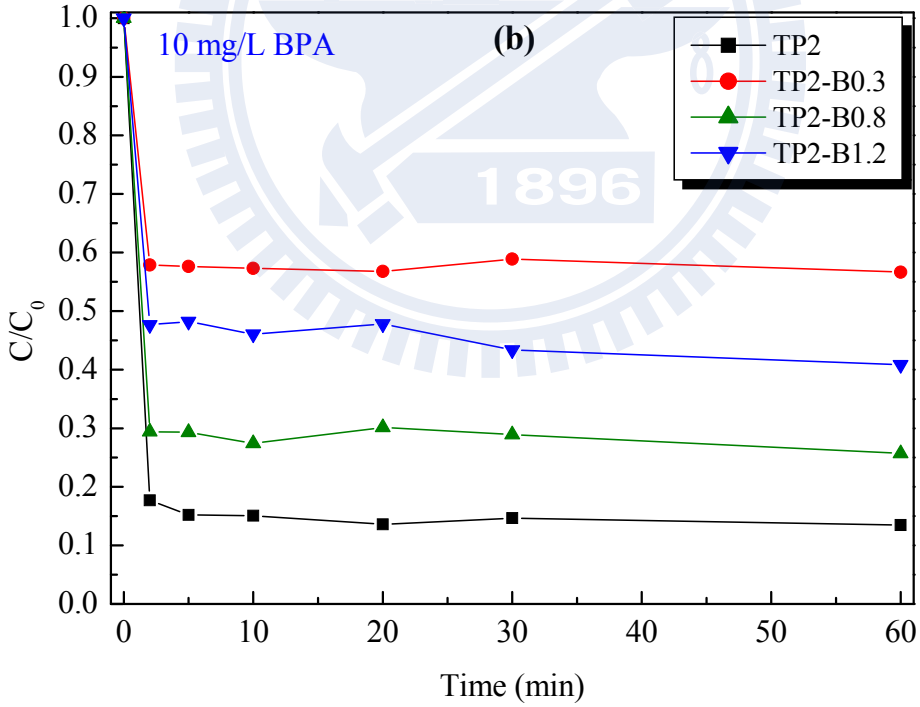

cd

Figure 4-13 Adsorption equilibrium of 10 mg/L BPA in the suspensions of (a) TP samples and pure TiO_2, (b) the TP 2-B samples.

4-5. Photocatalytic activity

Figure 4-14 shows the photocatalytic decomposition of 10 mg/L BPA in the presence of pure TiO_2, TP and TP-B samples. The TP samples reduced 46-75% BPA in the initial 30 minutes of dark adsorption. However, the pure TiO_2 and P25 reduced 1% BPA only. Photodegradation of BPA by the TP samples reached 95% removal efficiency in next 90 minutes, while the TiO_2 degraded 70% BPA in the same period. The high removal efficiencies of the TOPO-TiO_2 was mainly contributed by pore structure and lost of stabilized charges which improved compound from bulk solution diffuse to the surface effectively and facilitated interfacial charge transfer[8,101]. It is noted that the photodegradation by TP 2 was limited to 95% because its high surface tension inhibits the diffusion of BPA into the porous structure. TP-B samples showed relatively low removal efficiencies than TP 2. In addition, the initial photocatalytic degradation rate of TP 2, TP 2-B0.3, TP 2-B0.8, and TP 2-B1.2 was 0.19, 0.21, 0.15, and 0.11, respectively, for the initial concentration of 2.51, 8.23, 3.30, and 5.26 mL/g. Because degradation rates are correlated to concentrations of a target compound, TP 2 exhibited higher photocatalytic activity than TP 2-B samples. The higher photocatalytic activity was attributed to high adsorption ability of TP 2[101]. To compare the photocatalytic activity of the porous TOPO-modified TiO_2 with commercial product P25, TP 2 was selected as the model compound because it showed the highest adsorption affinity for BPA. The high adsorption ability of TP 2 led its photocatalytic kinetics not satisfying pseudo-first order kinetics. Thus, transformed Langmuir-Hinshelwood kinetics model is used (shown in equation 4-1):

$$\frac{1}{r} = \frac{1}{k_r} + \frac{1}{k_r K_a} \times \frac{1}{C} \qquad (4\text{-}1)$$

where r is the initial rate of photocatalytic degradation fro BPA, C represents the concentration of the BPA, k_r and K_a are the kinetic rate constant and adsorption coefficient,

respectively. The k_r and K_a were obtained from the intercept and slope of the linear fit of 1/r versus 1/C, respectively. Figure 4-15 shows the plot of the linear fit of 1/r versus 1/C for Langmuir-Hinshelwood model. Table 4-8 were summarized the rate constants and adsorption coefficients of BPA in the TP 2 and P25 suspensions. The TP 2 exhibited a k_r and K_a of 6.58×10^{-1} mg/L-min and 8.89×10^{-2} L/mg, respectively. P25 showed the k_r and K_a of 4.43×10^{-1} mg/L-min and 8.55 L/mg, respectively. The k_r of TP 2 was 1.5 times higher than P25. Higher adsorption ability improved the attachment of BPA to the surface of TP 2 and apparently enhanced electron transfer process. However, the K_a of TP 2 was relatively smaller than P25 due to its poor crystallinity. Large amounts of surface defect energy levels between bands inhibited the kinetic absorption. It also resulted in lower $k_r \times K_a$ product of TP 2 (5.85×10^{-2} min^{-1}) than that of P25 (3.71 min^{-1}). The poor crystallinity of TP samples is limited by the heating process used in this study. Conventional conductive heating causes poor and inhomogeneous dissipation of thermal energy through whole preparation systems, especially when solid TiO_2 gel is formed. Thus, short heating time was taken in order to avoid thermal decomposition of organic TOPO. This problem could be solved in case a heating method which allows thermal energy penetrating matrix rapidly and homogeneously, like microwave, is used for the preparation. However, this study demonstrated that surface modified porous TiO_2 was successfully obtained using a templated non-hydrolytic sol-gel method.

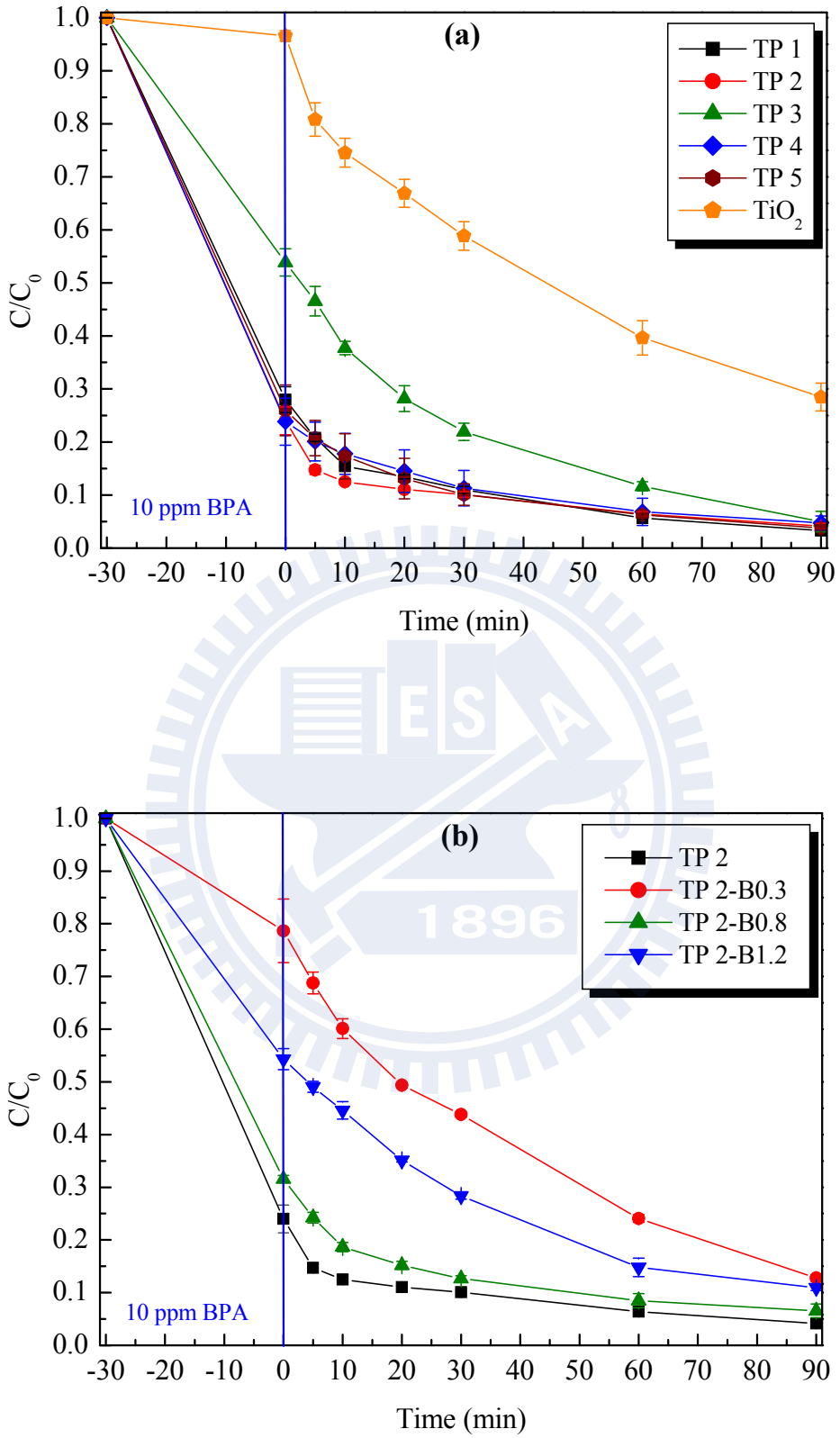

Figure 4-14 The photodegradation of 10 mg/L BPA by (a) TP samples and pure TiO_2, (b) TP 2-B samples.

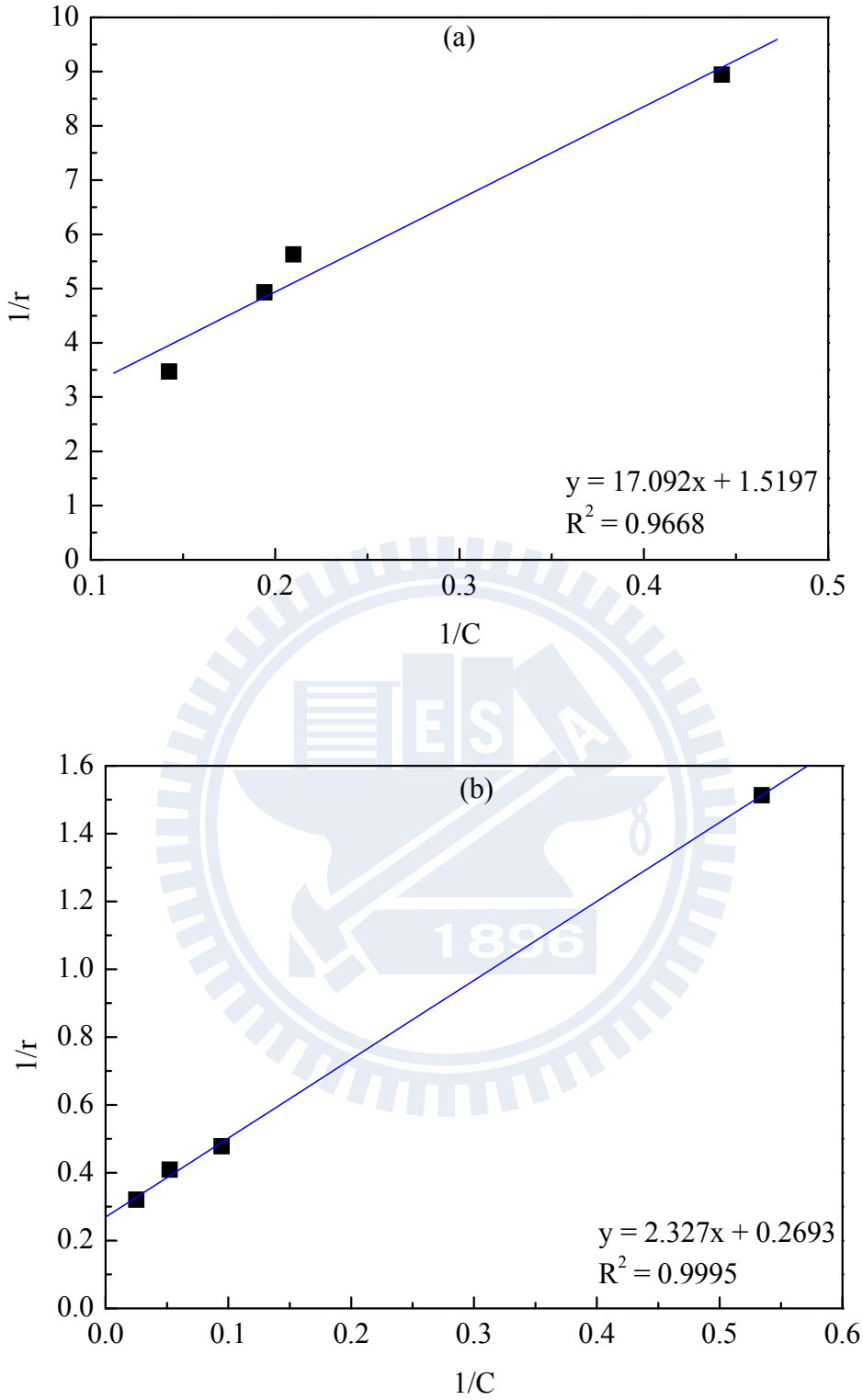

Figure 4-15 A plot of the linear fit of 1/r versus 1/C of (a) TP 2 and (b) P25.

Table 4-8 The rate constants (k_r) and adsorption coefficients (K_a) of BPA in the TP 2 and P25 suspensions.

	k_r (mg/L -min)	K_a (l/mg)	$k_r \times K_a$	R^2
TP 2	6.58×10^{-1}	8.89×10^{-2}	5.85×10^{-2}	0.967
P25	4.43×10^{-1}	8.55	3.71	0.999

Chapter 5. Conclusions

TOPO-modified mesoporous TiO_2 have been successfully synthesized via a non-hydrolytic sol-gel method. The mesoporous structure was formed when the TOPO/Ti ratio was 0.05. At the TOPO/Ti ratio of 0.1, the pore shape changed to microporous structure. TMB is a hydrophobic substance and can assist TOPO to self-assemble micelles in hydrophilic media. The TMB addition would led micro- and continuous porous samples exhibiting Type Ⅳ isotherm and increases in specific surface areas, pore volumes and pore size. High preparation temperature resulted in anatase crystals in the as-prepared samples. In addition, the TOPO was chemically bonded to the TiO_2 surface through the formation of P-O-Ti bonds. Hence, the TOPO-TiO_2 samples contained hydrophobic feature inside the pores and hydrophilic property on the outer surface. The TOPO played an important role in the mechanisms and kinetics of the photocatalysis in the modified mesoporous TiO_2 system. TOPO-modified micropores exhibited remarkably high adsorption affinity toward BPA because of high surface area, hydrophobic interactions and capillary force. In addition, the modified mesoporous samples exhibited higher photocatalytic activity over pure TiO_2 and P25. The improved adsorption resulting from the exceptional porous structure contributed to the high photocatalytic activity of the TOPO-modified TiO_2.

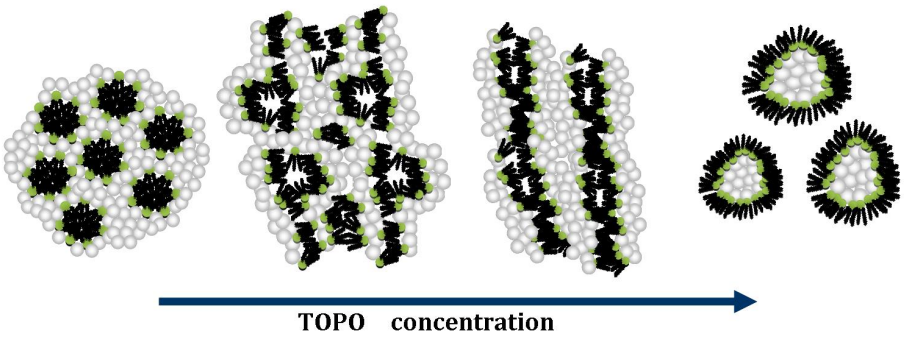

Figure 5-1 The TOPO concentration has influenced of pore structure.

References

(1) Kim, T. K.; Lee, M. N.; Lee, S. H.; Park, Y. C.; Jung, C. K.; Boo, J. H. *Thin Solid Films* **2005**, *475*, 171-77.

(2) Ren, W. J.; Ai, Z. H.; Jia, F. L.; Zhang, L. Z.; Fan, X. X.; Zou, Z. G. *Applied Catalysis B-Environmental* **2007**, *69*, 138-44.

(3) Wang, H. W.; Kuo, C. H.; Lin, H. C.; Kuo, I. T.; Cheng, C. F. *Journal of the American Ceramic Society* **2006**, *89*, 3388-92.

(4) Zhao, D.; Chen, C. C.; Wang, Y. F.; Ji, H. W.; Ma, W. H.; Zang, L.; Zhao, J. C. *Journal of Physical Chemistry C* **2008**, *112*, 5993-6001.

(5) Chang, S. M.; Chen, T. Y. "*Preparation of surface salicylic acid modified titanium dioxide photocatalyst using microwave assisted method*"; 236th ACS Annual Meeting, **2008**, Philadelphia, PA, USA.

(6) Chang, S. M.; Hou, C. Y.; Lo, P. H.; Chang, C. T. *Applied Catalysis B-Environmental* **2009**, *90*, 233-41.

(7) Bannat, I.; Wessels, K.; Oekermann, T.; Rathousky, J.; Bahnemann, D.; Wark, M. *Chemistry of Materials* **2009**, *21*, 1645-53.

(8) Chang, S. M.; Lo, P. H.; Chang, C. T. *Applied Catalysis B-Environmental* **2009**, *91*, 619-27.

(9) Yu, J. C.; Zhang, L. Z.; Zheng, Z.; Zhao, J. C. *Chemistry of Materials* **2003**, *15*, 2280-86.

(10) An, T. C.; Liu, J. K.; Li, G. Y.; Zhang, S. Q.; Zhao, H. J.; Zeng, X. Y.; Sheng, G. Y.; Fu, J. M. *Applied Catalysis A-General* **2008**, *350*, 237-43.

(11) Yu, J. G.; Zhang, L. J.; Cheng, B.; Su, Y. R. *Journal of Physical Chemistry C* **2007**, *111*, 10582-89.

(12) Yu, J. G.; Wang, G. H.; Cheng, B.; Zhou, M. H. *Applied Catalysis B-Environmental*

2007, *69*, 171-80.

(13) Rossmanith, R.; Weiss, C. K.; Geserick, J.; Husing, N.; Hormann, U.; Kaiser, U.; Landfester, K. *Chemistry of Materials* **2008**, *20*, 5768-80.

(14) Calleja, G.; Serrano, D. P.; Sanz, R.; Pizarro, P.; Garcia, A. *Industrial & Engineering Chemistry Research* **2004**, *43*, 2485-92.

(15) On, D. T. *Langmuir* **1999**, *15*, 8561-64.

(16) Kresge, C. T.; Leonowicz, M. E.; Roth, W. J.; Vartuli, J. C.; Beck, J. S. *Nature* **1992**, *359*, 710-12.

(17) Huang, D.; Wang, Y. J.; Yang, L. M.; Luo, G. S. *Microporous and Mesoporous Materials* **2006**, *96*, 301-06.

(18) Kim, D. S.; Kwak, S. Y. *Applied Catalysis A-General* **2007**, *323*, 110-18.

(19) Peng, T. Y.; Zhao, D.; Dai, K.; Shi, W.; Hirao, K. *Journal of Physical Chemistry B* **2005**, *109*, 4947-52.

(20) Tian, G. H.; Fu, H. G.; Jing, L. Q.; Xin, B. F.; Pan, K. *Journal of Physical Chemistry C* **2008**, *112*, 3083-89.

(21) Soler-Illia, G. J. D. A.; Louis, A.; Sanchez, C. *Chemistry of Materials* **2002**, *14*, 750-59.

(22) Kim, D. S.; Han, S. J.; Kwak, S. Y. *Journal of Colloid and Interface Science* **2007**, *316*, 85-91.

(23) Yu, J. C.; Zhang, L. Z.; Yu, J. G. *Chemistry of Materials* **2002**, *14*, 4647-53.

(24) Chen, L.; Yao, B.; Cao, Y.; Fan, K. *Journal of Physical Chemistry C* **2007**, *111*, 11849-53.

(25) Antonelli, D. M. *Microporous and Mesoporous Materials* **1999**, *30*, 315-19.

(26) Yoshitake, H.; Sugihara, T.; Tatsumi, T. *Chemistry of Materials* **2002**, *14*, 1023-29.

(27) Wang, Y. Q.; Tang, X. H.; Yin, L. X.; Huang, W. P.; Hacohen, Y. R.; Gedanken, A. *Advanced Materials* **2000**, *12*, 1183-86.

(28) Pavasupree, S.; Ngamsinlapasathian, S.; Suzuki, Y.; Yoshikawa, S. *Materials Letters* **2007**, *61*, 2973-77.

(29) Jitputti, J.; Pavasupree, S.; Suzuki, Y.; Yoshikawa, S. *Journal of Solid State Chemistry* **2007**, *180*, 1743-49.

(30) Kluson, P.; Kacer, P.; Cajthaml, T.; Kalaji, M. *Journal of Materials Chemistry* **2001**, *11*, 644-51.

(31) Ou, Y.; Lin, J. D.; Zou, H. M.; Liao, D. W. *Journal of Molecular Catalysis A-Chemical* **2005**, *241*, 59-64.

(32) Yu, J. C.; Ho, W. K.; Yu, J. G.; Hark, S. K.; Iu, K. *Langmuir* **2003**, *19*, 3889-96.

(33) Tian, G.; Fu, H.; Jing, L.; Xin, B.; Pan, K. *J. Phys. Chem. C* **2008**, *112*, 3083-89.

(34) Linsebigler, A. L.; Lu, G. Q.; Yates, J. T. *Chemical Reviews* **1995**, *95*, 735-58.

(35) Fujishima, A.; Honda, K. *Nature* **1972**, *238*, 37-38.

(36) Sreethawong, T.; Suzuki, Y.; Yoshikawa, S. *Journal of Solid State Chemistry* **2005**, *178*, 329-38.

(37) Vainshtein, B. K.; Fridkin, W. M.; Indenbom, V. L. *Structure of Crystals. Berlin:Macmillan India Ltd* **1994**.

(38) Corma, A. *Chemical Reviews* **1997**, *97*, 2373-419.

(39) Lin, J.; Brown, C. W. *Trac-Trends in Analytical Chemistry* **1997**, *16*, 200-11.

(40) Chandrappa, G. T.; Steunou, N.; Livage, J. *Nature* **2002**, *416*, 702-02.

(41) Corbin, S. F.; Apte, P. S. *Journal of the American Ceramic Society* **1999**, *82*, 1693-701.

(42) Behrens, P. *Advanced Materials* **1993**, *5*, 127-32.

(43) Beck, J. S.; Vartuli, J. C.; Roth, W. J.; Leonowicz, M. E.; Kresge, C. T.; Schmitt, K. D.; Chu, C. T. W.; Olson, D. H.; Sheppard, E. W.; Mccullen, S. B.; Higgins, J. B.; Schlenker, J. L. *Journal of the American Chemical Society* **1992**, *114*, 10834-43.

(44) Ying, J. Y.; Mehnert, C. P.; Wong, M. S. *Angewandte Chemie-International Edition* **1999**, *38*, 56-77.

(45) Vartuli, J. C.; Kresge, C. T.; Roth, W. J.; McCullen, S. B.; Beck, J. S.; Schmitt, K. D.; Leonowicz, M. E.; Lutner, J. D.; W., E. Advanced Catalysis and Nanostructured Materials: Modern Synthesis Methods. New York, **1996**

(46) Huo, Q. S.; Margolese, D. I.; Ciesla, U.; Feng, P. Y.; Gier, T. E.; Sieger, P.; Leon, R.; Petroff, P. M.; Schuth, F.; Stucky, G. D. *Nature* **1994**, *368*, 317-21.

(47) Schmidt-Winkel, P.; Glinka, C. J.; Stucky, G. D. *Langmuir* **2000**, *16*, 356-61.

(48) Antonelli, D. M.; Ying, J. Y. *Angewandte Chemie-International Edition* **1995**, *34*, 2014-17.

(49) Luzzati, V.; Vargas, R.; Mariani, P.; Gulik, A.; Delacroix, H. *Journal of Molecular Biology* **1993**, *229*, 540-51.

(50) Smarsly, B.; Grosso, D.; Brezesinski, T.; Pinna, N.; Boissiere, C.; Antonietti, M.; Sanchez, C. *Chemistry of Materials* **2004**, *16*, 2948-52.

(51) Miao, S. D.; Miao, Z. J.; Liu, Z. M.; Han, B. X.; Zhang, H.; Zhang, J. *Microporous and Mesoporous Materials* **2006**, *95*, 26-30.

(52) Wong, M. S.; Ying, J. Y. *Chemistry of Materials* **1998**, *10*, 2067-77.

(53) Serrano, D. P.; Calleja, G.; Sanz, R.; Pizarro, P. *Journal of Materials Chemistry* **2007**, *17*, 1178-87.

(54) Wang, L.; Yan, Z.; Qiao, S.; Lu, G. Q. M.; Huang, Y. *Journal of Colloid and Interface Science* **2007**, *316*, 954-61.

(55) Stone, V. F.; Davis, R. J. *Chemistry of Materials* **1998**, *10*, 1468-74.

(56) Konishi, J.; Fujita, K.; Nakanishi, K.; Hirao, K. *Chemistry of Materials* **2006**, *18*, 6069-74.

(57) Addamo, M.; Augugliaro, V.; Di Paola, A.; Garcia-Lopez, E.; Loddo, V.; Marci, G.; Molinari, R.; Palmisano, L.; Schiavello, M. *Journal of Physical Chemistry B* **2004**, *108*, 3303-10.

(58) Wu, L.; Yu, J. C.; Wang, X. C.; Zhang, L. H.; Yu, J. G. *Journal of Solid State Chemistry*

2005, *178*, 321-28.

(59) Huang, D.; Wang, Y. J.; Cui, Y. C.; Luo, G. S. *Microporous and Mesoporous Materials* **2008**, *116*, 378-85.

(60) Keller, V.; Bernhardt, P.; Garin, F. *Journal of Catalysis* **2003**, *215*, 129-38.

(61) Li, H. X.; Bian, Z. F.; Zhu, J.; Huo, Y. N.; Li, H.; Lu, Y. F. *Journal of the American Chemical Society* **2007**, *129*, 4538-39.

(62) Krylova, G. V.; Gnatyuk, Y. I.; Smirnova, N. P.; Eremenko, A. M.; Gun'ko, V. M. *Journal of Sol-Gel Science and Technology* **2009**, *50*, 216-28.

(63) Zhang, F. L.; Zheng, Y. H.; Cao, Y. N.; Chen, C. Q.; Zhan, Y. Y.; Lin, X. Y.; Zheng, Q.; Wei, K. M.; Zhu, J. F. *Journal of Materials Chemistry* **2009**, *19*, 2771-77.

(64) Jin, S.; Shiraishi, F. *Chemical Engineering Journal* **2004**, *97*, 203-11.

(65) Yan, P. F.; Zhou, D. R.; Wang, J. Q.; Yang, L. B.; Zhang, D.; Fu, H. G. *Chemical Journal of Chinese Universities-Chinese* **2002**, *23*, 2317-21.

(66) Yamashita, H.; Harada, M.; Misaka, J.; Takeuchi, M.; Neppolian, B.; Anpo, M. *Catalysis Today* **2003**, *84*, 191-96.

(67) Wu, S. X.; Ma, Z.; Qin, Y. N.; Qi, X. Z.; Liang, Z. C. *Acta Physico-Chimica Sinica* **2004**, *20*, 138-43.

(68) Quan, X. J.; Zhao, Q. H.; Tan, H. Q.; Sang, X. M.; Wang, F. P.; Dai, Y. *Materials Chemistry and Physics* **2009**, *114*, 90-98.

(69) Huo, Y. N.; Zhu, J.; Li, J. X.; Li, G. S.; Li, H. X. *Journal of Molecular Catalysis A-Chemical* **2007**, *278*, 237-43.

(70) Makarova, O. V.; Rajh, T.; Thurnauer, M. C.; Martin, A.; Kemme, P. A.; Cropek, D. *Environmental Science & Technology* **2000**, *34*, 4797-803.

(71) Xagas, A. P.; Bernard, M. C.; Hugot-Le Goff, A.; Spyrellis, N.; Loizos, Z.; Falaras, P. *Journal of Photochemistry and Photobiology A-Chemistry* **2000**, *132*, 115-20.

(72) Jiang, D.; Xu, Y.; Hou, B.; Wu, D.; Sun, Y. H. *Journal of Solid State Chemistry* **2007**,

180, 1787-91.

(73) Yamashita, H.; Nishida, Y.; Yuan, S.; Mori, K.; Narisawa, M.; Matsumura, Y.; Ohmichi, T.; Katayama, I. *Catalysis Today* **2007**, *120*, 163-67.

(74) Comparelli, R.; Fanizza, E.; Curri, M. L.; Cozzoli, P. D.; Mascolo, G.; Passino, R.; Agostiano, A. *Applied Catalysis B-Environmental* **2005**, *55*, 81-91.

(75) Angelome, P. C.; Soler-Illia, G. J. D. A. A. *Chemistry of Materials* **2005**, *17*, 322-31.

(76) Hench, L. L.; West, J. K. *Chemical Reviews* **1990**, *90*, 33-72.

(77) Su, C.; Hong, B. Y.; Tseng, C. M. *Catalysis Today* **2004**, *96*, 119-26.

(78) Cushing, B. L.; Kolesnichenko, V. L.; O'Connor, C. J. *Chemical Reviews* **2004**, *104*, 3893-946.

(79) Corriu, R. J. P.; Leclercq, D.; Lefevre, P.; Mutin, P. H.; Vioux, A. *Journal of Materials Chemistry* **1992**, *2*, 673-74.

(80) Andrianainarivelo, M.; Corriu, R. J. P.; Leclercq, D.; Mutin, P. H.; Vioux, A. *Journal of Materials Chemistry* **1997**, *7*, 279-84.

(81) Hay, J. N.; Raval, H. M. *Chemistry of Materials* **2001**, *13*, 3396-403.

(82) Guo, G. Q.; Whitesell, J. K.; Fox, M. A. *Journal of Physical Chemistry B* **2005**, *109*, 18781-85.

(83) Nakada, N.; Shinohara, H.; Murata, A.; Kiri, K.; Managaki, S.; Sato, N.; Takada, H. *Water Research* **2007**, *41*, 4373-82.

(84) Esplugas, S.; Bila, D. M.; Krause, L. G. T.; Dezotti, M. *Journal of Hazardous Materials* **2007**, *149*, 631-42.

(85) Rodriguez-Mozaz, S.; de Alda, M. J. L.; Barcelo, D. *Journal of Chromatography A* **2007**, *1152*, 97-115.

(86) Lee, W. S.; Takeuchi, T. *Analytical Sciences* **2005**, *21*, 1125-28.

(87) Tai, C.; Jiang, G. B.; Liu, J. F.; Zhou, Q. F.; Liu, J. Y. *Journal of Photochemistry and Photobiology A-Chemistry* **2005**, *172*, 275-82.

(88) Wang, G. H.; Wu, F.; Zhang, X.; Luo, M. D.; Deng, N. S. *Journal of Photochemistry and Photobiology A-Chemistry* **2006**, *179*, 49-56.

(89) Kaneco, S.; Rahman, M. A.; Suzuki, T.; Katsumata, H.; Ohta, K. *Journal of Photochemistry and Photobiology A-Chemistry* **2004**, *163*, 419-24.

(90) Kang, J. H.; Kondo, F. *Archives of Environmental Contamination and Toxicology* **2002**, *43*, 265-69.

(91) Xuan, Y. J.; Endo, Y.; Fujimoto, K. *Journal of Agricultural and Food Chemistry* **2002**, *50*, 6575-78.

(92) Sajiki, J. *Environment International* **2001**, *27*, 315-20.

(93) Belfroid, A.; van Velzen, M.; van der Horst, B.; Vethaak, D. *Chemosphere* **2002**, *49*, 97-103.

(94) Boscoletto, A. B.; Gottardi, F.; Milan, L.; Pannocchia, P.; Tartari, V.; Tavan, M.; Amadelli, R.; Debattisti, A.; Barbieri, A.; Patracchini, D.; Battaglin, G. *Journal of Applied Electrochemistry* **1994**, *24*, 1052-58.

(95) Ioan, I.; Wilson, S.; Lundanes, E.; Neculai, A. *Journal of Hazardous Materials* **2007**, *142*, 559-63.

(96) Watanabe, N.; Horikoshi, S.; Kawabe, H.; Sugie, Y.; Zhao, J. C.; Hidaka, H. *Chemosphere* **2003**, *52*, 851-59.

(97) Fukahori, S.; Ichiura, H.; Kitaoka, T.; Tanaka, H. *Environmental Science & Technology* **2003**, *37*, 1048-51.

(98) Chin, Y. P.; Miller, P. L.; Zeng, L. K.; Cawley, K.; Weavers, L. K. *Environmental Science & Technology* **2004**, *38*, 5888-94.

(99) Wang, R. C.; Ren, D. J.; Xia, S. Q.; Zhang, Y. L.; Zhao, J. F. *Journal of Hazardous Materials* **2009**, *169*, 926-32.

(100) Gao, B. F.; Lim, T. M.; Subagio, D. P.; Lim, T. T. *Applied Catalysis A-General* **2010**, *375*, 107-15.

(101) Guo, C. S.; Ge, M.; Liu, L.; Gao, G. D.; Feng, Y. C.; Wang, Y. Q. *Environmental Science & Technology* **2010**, *44*, 419-25.

(102) Staples, C. A.; Dorn, P. B.; Klecka, G. M.; O'Block, S. T.; Harris, L. R. *Chemosphere* **1998**, *36*, 2149-73.

(103) Uvarov, V.; Popov, I. *Materials Characterization* **2007**, *58*, 883-91.

(104) Lacombe, S.; Cardy, H.; Soggiu, N.; Blanc, S.; Habib-Jiwan, J. L.; Soumillion, J. P. *Microporous and Mesoporous Materials* **2001**, *46*, 311-25.

(105) Wilson, R. G.; Stevie, F. A.; Magee, C. W. *Secondary Ion Mass Spectrometry: A Practical Handbook for Depth Profiling and Bulk Impurity Analysis*, 1989.

(106) Chen, X.; Mao, S. S. *Chemical Reviews* **2007**, *107*, 2891-959.

(107) Korosi, L.; Papp, S.; Bertoti, I.; Dekany, I. *Chemistry of Materials* **2007**, *19*, 4811-19.

(108) Sing, K. S. W.; Everett, D. H.; Haul, R. A. W.; Moscou, L.; Pierotti, R. A.; Rouquerol, J.; Siemieniewska, T. *Pure and Applied Chemistry* **1985**, *57*, 603-19.

Appendix A. Zeta potential of TOPO-TiO_2 and Pure TiO_2

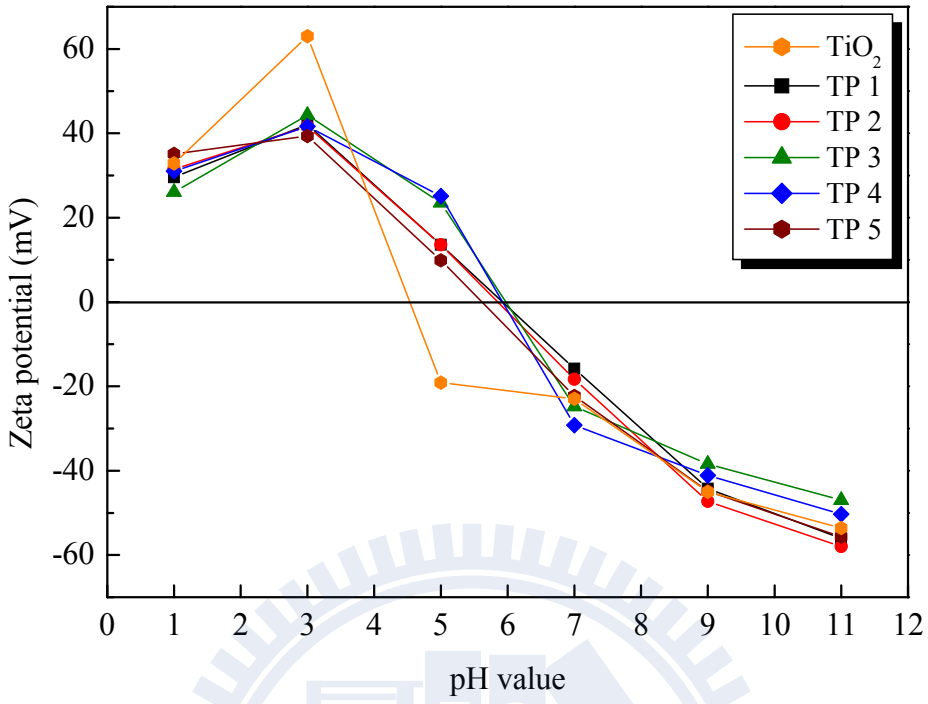

Appendix A-1 Zeta potential as a function of pH of TOPO-TiO_2 and TiO_2.

Appendix A-2 Surface zero point charge of TOPO-TiO_2 and TiO_2.

Sample	**TP 1**	**TP 2**	**TP 3**	**TP 4**	**TP 5**	**TiO_2**
Zpc	5.9	5.8	6.0	5.9	5.6	4.6

Appendix B. JCPDS database of TiO_2 (anatase)

21-1272 Quality: *

CAS Number:

Molecular Weight: 79.90
Volume[CD]: 136.31
Dx: 3.893 Dm:

S.G.: $I4_1/amd$ (141)
Cell Parameters:
a 3.785 b c 9.513
α β γ

SS/FOM: F30=74(.0116, 35)
I/Icor: 3.3
Rad:
Lambda:
Filter:
d-sp:

Mineral Name:
Anatase, syn

Ti O2
Titanium Oxide
Ref: Natl. Bur. Stand. (U.S.) Monogr. 25, 7, 82 (1969)

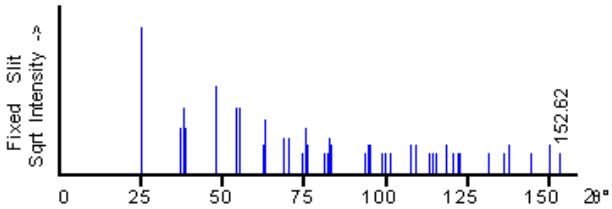

2θ	int-f	h	k	l	2θ	int-f	h	k	l	2θ	int-f	h	k	l
25.281	100	1	0	1	76.017	4	3	0	1	112.83	<2	3	0	7
36.946	10	1	0	3	80.725	<2	0	0	8	113.85	2	3	2	5
37.800	20	0	0	4	82.136	2	3	0	3	114.90	2	4	1	1
38.575	10	1	1	2	82.659	6	2	2	4	118.43	4	2	1	9
48.049	35	2	0	0	83.147	4	3	1	2	120.09	2	2	2	8
53.890	20	1	0	5	93.217	2	2	1	7	121.72	<2	4	1	3
55.060	20	2	1	1	94.178	4	3	0	5	122.33	2	4	0	4
62.119	4	2	1	3	95.139	4	3	2	1	131.02	2	4	2	0
62.688	14	2	0	4	98.315	2	1	0	9	135.99	<2	3	2	7
68.760	6	1	1	6	99.801	2	2	0	8	137.38	4	4	1	5
70.309	6	2	2	0	101.21	2	3	2	3	143.87	2	3	0	9
74.029	<2	1	0	7	107.44	4	3	1	6	150.02	4	4	2	4
75.029	10	2	1	5	108.95	4	4	0	0	152.62	2	0	0	12

Appendix B-1 JCPDS database of TiO_2.

Appendix C. EDX patterns of TP and TP 2-B samples

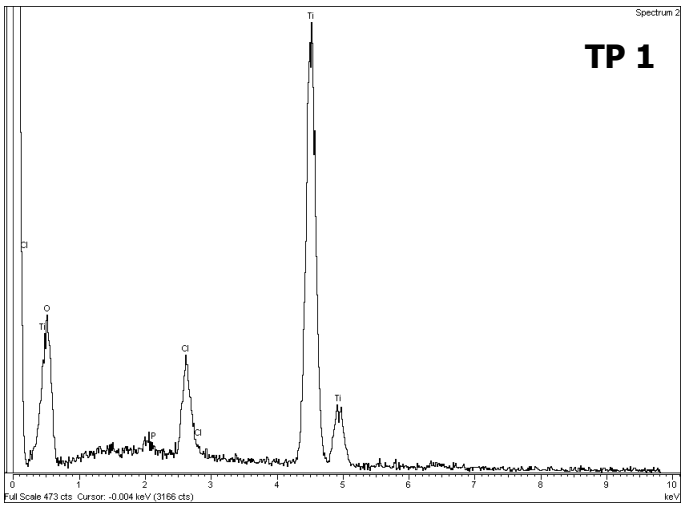
Spectrum 2
TP 1
Ti
Cl
O
Ti
Cl
P
Cl
Ti
0 1 2 3 4 5 6 7 8 9 10
Full Scale 473 cts Cursor: -0.004 keV (3166 cts)
keV

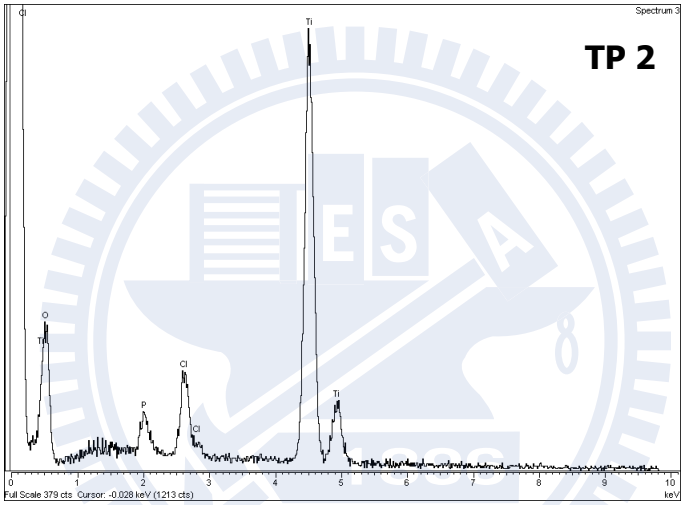
Spectrum 3
TP 2
Cl
Ti
O
Ti
Cl
P
Cl
Ti
0 1 2 3 4 5 6 7 8 9 10
Full Scale 379 cts Cursor: -0.028 keV (1213 cts)
keV

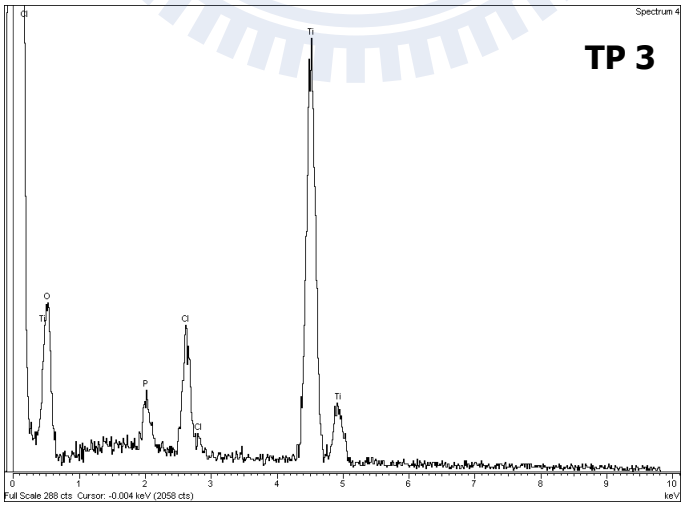
Spectrum 4
TP 3
Cl
Ti
O
Ti
Cl
P
Cl
Ti
0 1 2 3 4 5 6 7 8 9 10
Full Scale 288 cts Cursor: -0.004 keV (2058 cts)
keV

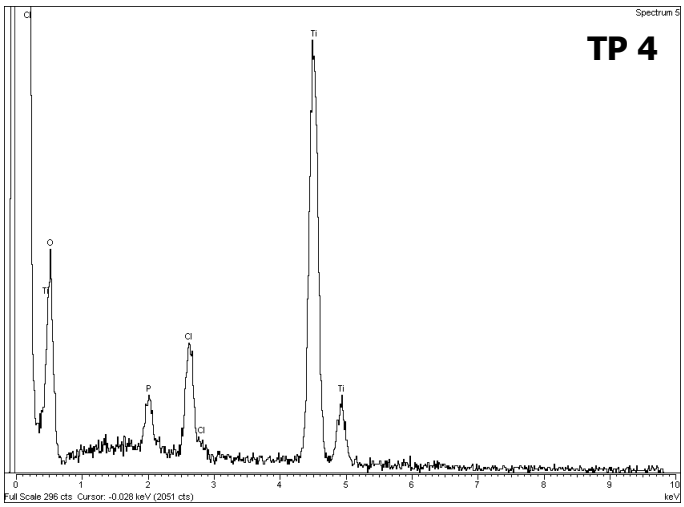
Spectrum 5
TP 4
Cl
Ti
O
Ti
Cl
P
Cl
Ti
0 1 2 3 4 5 6 7 8 9 10
Full Scale 296 cts Cursor: -0.028 keV (2051 cts)
keV

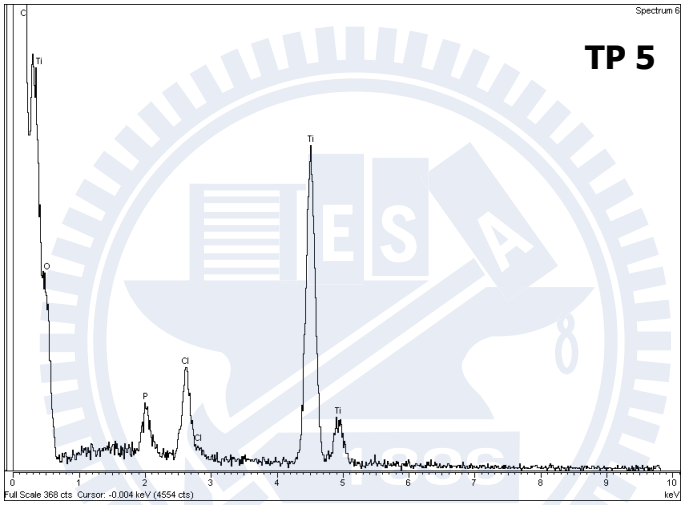
Spectrum 6
TP 5
C
Ti
O
Ti
Cl
P
Cl
Ti
0 1 2 3 4 5 6 7 8 9 10
Full Scale 368 cts Cursor: -0.004 keV (4554 cts)
keV

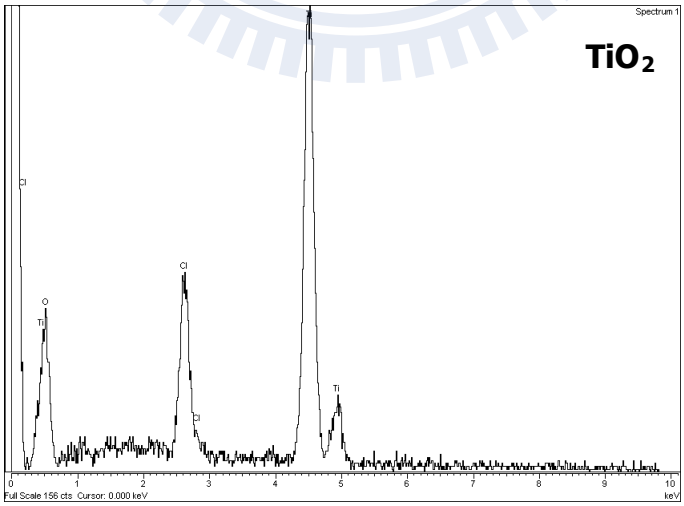
Spectrum 1
TiO_2
Cl
O
Ti
Cl
Cl
Ti
0 1 2 3 4 5 6 7 8 9 10
Full Scale 156 cts Cursor: 0.000 keV
keV

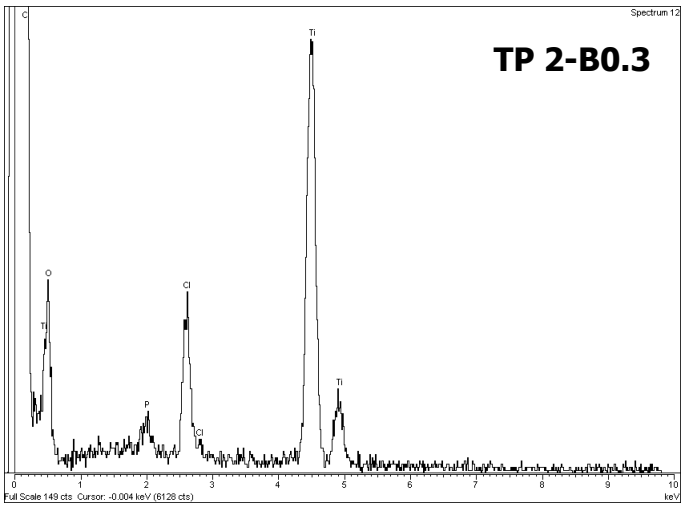

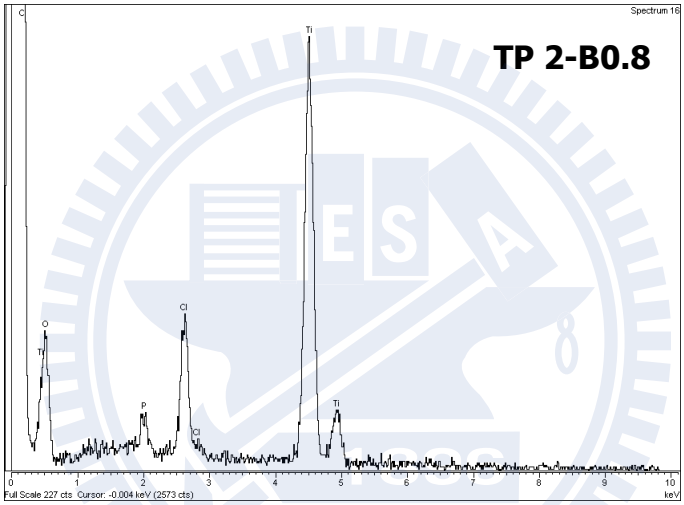

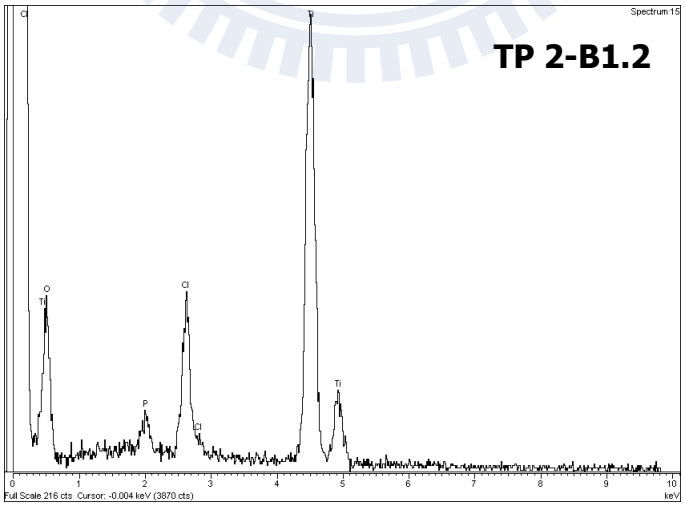

Appendix C-1 EDX patterns of TP, TP 2-B samples and TiO_2.

Appendix D. TGA/DSC curve of TP and TP 2-B samples

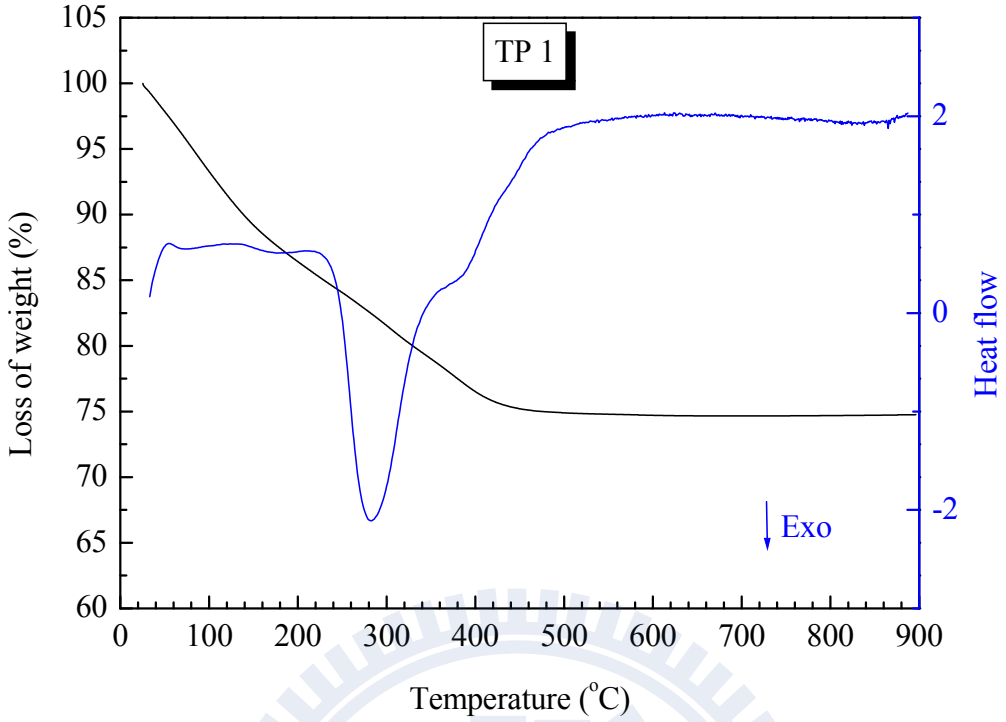
TP 1
Loss of weight (%)
Heat flow
Exo
Temperature (°C)
105
100
95
90
85
80
75
70
65
60
2
0
-2
0
100
200
300
400
500
600
700
800
900

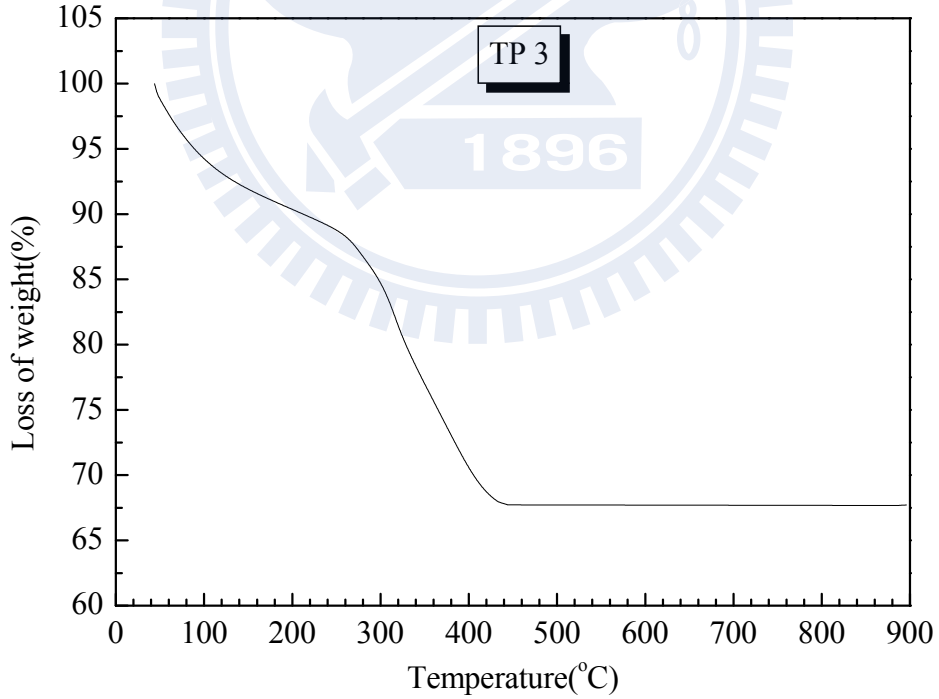
TP 3
Loss of weight(%)
Temperature(°C)
105
100
95
90
85
80
75
70
65
60
0
100
200
300
400
500
600
700
800
900

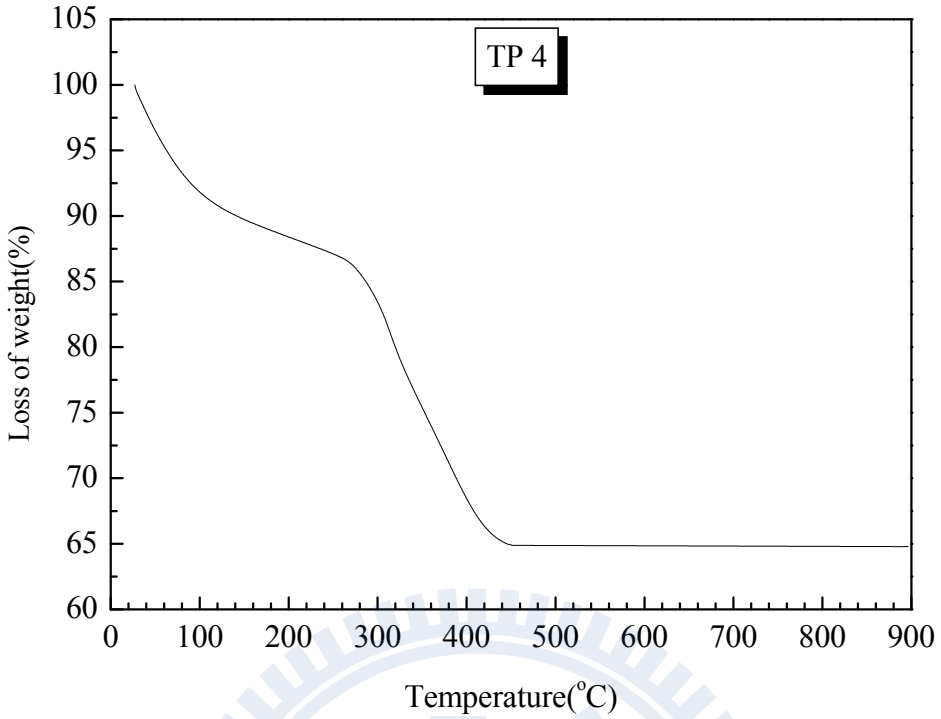
TP 4
Loss of weight(%)
105
100
95
90
85
80
75
70
65
60
0
100
200
300
400
500
600
700
800
900
Temperature(°C)

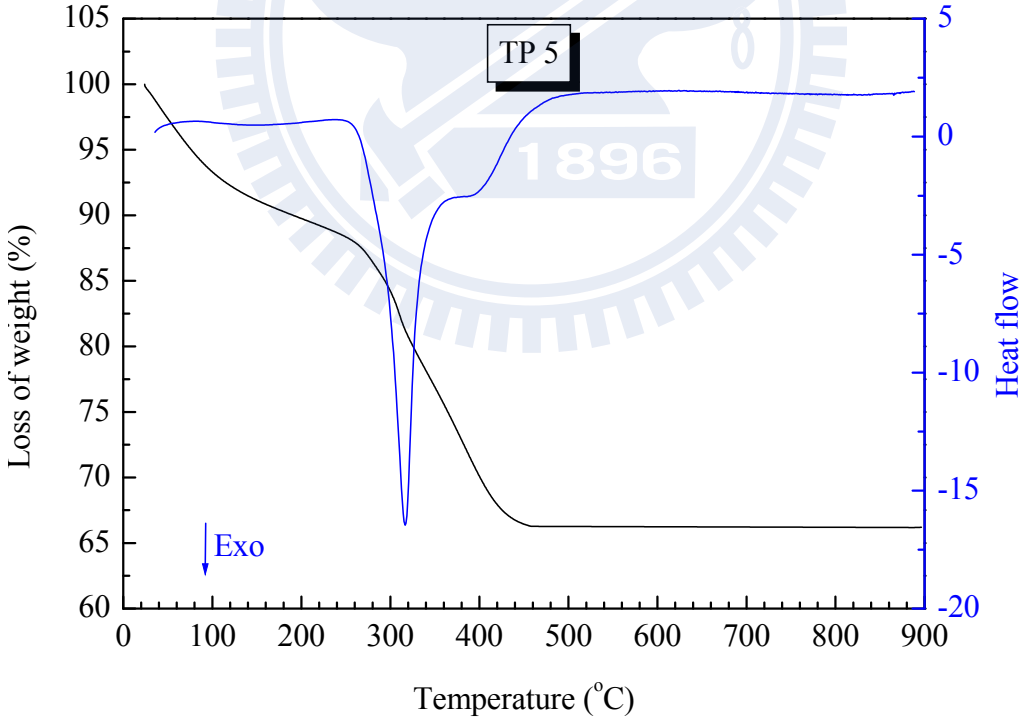
TP 5
Loss of weight (%)
105
100
95
90
85
80
75
70
65
60
Exo
5
0
-5
-10
-15
-20
Heat flow
0
100
200
300
400
500
600
700
800
900
Temperature (°C)

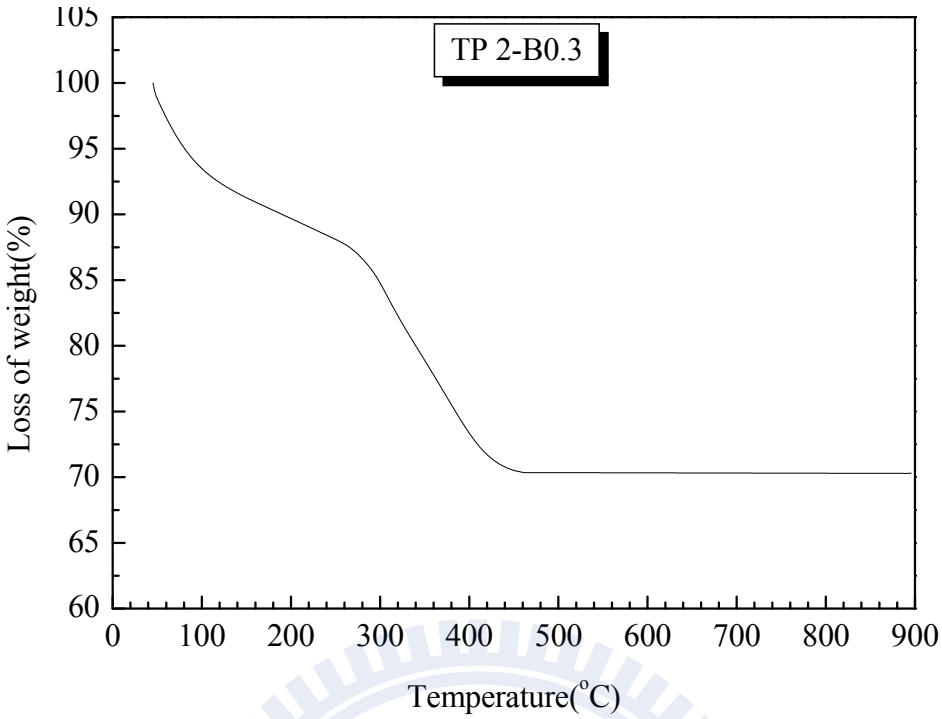
TP 2-B0.3
Loss of weight(%)
Temperature(°C)
105
100
95
90
85
80
75
70
65
60
0
100
200
300
400
500
600
700
800
900

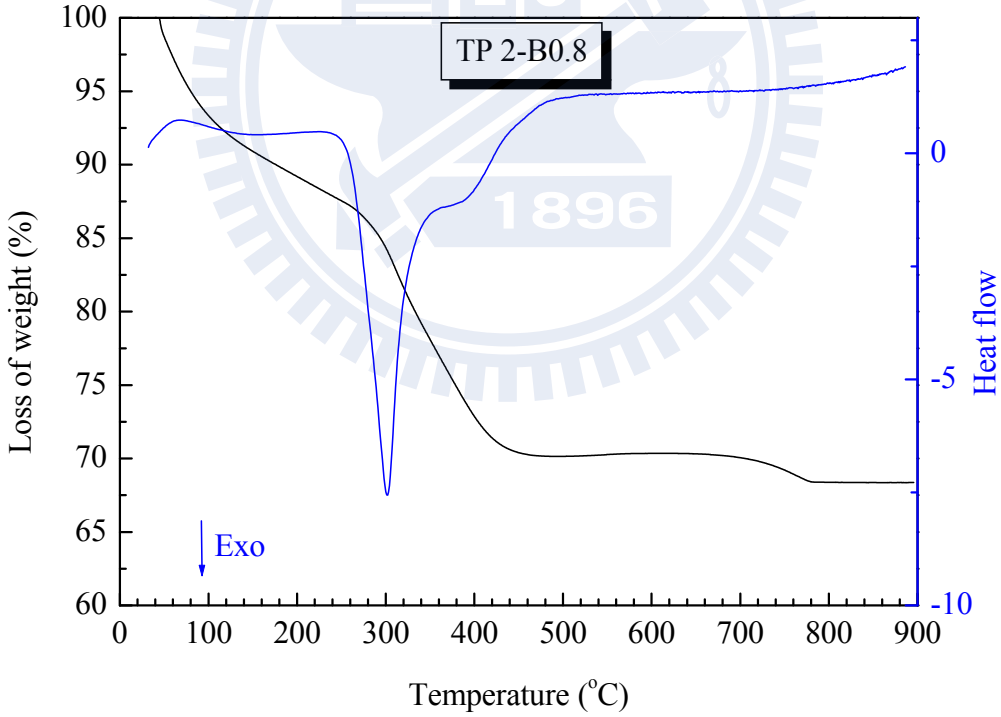
TP 2-B0.8
Loss of weight (%)
Heat flow
Temperature (°C)
Exo
100
95
90
85
80
75
70
65
60
0
-5
-10
0
100
200
300
400
500
600
700
800
900

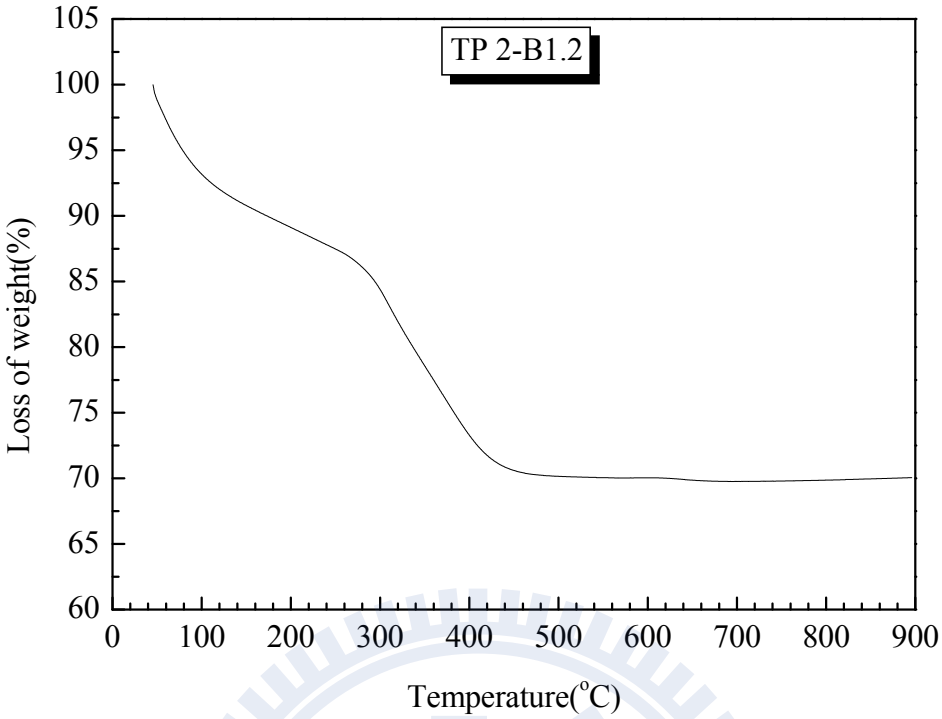

Appendix D-1 TGA/DSC curve of TP and TP 2-B samples.

Appendix E. Calibration curve of BPA solution

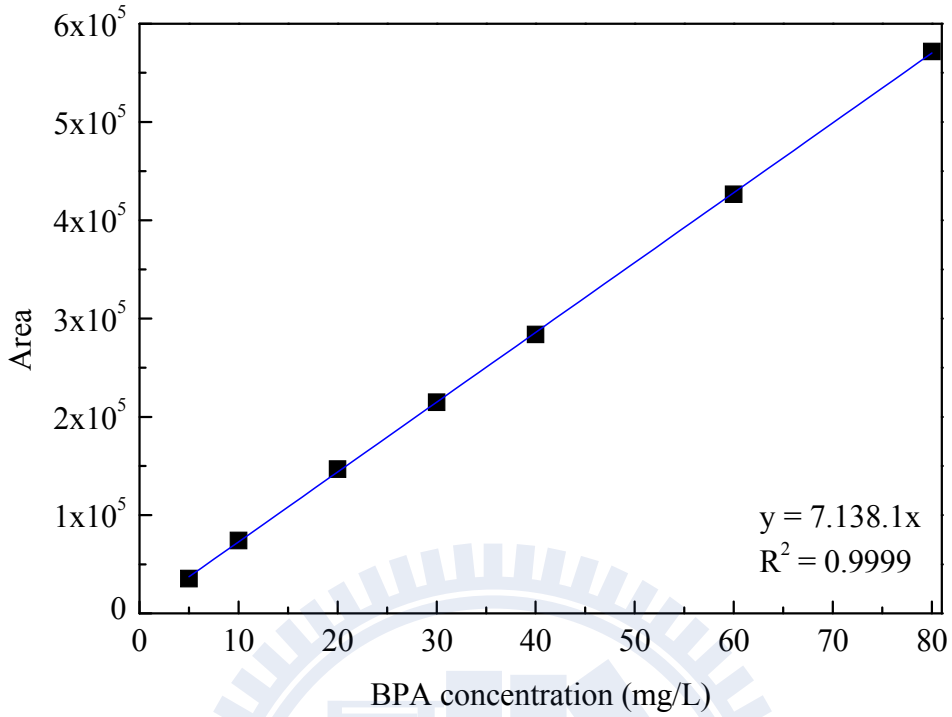

Appendix E-1 Calibration curve of BPA solution.

Appendix F. Photodegradation of various BPA concentrations

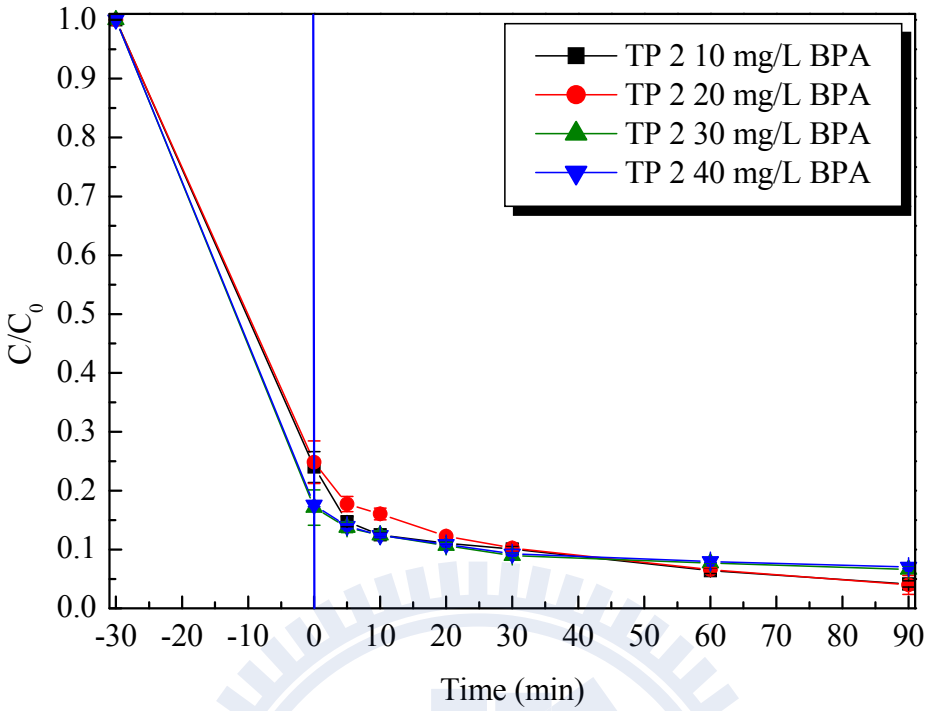

Appendix F-1 The photodegradation of various BPA concentrations by TP 2.

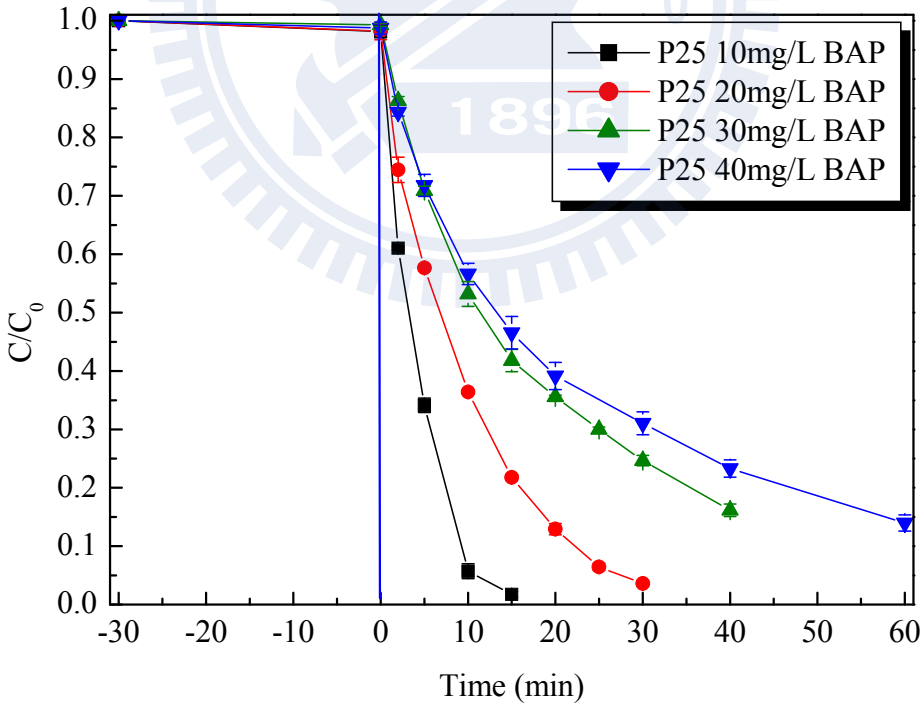

Appendix F-2 The photodegradation of various BPA concentrations by P25.